正电子技术的在材料科学中应用

Ye Bangjiao

叶邦角

中国科学技术大学
核固体物理实验室
Laboratory of Nuclear Solid State Physics, USTC

内容提要

- 正电子概况
- 正电子湮灭探测技术
- 正电子技术的应用

正电子发现

1928	Predicted by Dirac
1930	Found by Z.Y.Zhao
1932	Found in cosmic Radiations by Anderson
1940’s	First studies of Electronic structures
1950’s	Establishment of Positron Annihilation Spectroscopy
1968	First LINAC based Positron Generation
1982	Slow positron beams

Relativity + Quantum Theory = Antimatter

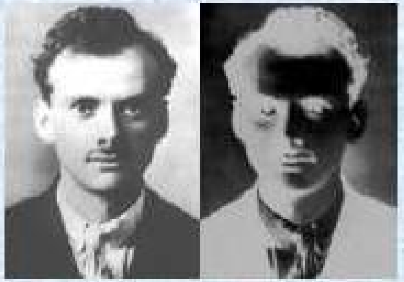

Paul A.M. Dirac (1928)

$$(i\gamma^\mu\partial_\mu - m)\psi = 0$$

$$\psi_+ = \begin{pmatrix}1\\0\\0\\0\end{pmatrix} \text{ or } \begin{pmatrix}0\\1\\0\\0\end{pmatrix} e^{-imt} \qquad \psi_- = \begin{pmatrix}0\\0\\1\\0\end{pmatrix} \text{ or } \begin{pmatrix}0\\0\\0\\1\end{pmatrix} e^{+imt}$$

Electron: spin 1/2

Another spin-1/2 particle??

- For $v \neq 0$, upper and lower components mix
- 1929: Positive electron = proton ????
- 1931: m(e-) = m(e+) ! Annihilation possible ...

赵忠尧

(1902—1998)

中国科学技术大学近代物理系的创建者和首任系主任

1930年春天，赵忠尧先生在CIT实验时发现，γ射线被铅散射时，除康普顿散射外，伴随着反常吸收还有一种特殊的光辐射出现。当时测定的这种特殊辐射的强度是大致各向同性的，并且每个光子的能量与一个电子质量的相当能量很接近。它揭示了一种新的反应机制。赵忠尧将这个实验结果写成第二篇论文，题目为《硬γ射线的散射》，并于1930年10月在美国《物理评论》杂志上发表。

Cloud Chamber Photograph

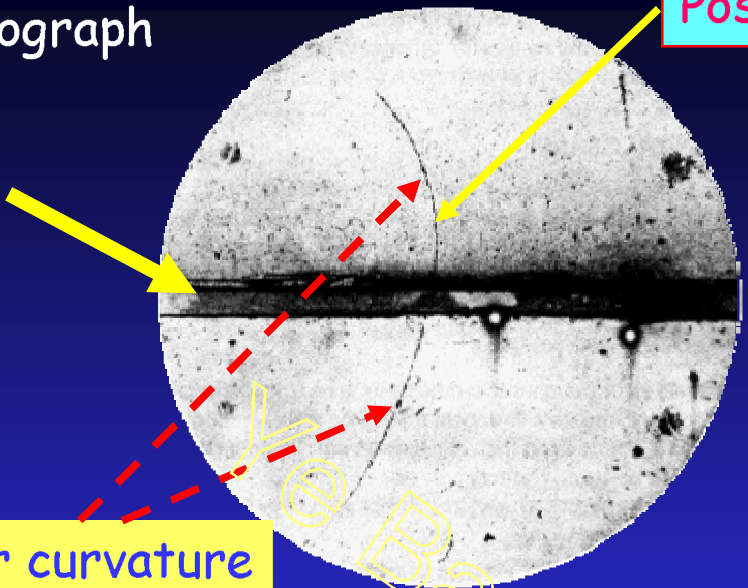

Lead plate

Positron

Larger curvature of particle above plate means it's moving slower (lost energy as it passed through)

Carl Anderson 1905-1991

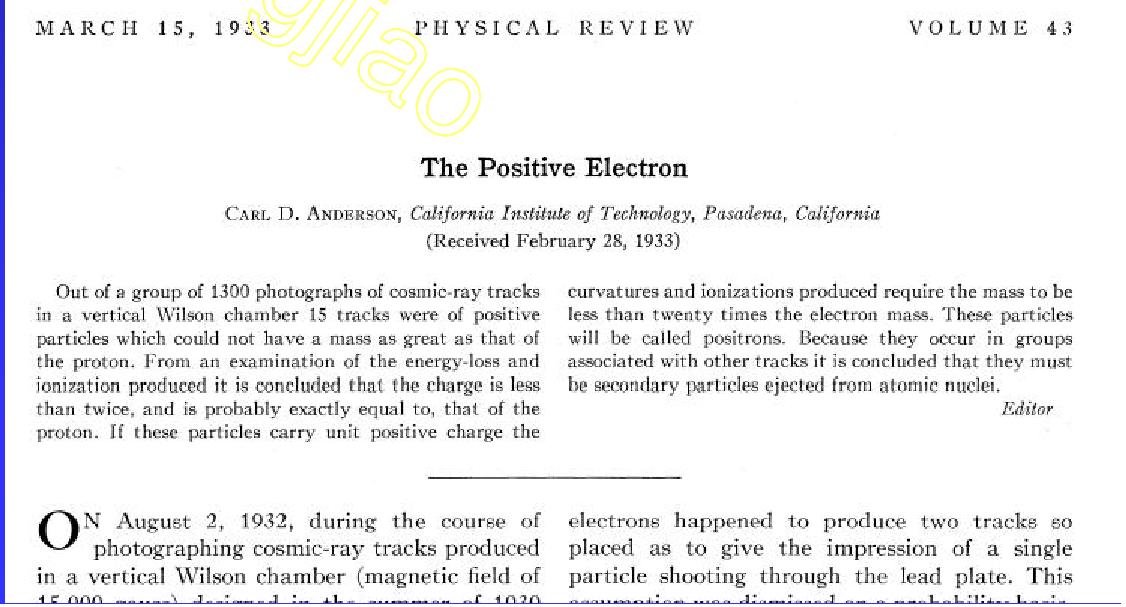

MARCH 15, 1933 PHYSICAL REVIEW VOLUME 43

The Positive Electron

Carl D. Anderson, *California Institute of Technology, Pasadena, California*

(Received February 28, 1933)

Out of a group of 1300 photographs of cosmic-ray tracks in a vertical Wilson chamber 15 tracks were of positive particles which could not have a mass as great as that of the proton. From an examination of the energy-loss and ionization produced it is concluded that the charge is less than twice, and is probably exactly equal to, that of the proton. If these particles carry unit positive charge the curvatures and ionizations produced require the mass to be less than twenty times the electron mass. These particles will be called positrons. Because they occur in groups associated with other tracks it is concluded that they must be secondary particles ejected from atomic nuclei.

Editor

On August 2, 1932, during the course of photographing cosmic-ray tracks produced in a vertical Wilson chamber (magnetic field of

electrons happened to produce two tracks so placed as to give the impression of a single particle shooting through the lead plate. This

正电子的性质

- 质量：等于电子质量
- 电荷：与电子电荷数量相等
- 磁矩：与电子磁矩相等，$ge/2m_0c$
- 寿命：在真空无电子环境，$>2\times10^{21}$年

正电子属轻子族，

所以它是费米子，遵守**Fermi-Dirac**统计；

不直接参与强相互作用。

正电子产生

- β^+-decay ($^{22}Na \rightarrow {}^{22}Ne + e^+ + \upsilon_e + \gamma\,(1.28\ MeV)$)
- pair production ($\gamma \rightarrow e^+ + e^-$)

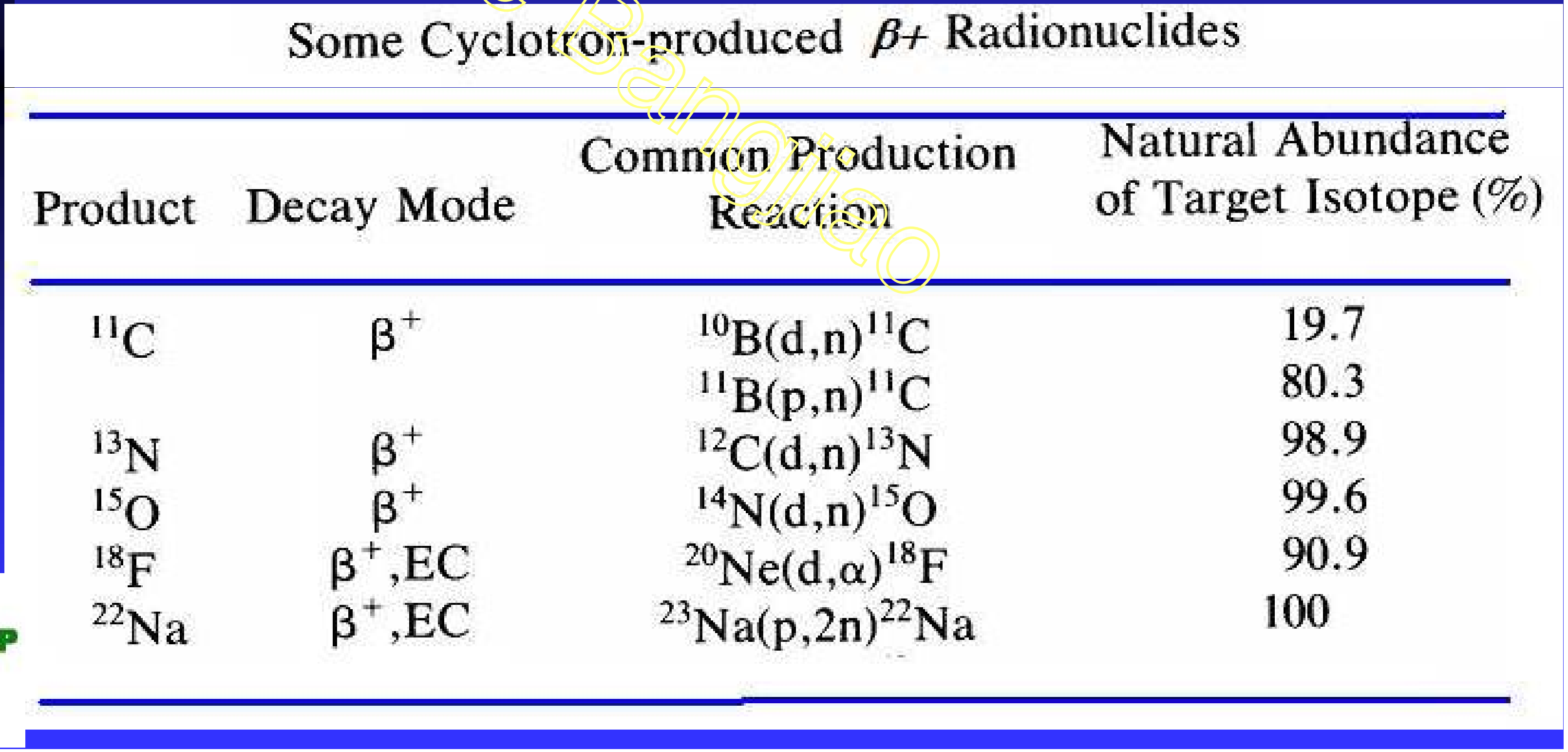

Some Cyclotron-produced β+ Radionuclides

Product	Decay Mode	Common Production Reaction	Natural Abundance of Target Isotope (%)
^{11}C	β^+	$^{10}B(d,n)^{11}C$	19.7
		$^{11}B(p,n)^{11}C$	80.3
^{13}N	β^+	$^{12}C(d,n)^{13}N$	98.9
^{15}O	β^+	$^{14}N(d,n)^{15}O$	99.6
^{18}F	β^+,EC	$^{20}Ne(d,\alpha)^{18}F$	90.9
^{22}Na	β^+,EC	$^{23}Na(p,2n)^{22}Na$	100

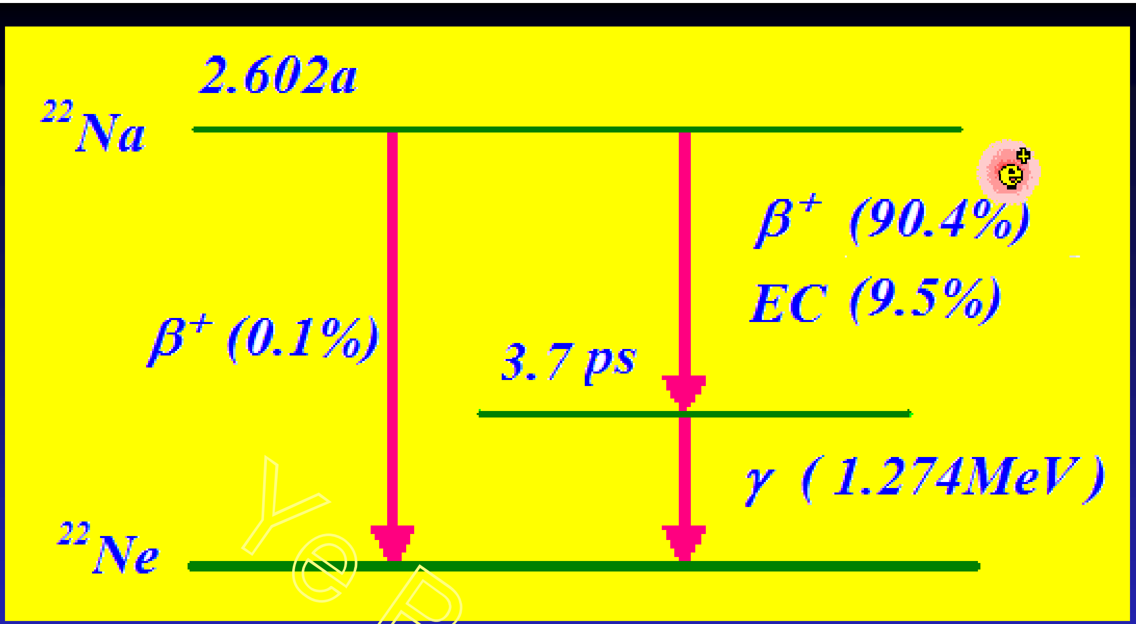

^{22}Na 2.602a

β^+ (90.4%)

EC (9.5%)

β^+ (0.1%)

3.7 ps

γ (1.274MeV)

^{22}Ne

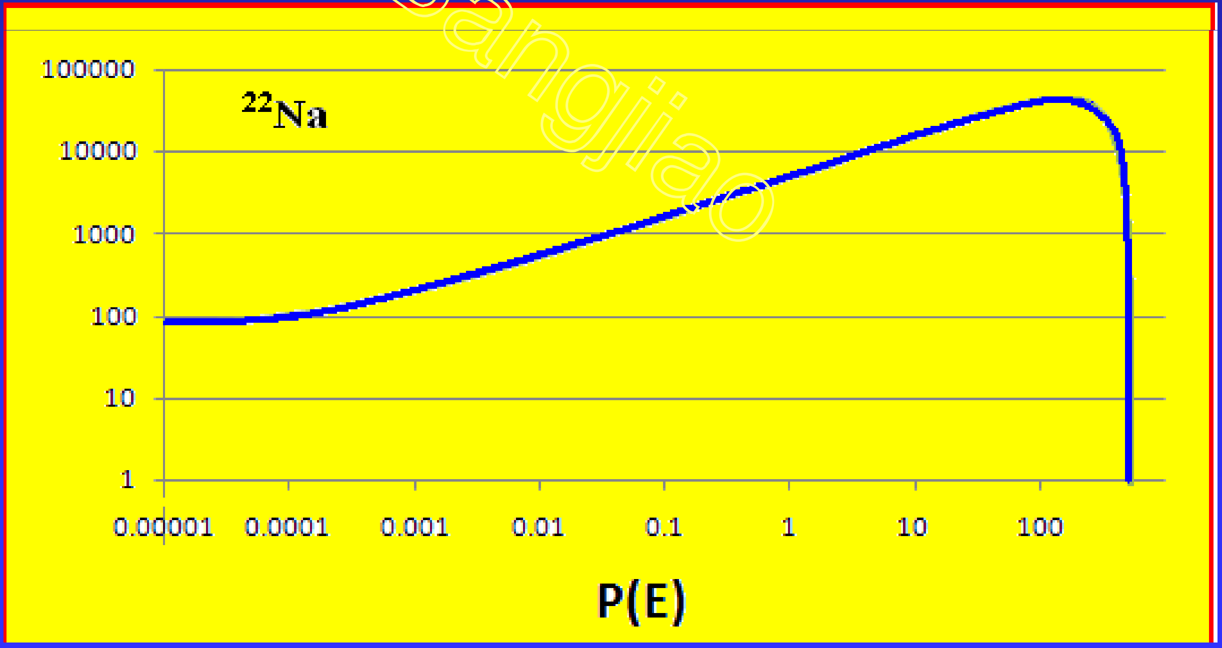

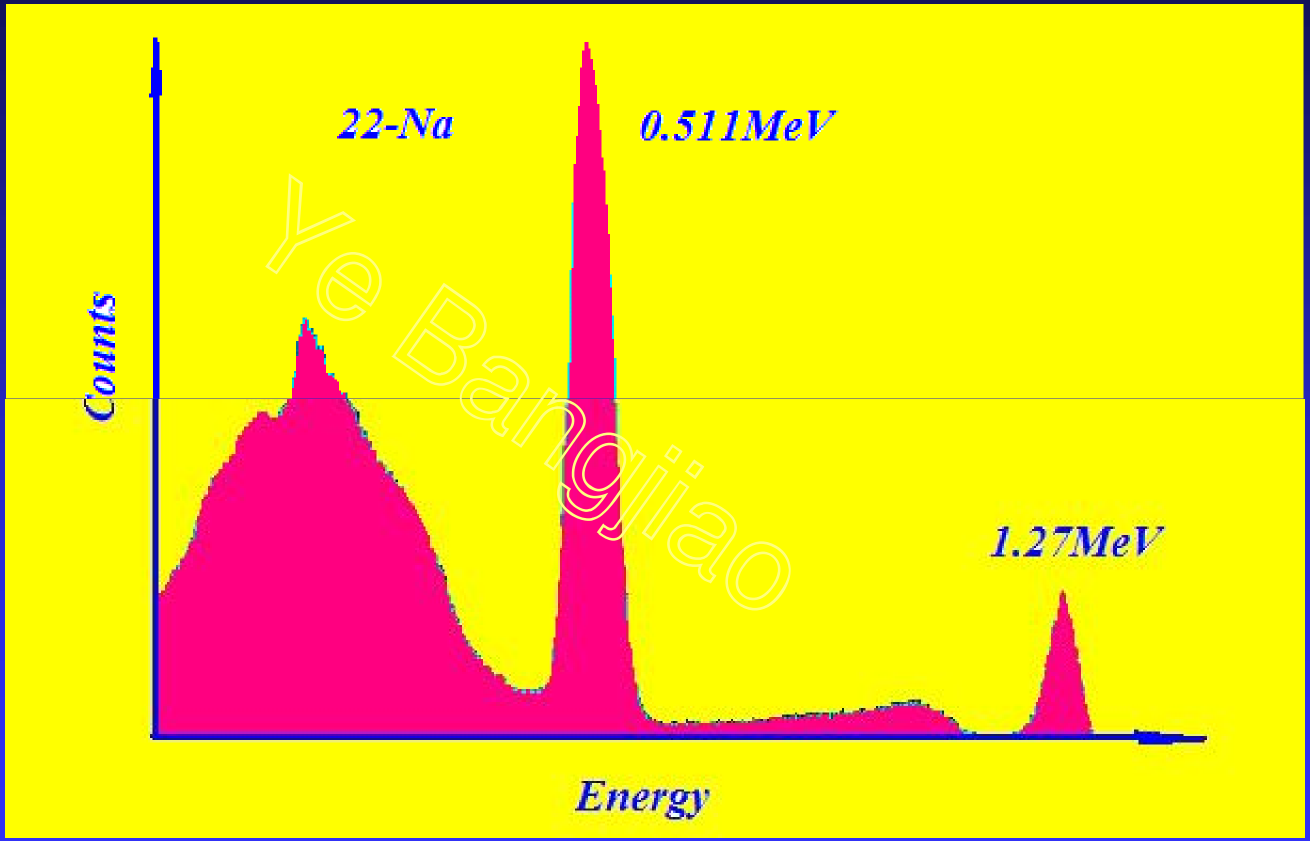
22-Na
0.511MeV
1.27MeV
Counts
Energy

二、正电子湮灭探测技术

- 正电子寿命测量技术
- 多普勒展宽测量技术
- 二维角关联技术
- 寿命-动量关联测量技术
- 3γ测量技术
- 寿命-幅度关联测量技术
- 慢 束
- 正电子衍射技术
- PAES
- 微 束

正电子技术应用

- 半导体
- 超导体
- 薄　膜
- 界　面
- 多孔材料

- 纳米材料
- 巨磁阻
- 金　属
- 多聚物
- 量子点

正电子技术的优越性

各种电镜、卢瑟福背散射、中子衍射、深能级瞬发谱、二次离子谱等，虽然各自给出了许多有价值的结果，但这些方法基本上不能给出原子尺度局域缺陷及微观物相变化的信息，并且多为破坏性测量或造成较大的辐照损伤。

正电子技术是一种无损和高灵敏的探测技术，对复杂材料的分析具有明显的优越性。正电子探针已在基础研究中发挥了巨大的作用，广泛地应用于研究凝聚态材料、介孔材料、半导体和超导体、纳米材料、高聚物化学、量子信息等学科，同时也在工业方面有着巨大的应用潜力，受到各国科学接和工业界的重视。

正电子技术的优越性

- 对缺陷及原子尺度的微结构变化极为灵敏；
- 无损探测；
- 可探测真实表面（几个原子层）的物理化学信息；
- 探测物体内部局域电子密度及动量分布；
- 正电子是电子的反粒子，容易与电子分辨,又可形成电子偶素；
- 慢正电子技术具有能量可调性，因而可获得缺陷或结构不均匀性沿样品深度的分布。

正电子技术与其它技术

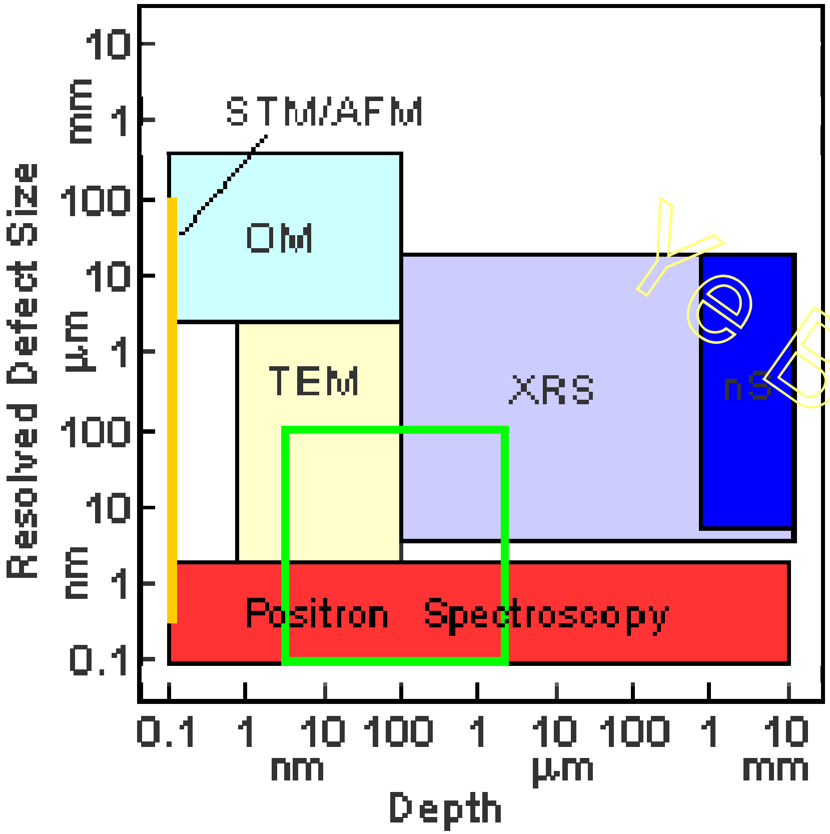

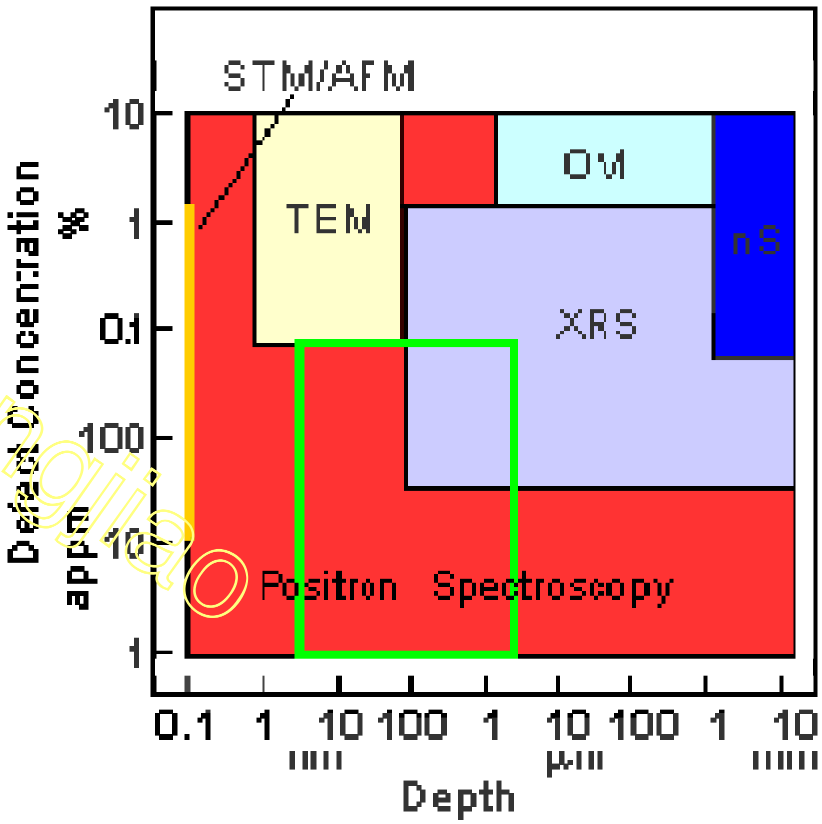

OM: Optical Microscopy

nS: neutron Scattering

TEM: Transmission Electron Microscopy

XRS: X-Ray Scattering

STM: Scanning Tunneling Microscopy

AFM: Atomic Force Microscopy

正电子湮灭

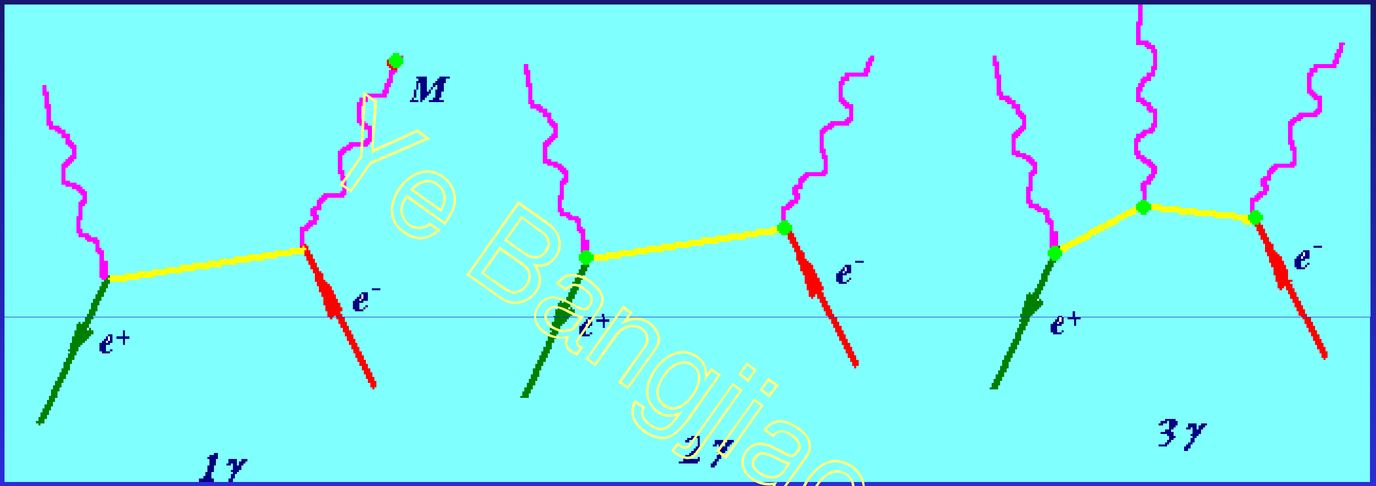

主要湮灭途径：单光子，双光子和三光子

单光子湮灭只有存在着吸收反冲动量的第三个粒子时才有可能

在费曼图中，每增加一个顶点，湮灭截面就要乘以一个因子α，α是精细结构常数

$$\alpha = \frac{e^2}{hc} = \frac{1}{137}$$

对单光子湮灭，还要乘以减弱因子，因为湮灭只有存在着吸收反冲动量的原子附近发生，这个因子正比于α^3。

所以三种湮灭之间的关系为：

$$\frac{\sigma_{3\gamma}}{\sigma_{2\gamma}} = \frac{\alpha^3}{\alpha^2} = \alpha = \frac{1}{137}, \quad \frac{\sigma_{1\gamma}}{\sigma_{2\gamma}} = \frac{\alpha^6}{\alpha^2} = \alpha^4 \approx 10^{-8},$$

正电子湮灭基本测量技术

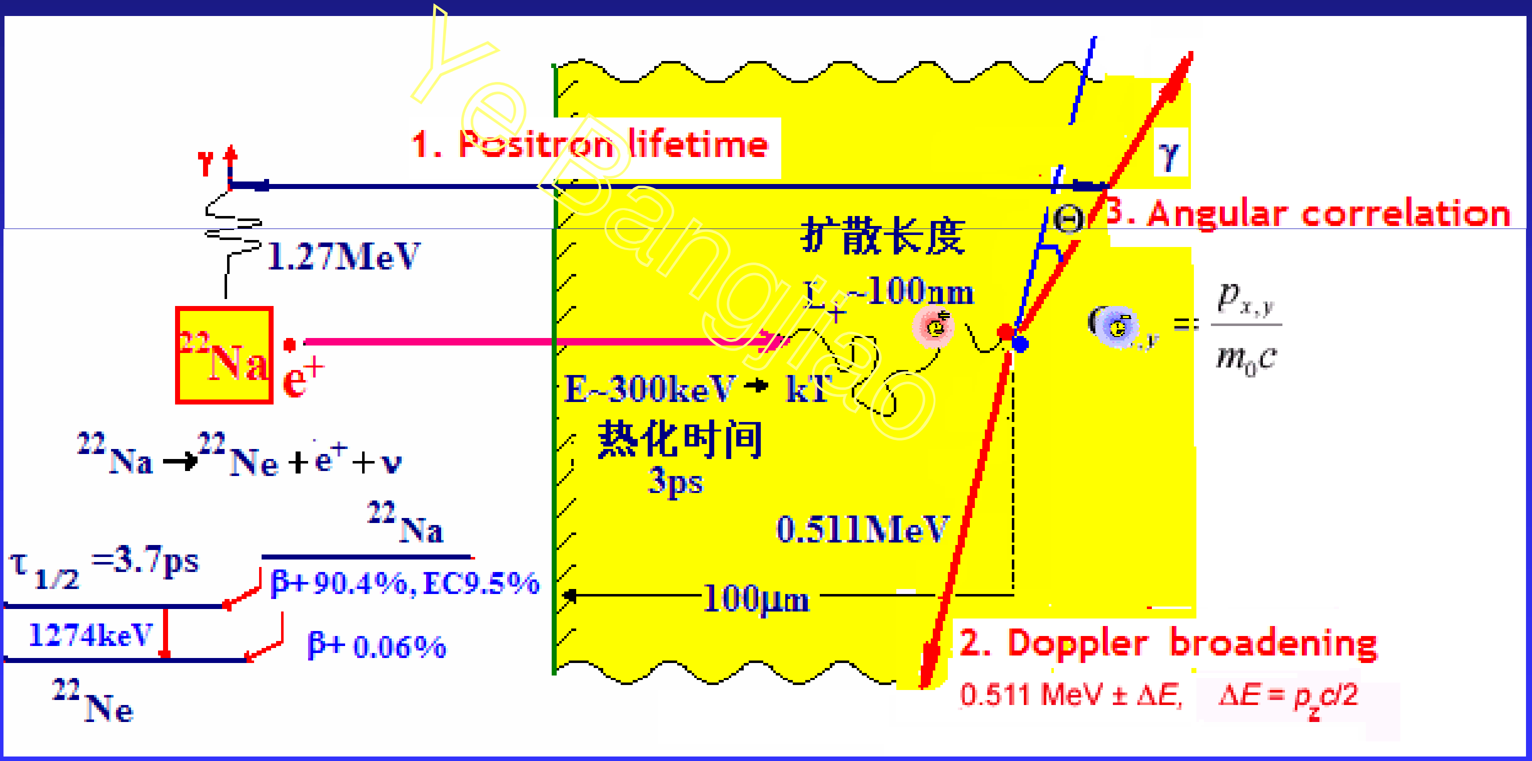

●寿命测量

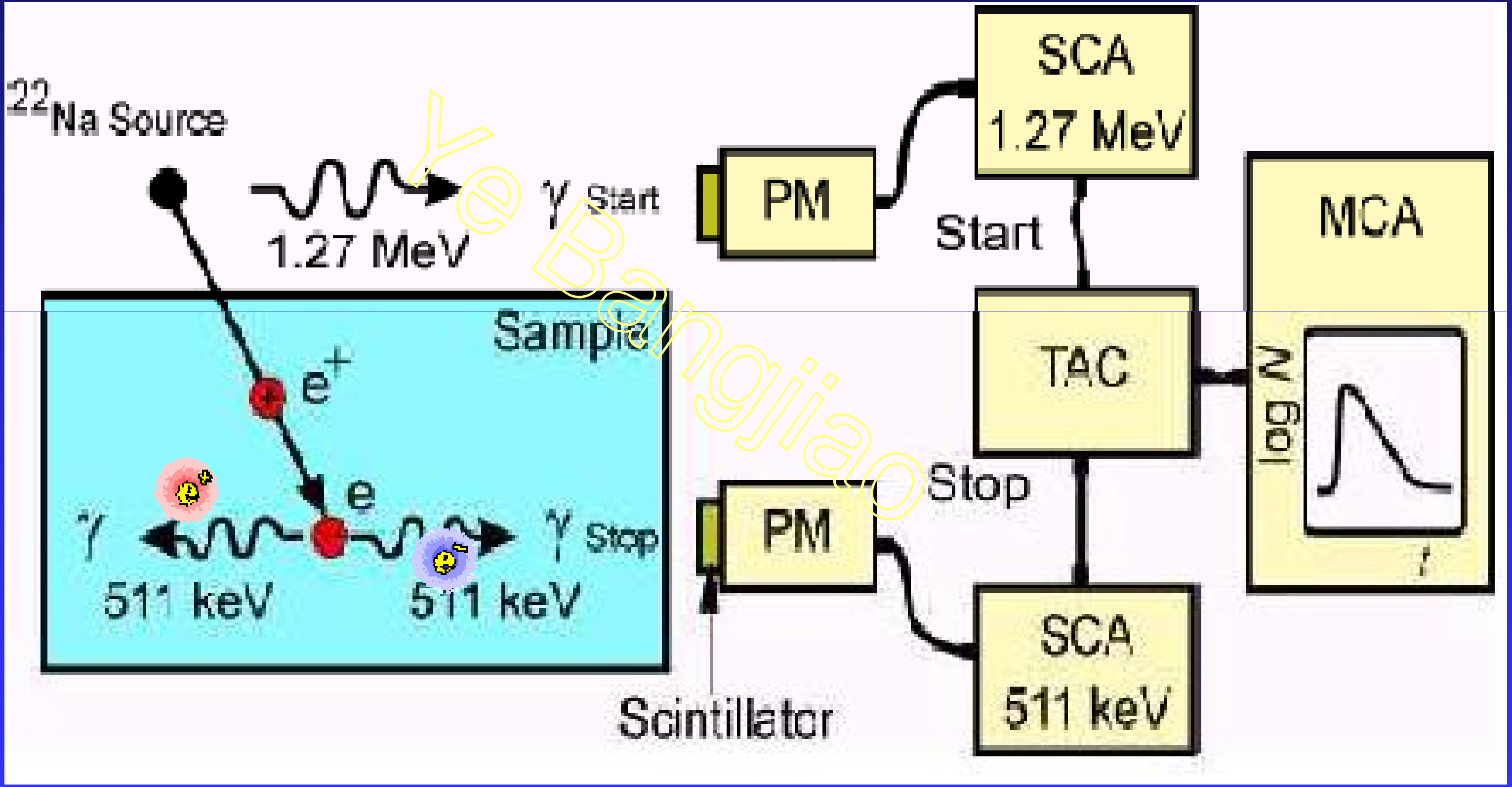
^{22}Na Source
1.27 MeV
γ Start
PM
SCA
1.27 MeV
Start
MCA
Sample
e+
e
γ
511 keV
511 keV
γ Stop
TAC
log N
t
Stop
PM
SCA
511 keV
Scintillator

Defects in Materials

Defect Type		Size	Materials
Atomic Vacancies	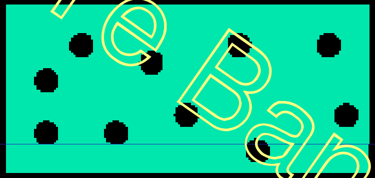	.1 nm	Metals
Dislocations	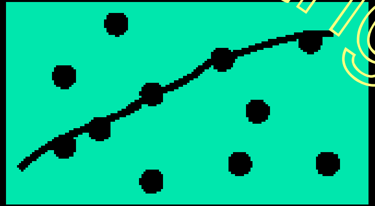	1 nm-10 µm	Metals
Voids	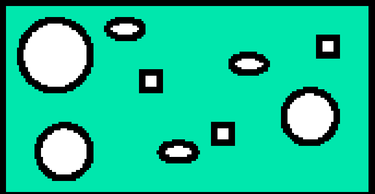	.1 nm-1 µm	Composites
Holes	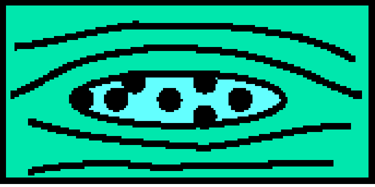	.1 nm-10 µm	Polymers

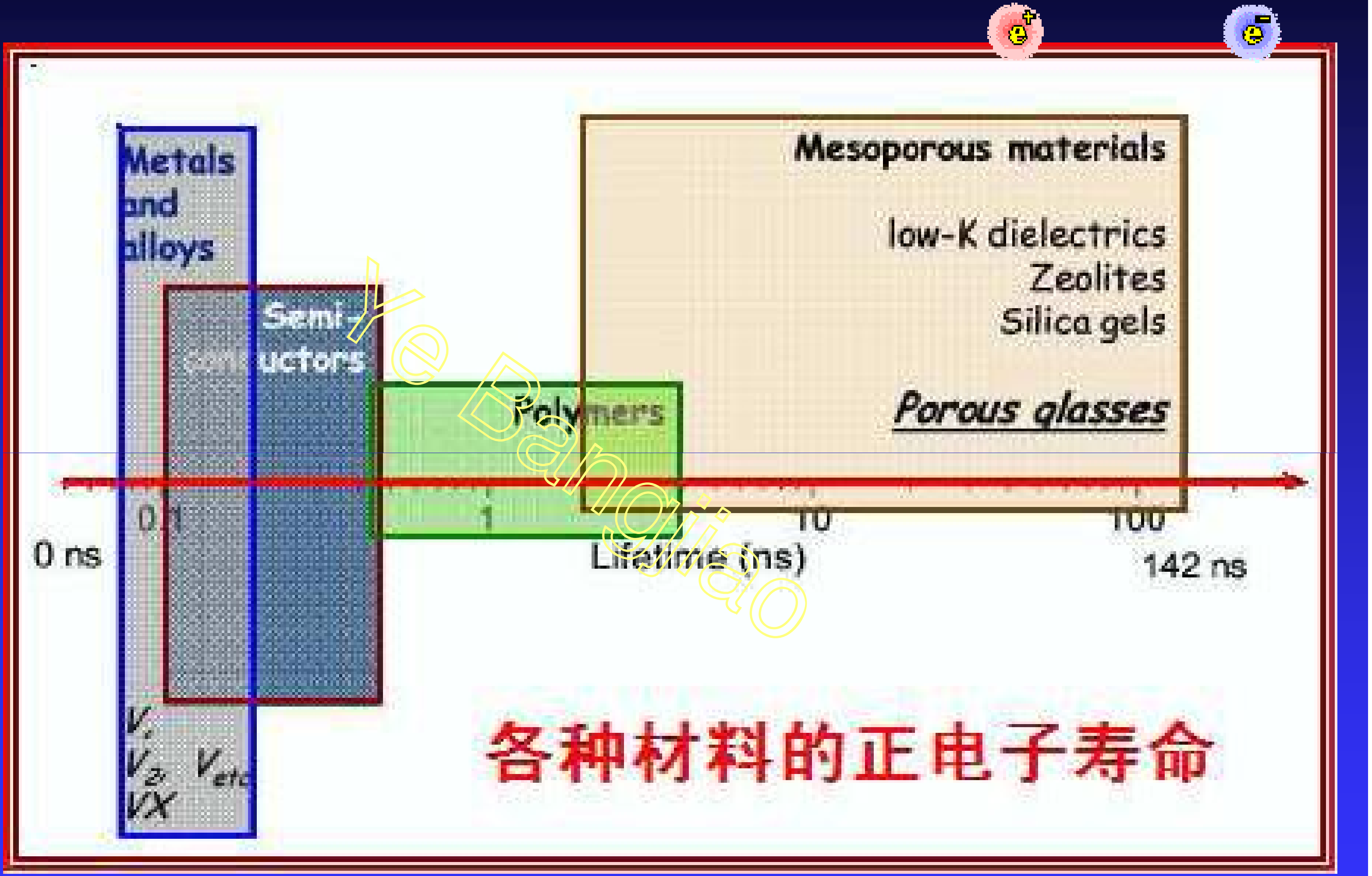
Metals and alloys
Semi-conductors
Polymers
Mesoporous materials
low-K dielectrics
Zeolites
Silica gels
Porous glasses
0 ns
0.1
1
10
100
Lifetime (ns)
142 ns
V, V2, VX
Vetc

各种材料的正电子寿命

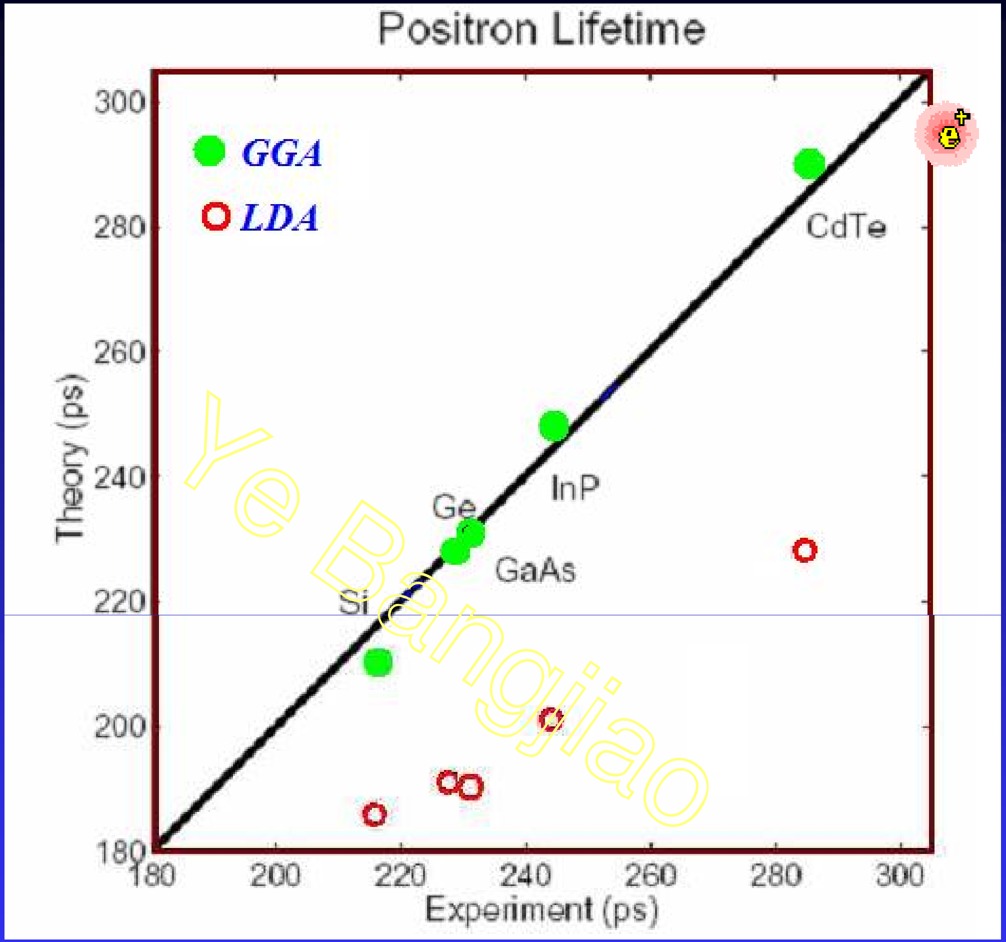

Positron lifetimes for some semiconductors. The solid and open circles give the Generalized Gradient Approximation (GGA) and the Local-Density Approximation (LDA) results as a function of the experimental ones, respectively.

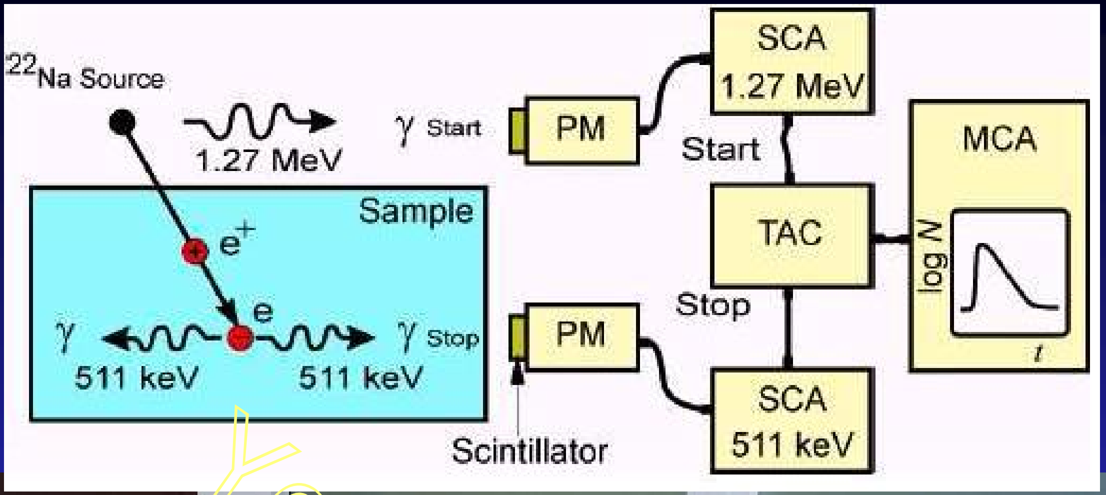
^{22}Na Source
1.27 MeV
γ Start
PM
SCA
1.27 MeV
Start
MCA
Sample
e^+
e
TAC
log N
t
γ
511 keV
511 keV
γ Stop
PM
Stop
Scintillator
SCA
511 keV

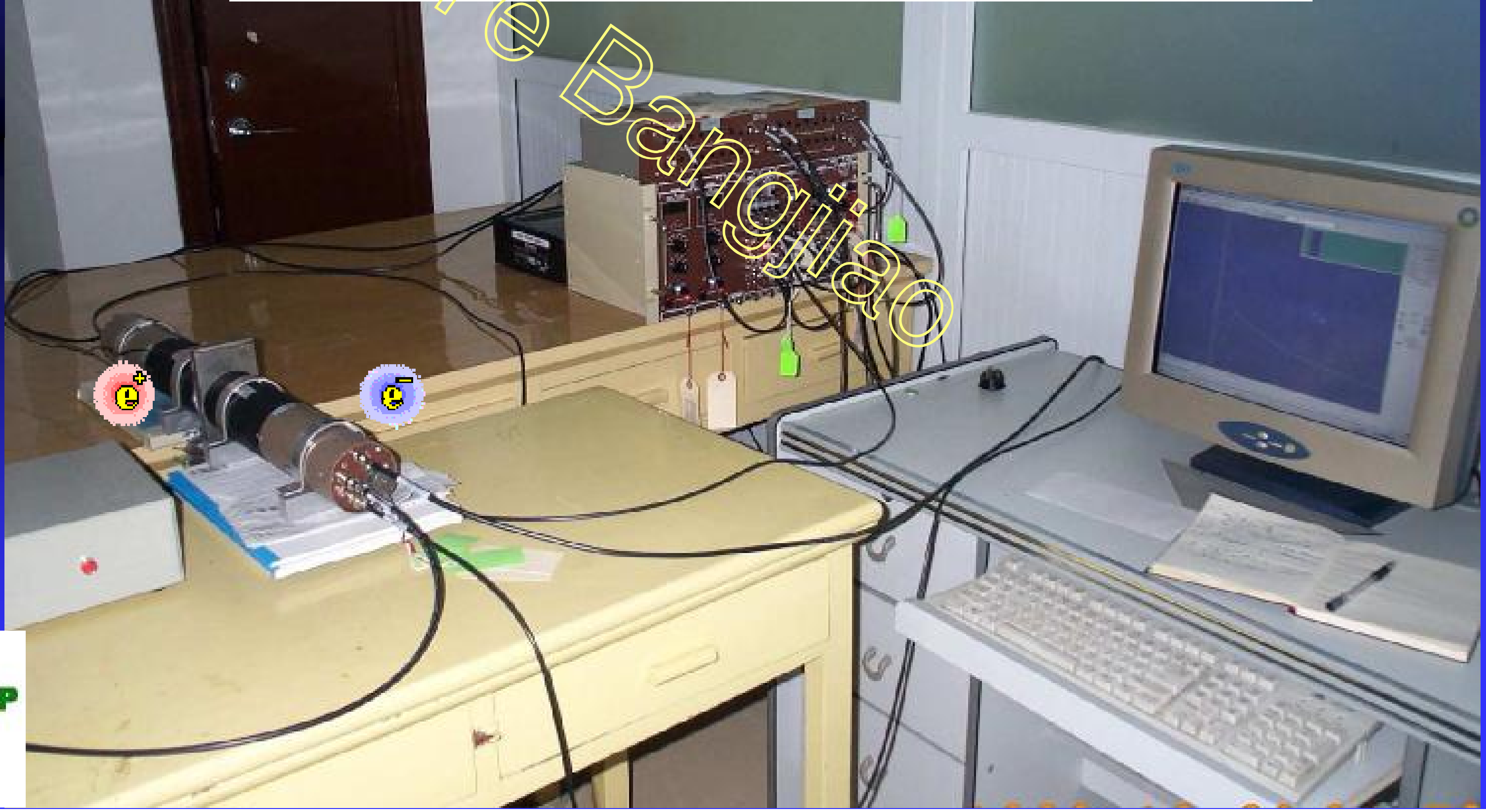


HV
BaF₂
CFD
DE
Ye Bangjiao
LNSSP

实测的正电子寿命谱

$$N(t)=\sum_{i=1}^{k+1}\frac{I_i}{\tau_i}\exp(-\frac{t}{\tau_i})$$

MELT拟合结果

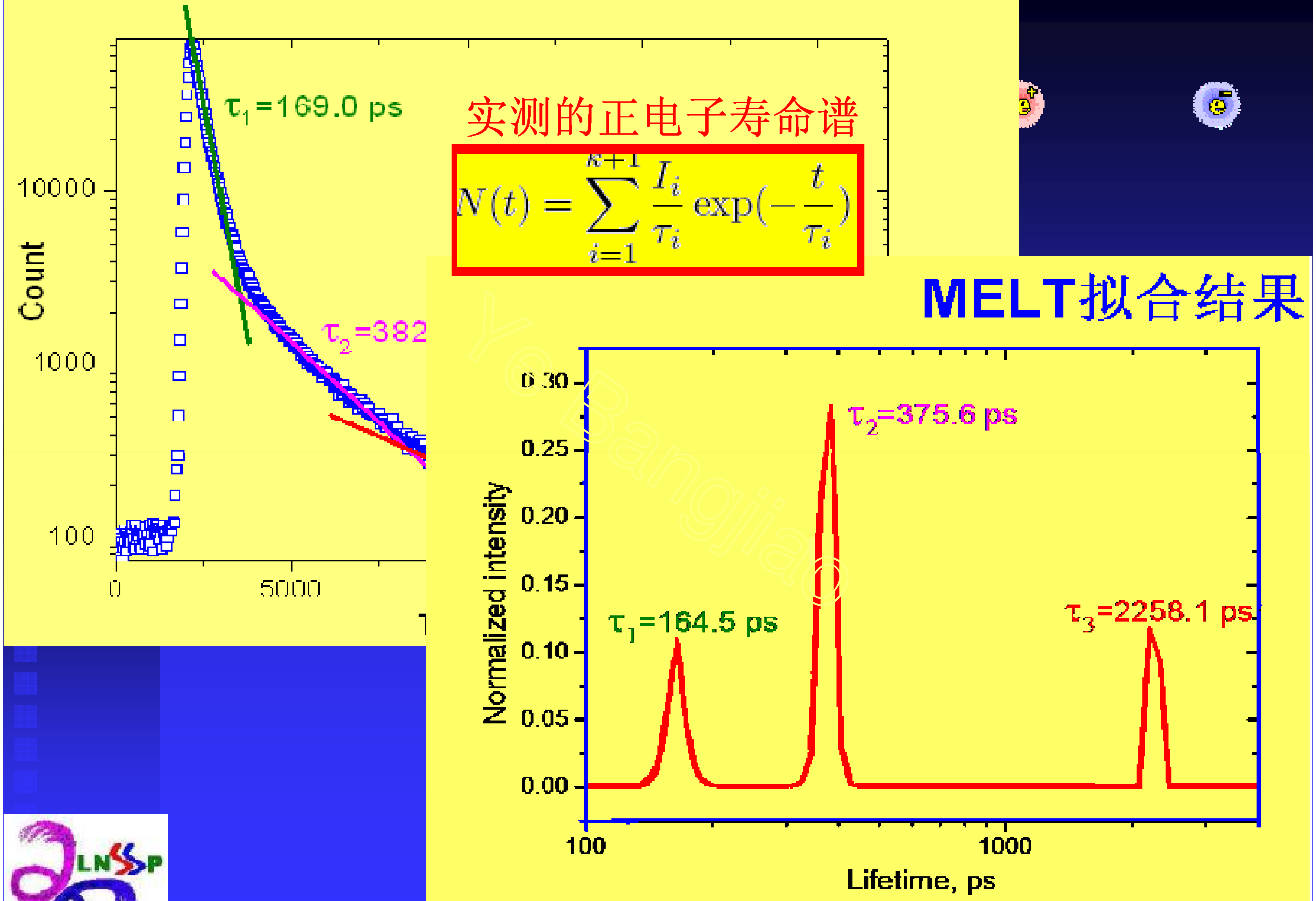

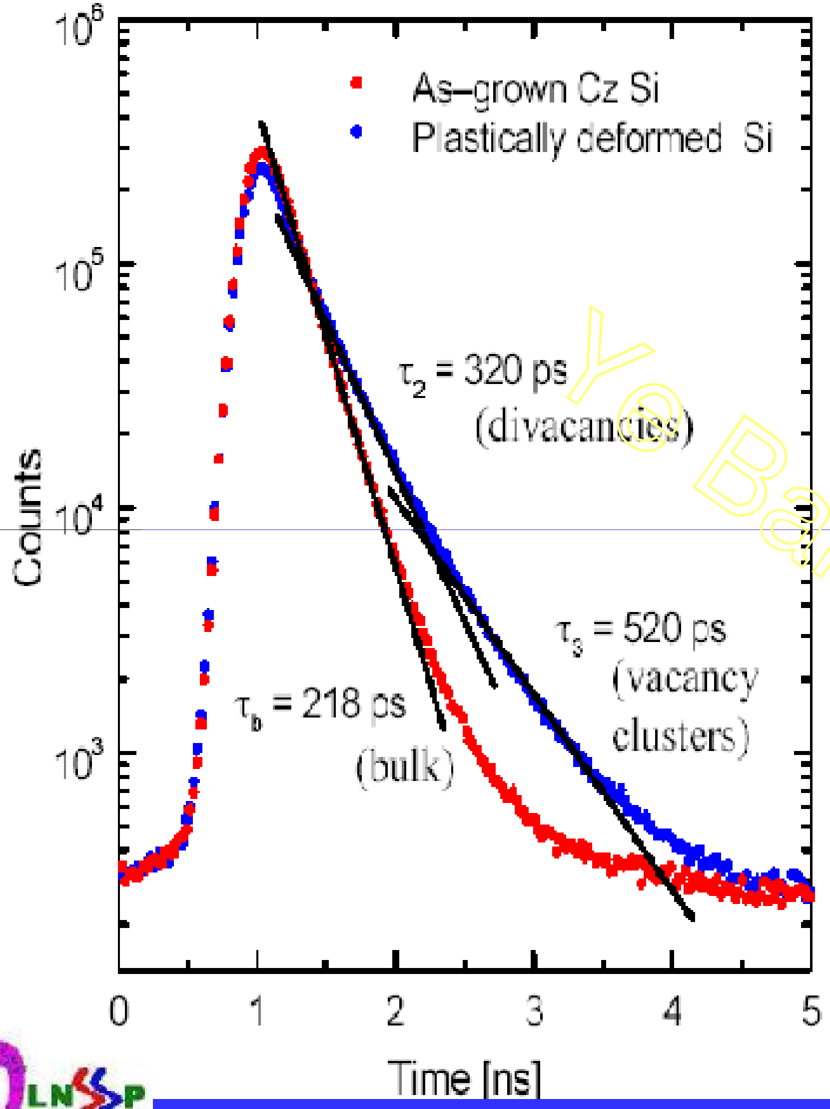

- positron lifetime spectra consist of exponential decay components
- positron trapping in open-volume defects leads to long-lived components
- longer lifetime due to lower electron density
- analysis by non-linear fitting: lifetimes τ_i and intensities I_i
- positron lifetime spectrum: $$N(t) = \sum_{i=1}^{k+1} \frac{I_i}{\tau_i} \exp\left(-\frac{t}{\tau_i}\right)$$

trapping coefficient

- $$\boxed{\kappa_d = \mu C_d} = \frac{I_2}{I_1}\left(\frac{1}{\tau_b} - \frac{1}{\tau_d}\right)$$

trapping rate

defect concentration

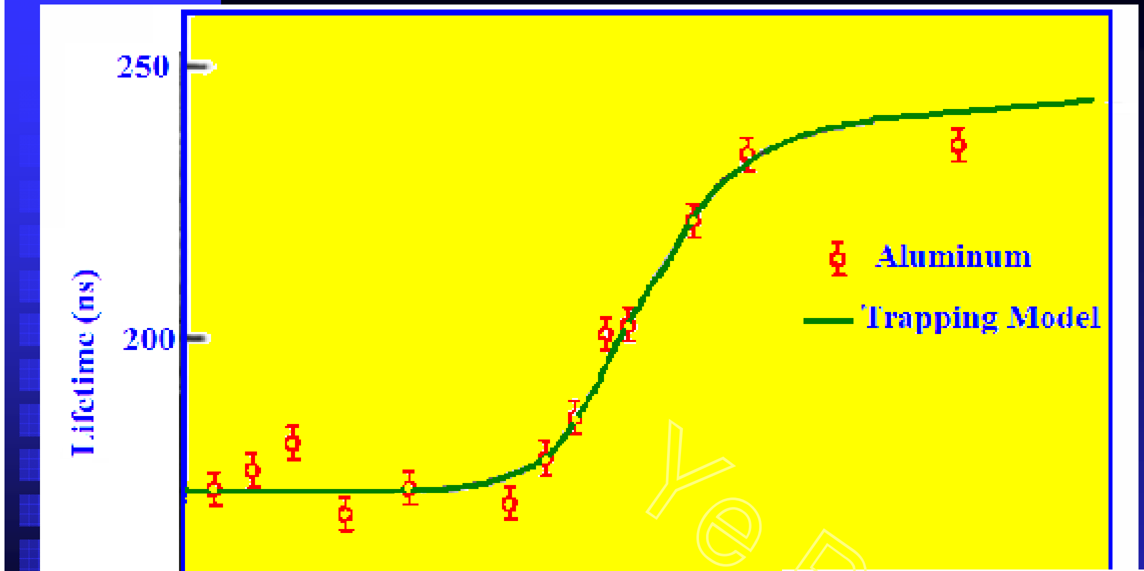

铝的热平衡缺陷

聚乙烯的热弛豫过程

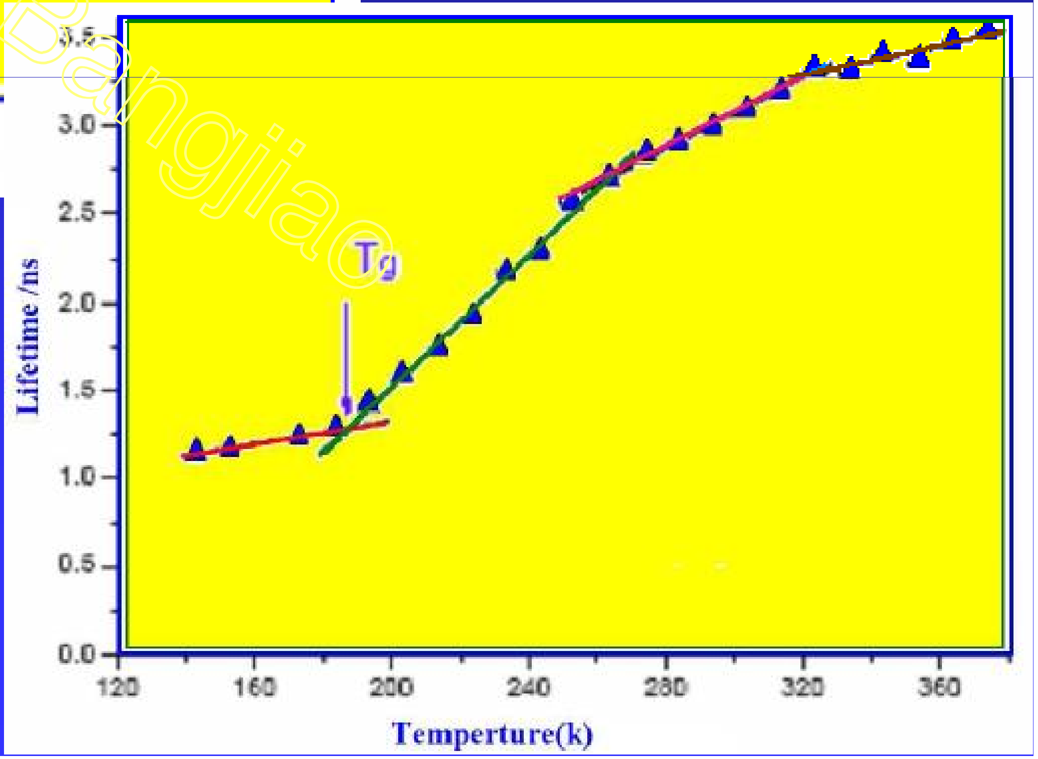

Positron interactions with condensed matter

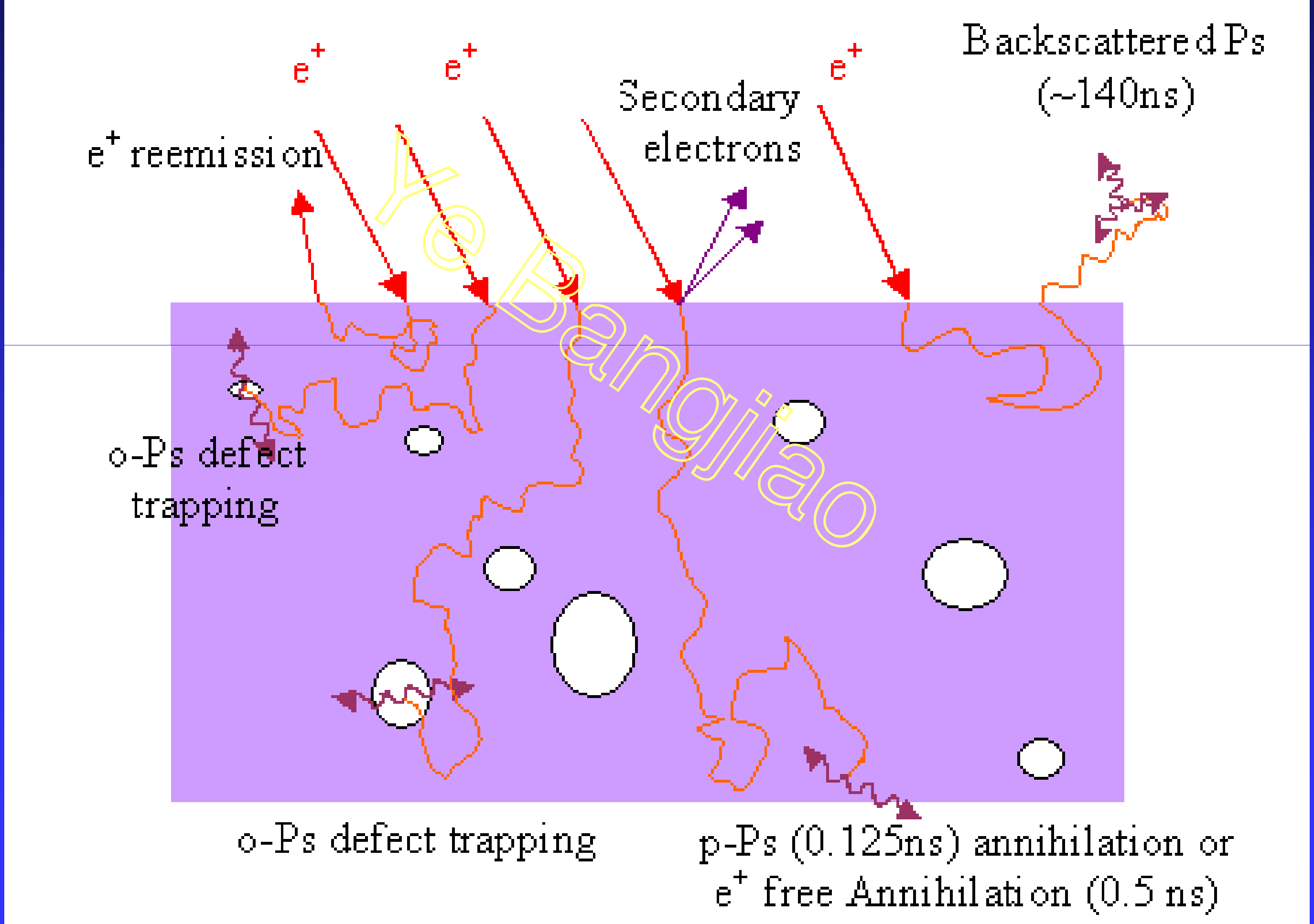

介孔结构和尺寸

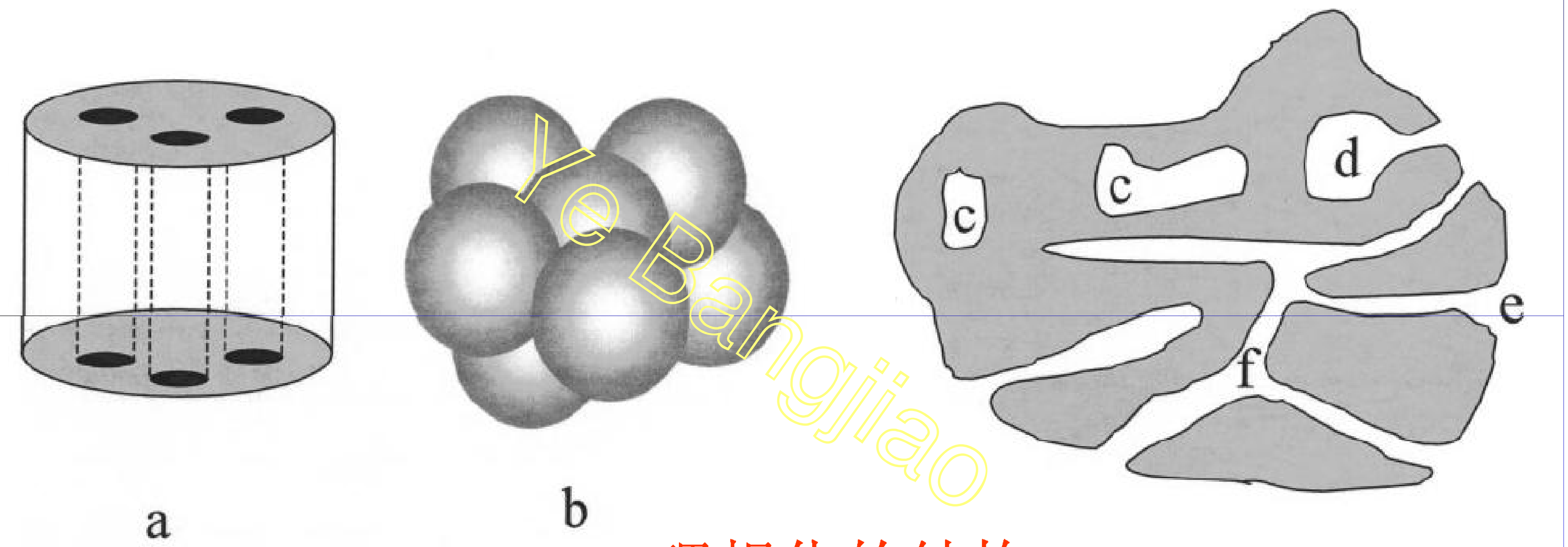

理想化的结构

(a) cylindrical pores; (b) voids between packed spheres and schematic boundary structure showing.

(c) closed (latent) pores; (d) ink bottle; (e) funnel; and (f) open pores.

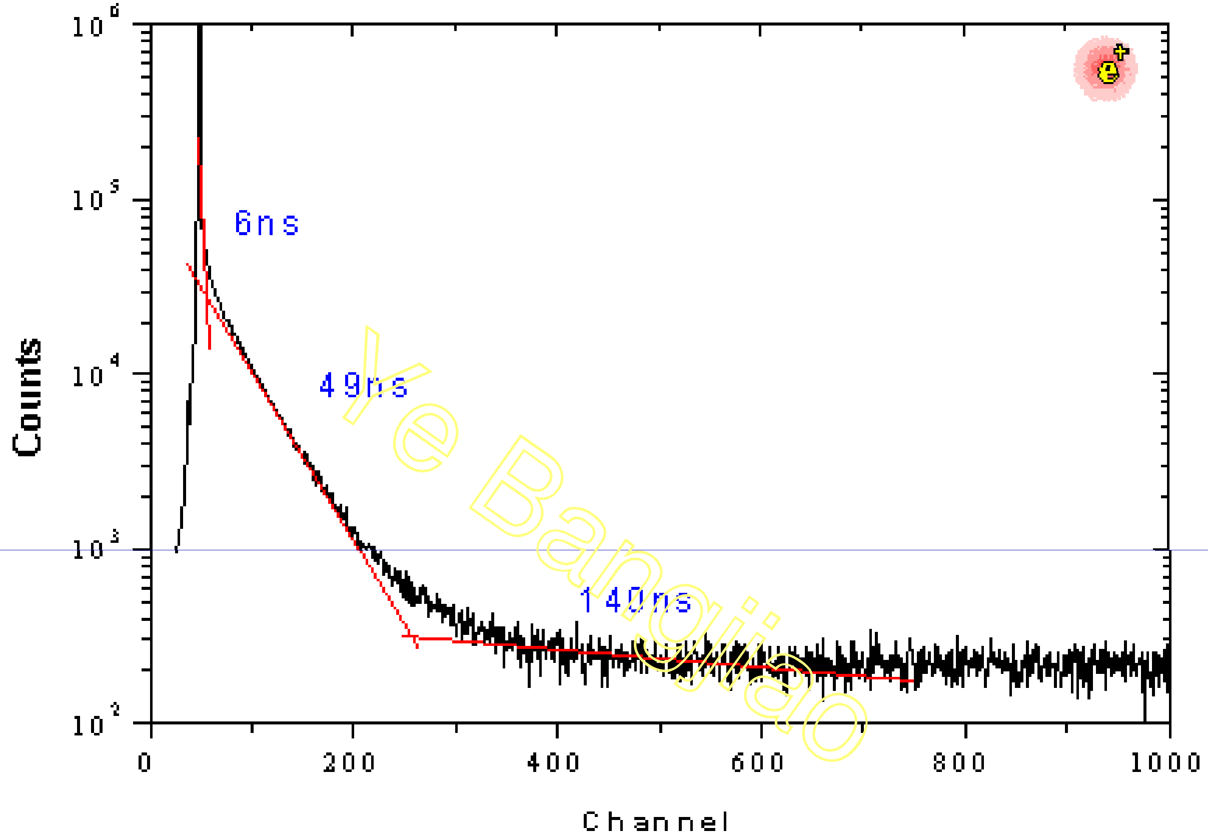

- A typical PALS spectrum with three film Ps lifetimes fitted using POSFIT.

T-E公式

Tao 1972,
J.Chem.Phys. **56**, 5499

Eldrup et al. 1981
Chem. Phys. **63**, 51

$$\tau_3 = \frac{1}{2}\left(1 - \frac{R}{R_0} + \frac{1}{2\pi}\sin\frac{2\pi R}{R_0}\right)^{-1}$$

$$f_v = aV_f I_3$$

R : free volume radius

$$R_0 = R + 1.66\ \text{Å}$$

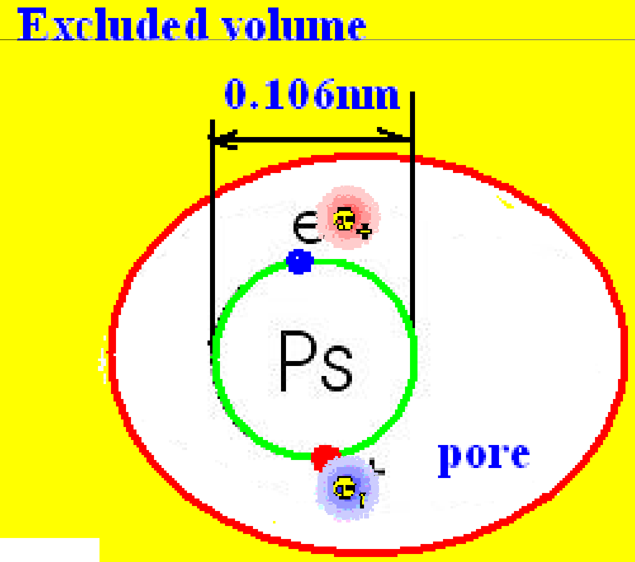

如果半径>2.3 nm

$$\frac{1}{\tau} = \frac{1}{\tau_{pick-off}} + \frac{1}{\tau_{self}}$$

where in air =100 ns but in vacuum 142 ns

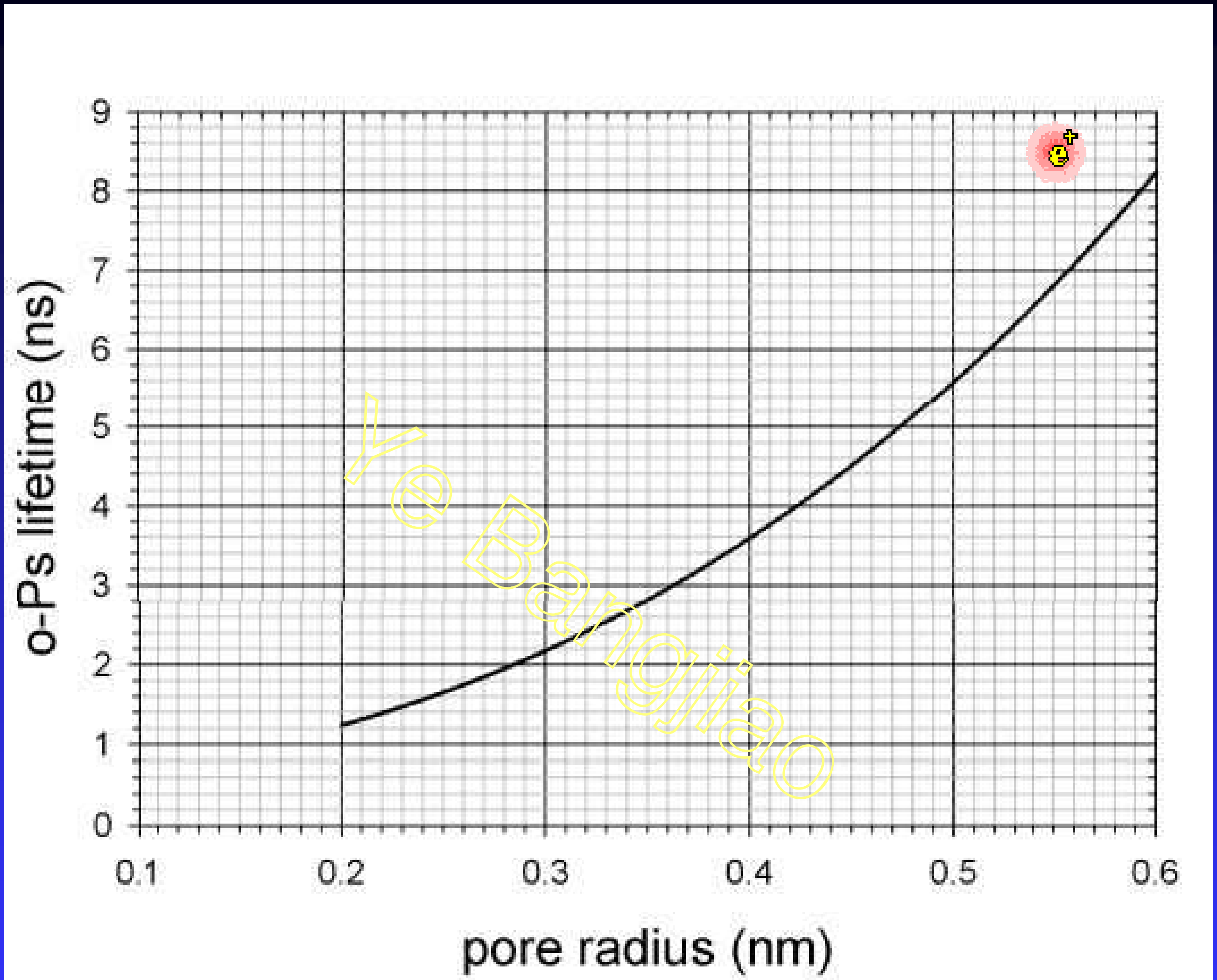

The dependency of o-Ps lifetime versus the pore radius according to the Tao-Eldrup equation

介孔尺寸标定

介孔分类

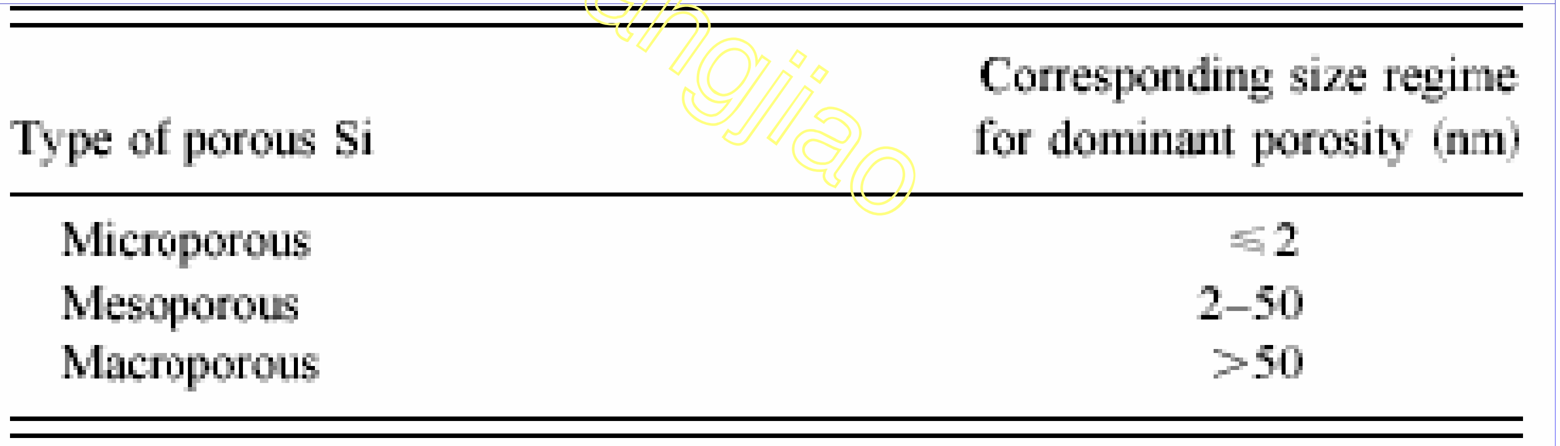

Type of porous Si	Corresponding size regime for dominant porosity (nm)
Microporous	≤2
Mesoporous	2–50
Macroporous	>50

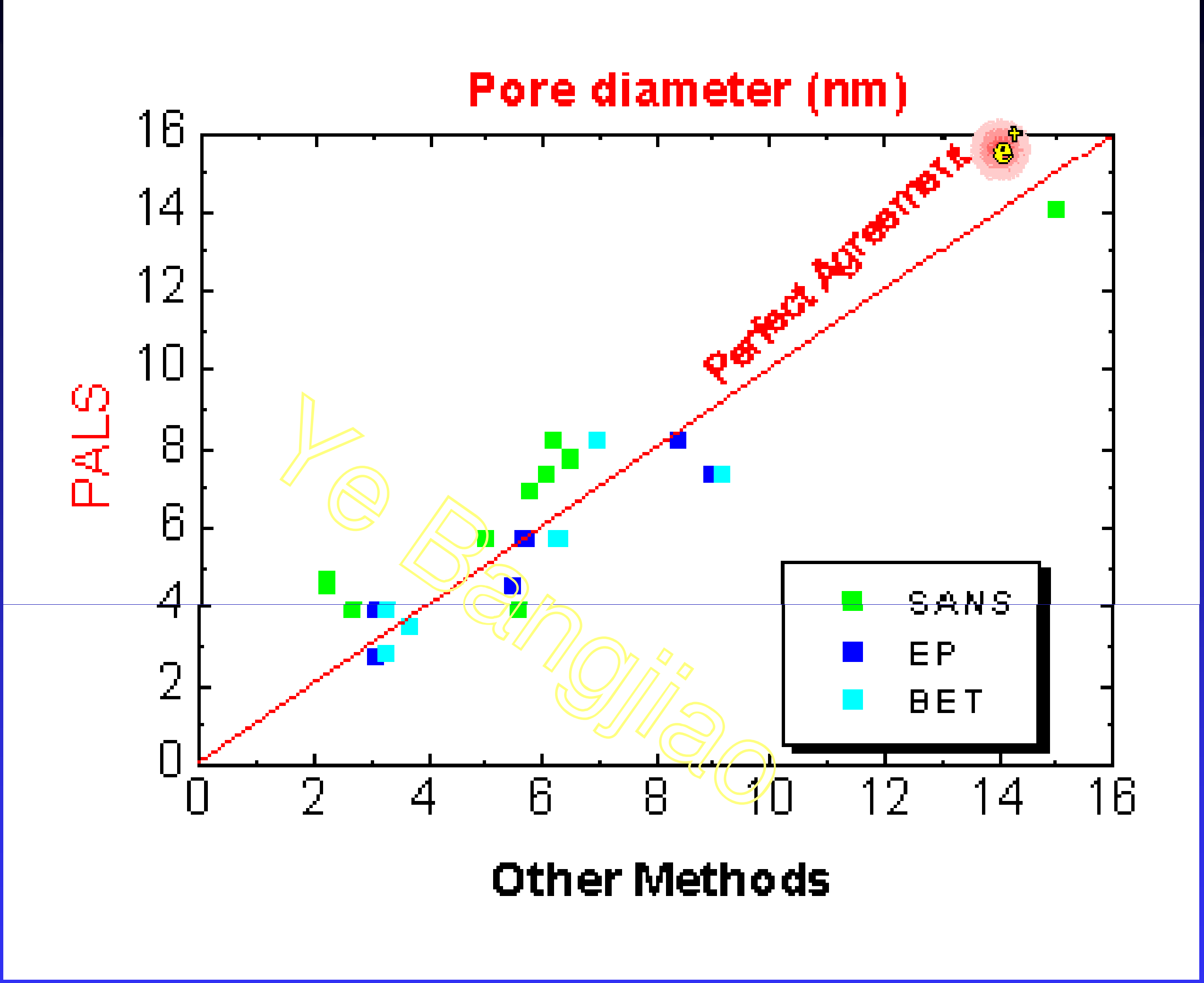

Comparison on PALS technique with other methods

Open Porosity

- Ps 在室温下的速率为 8×10^6 cm/s, 在寿命期内在直径为5-10nm的介孔内可以有1-2 × 10^6次碰撞.
- Ps 可以容易地扩散回到真空表面, 大部分的Ps湮灭发生在表面真空(142 ns).

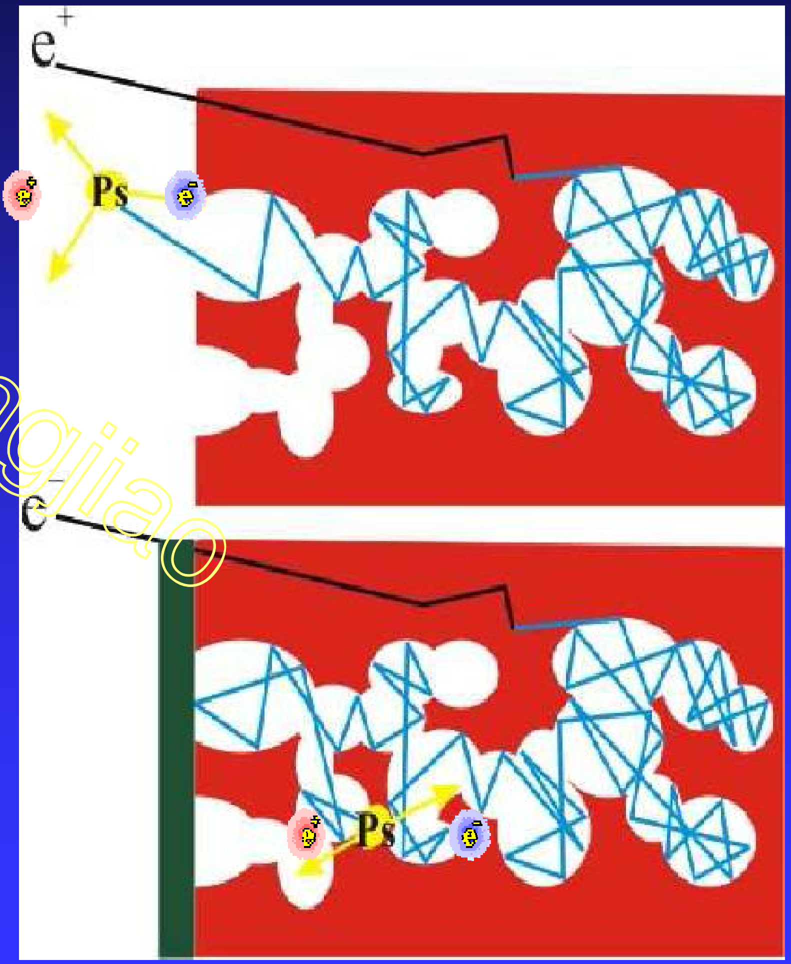

开介孔

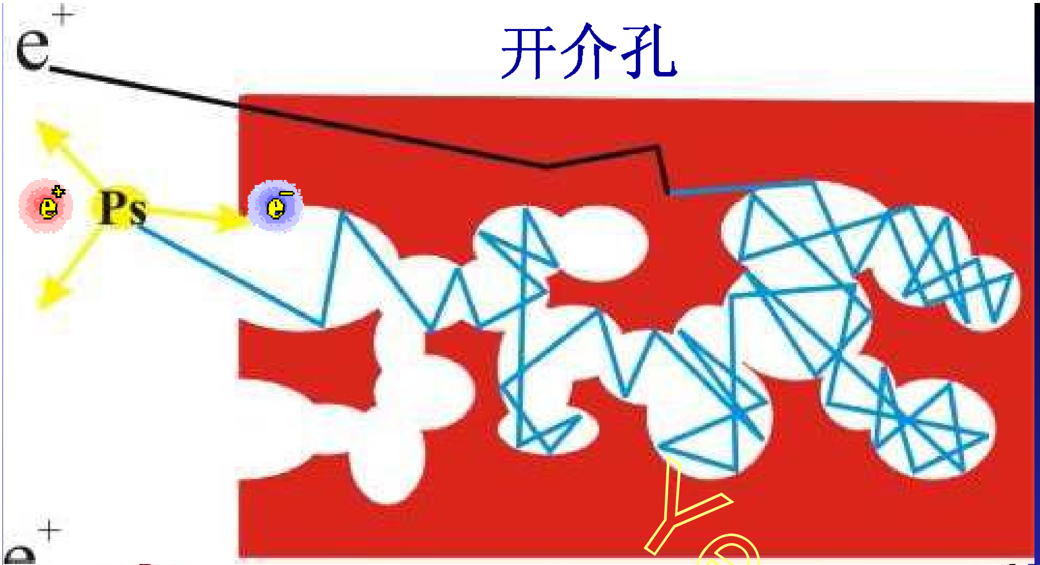

a porous silica film

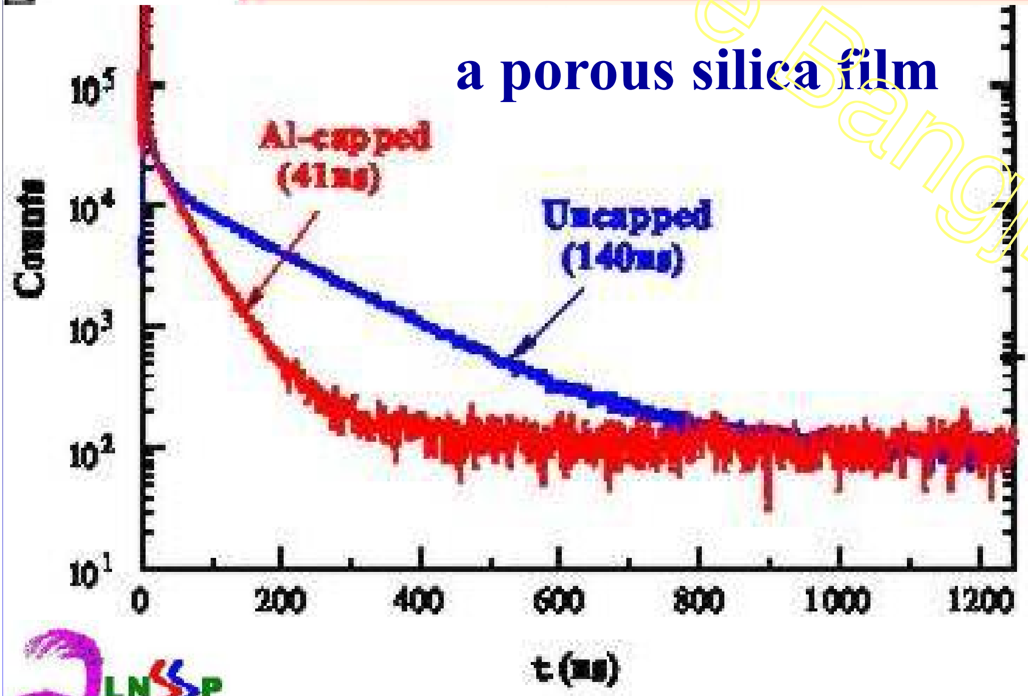

- 典型的开介孔寿命谱.
- 一个较短寿命(<0.5 ns)的特征峰来自于正电子或 Ps 在介孔和块体上的湮灭;
- 另一个长寿命分量占(35 - 40%).
- 长寿命分量的拟合值是140 ns ,即在真空中湮灭. 表明介孔内部是高度连通, Ps 可以容易扩散到真空表面.

Closed Porosity

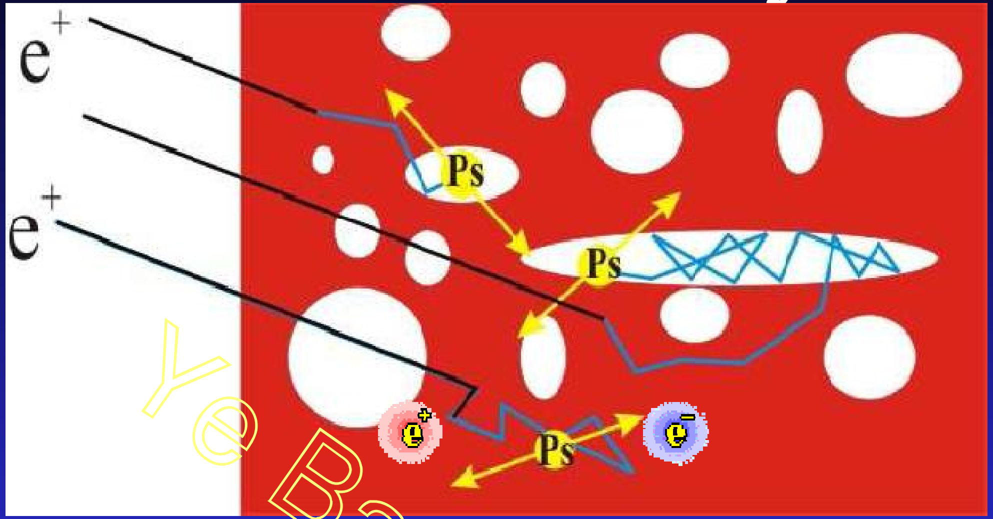

Capped Porosity

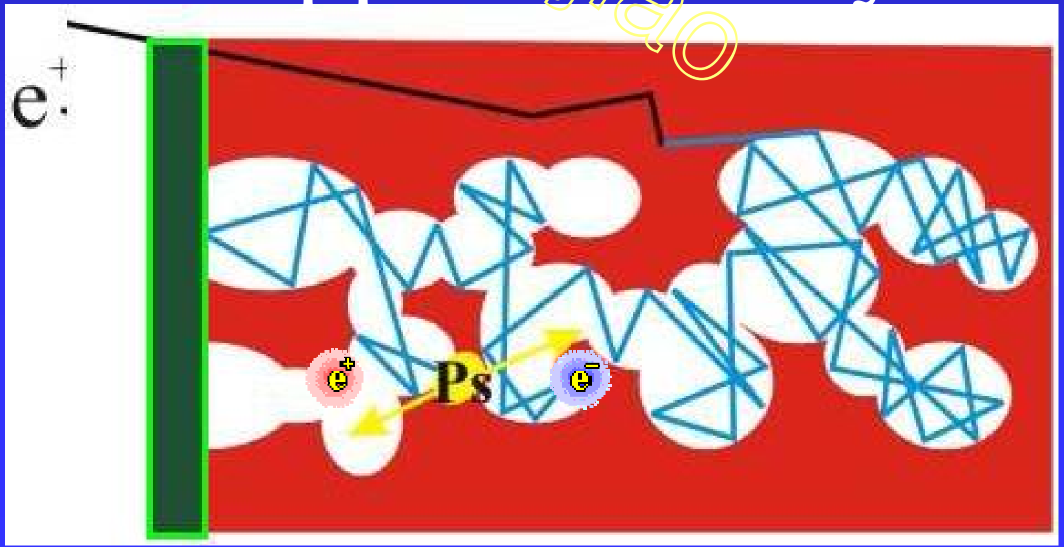

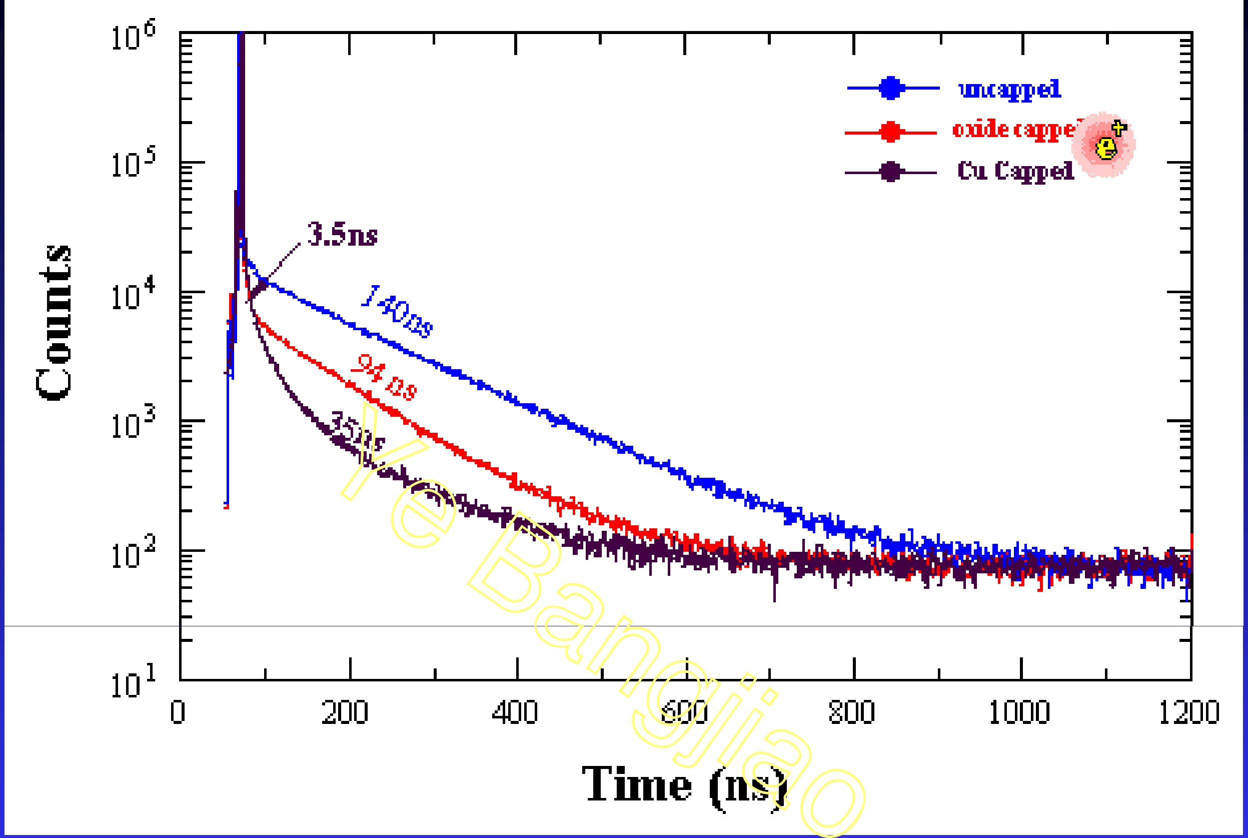

- A Cu-capped porous silica film : 35ns and 3.5 ns;
- Oxide-capped silica film : 94 ns;
- This reduction of the Ps lifetime is almost certainly due to Cu coating on the inner pore surfaces where Ps annihilation would be enhanced by the high density of free electrons in Cu.

●多普勒展宽

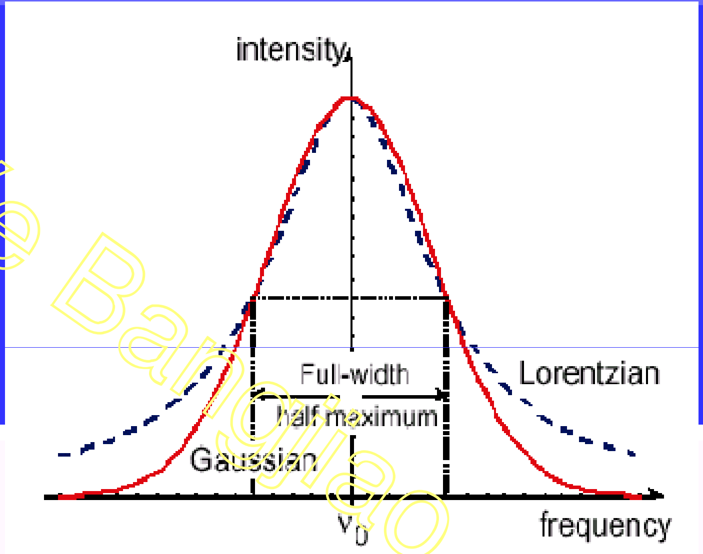

intensity
Full-width
half maximum
Lorentzian
Gaussian
ν_0
frequency

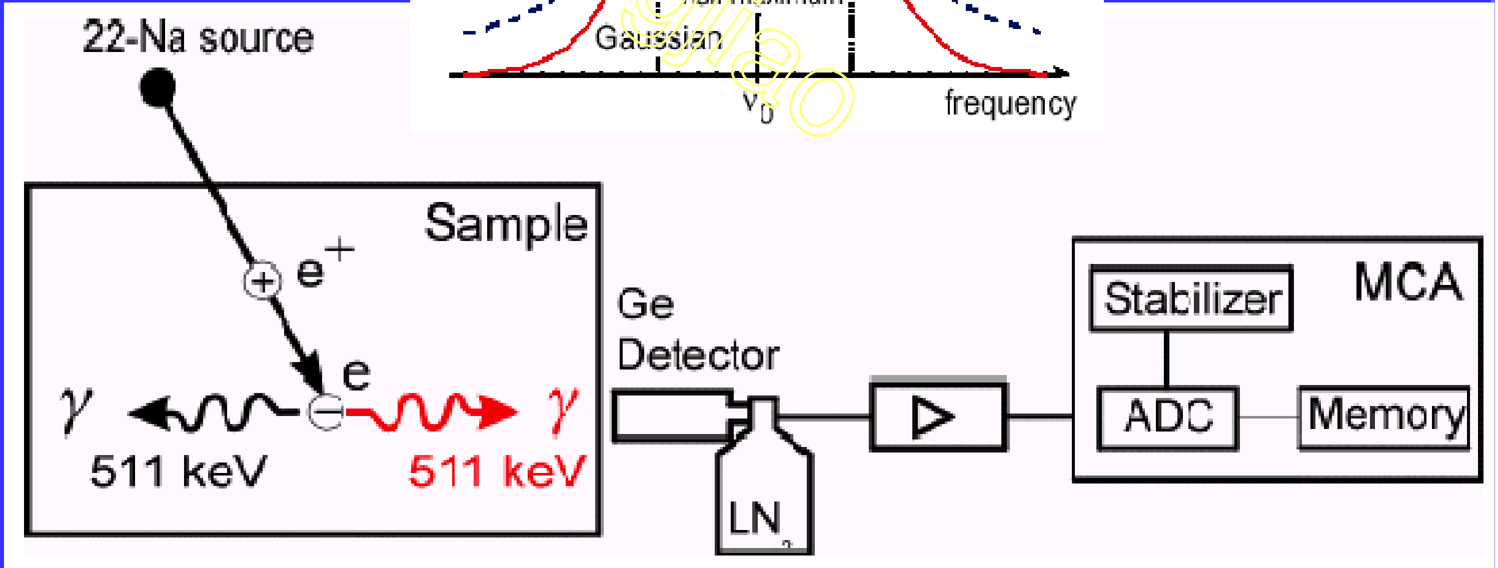

22-Na source
Sample
e^+
e
γ
511 keV
γ
511 keV
Ge
Detector
LN_2
MCA
Stabilizer
ADC
Memory

- Doppler effect
  - electron momentum in propagation direction of 511 keV γ-ray leads to Doppler broadening of annihilation line

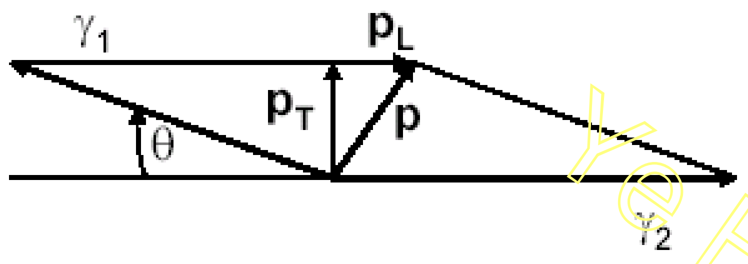

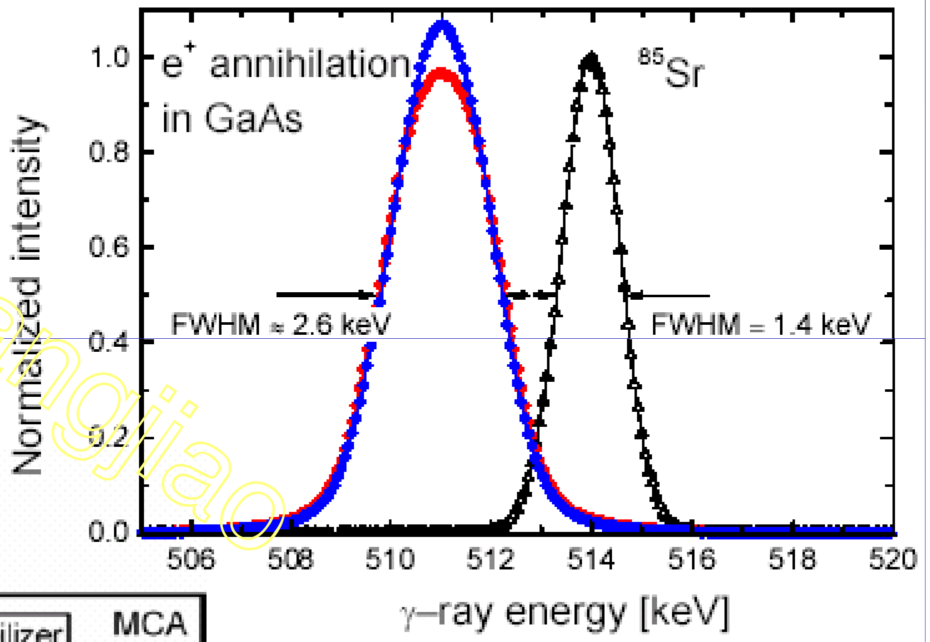

- Technique

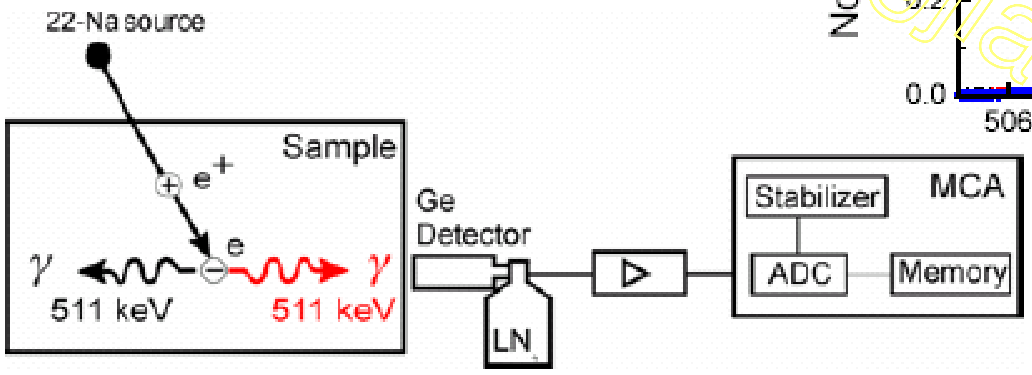

$$E_1 - E_2 = p_L c$$

E_1, E_2 – energy of γ quanta

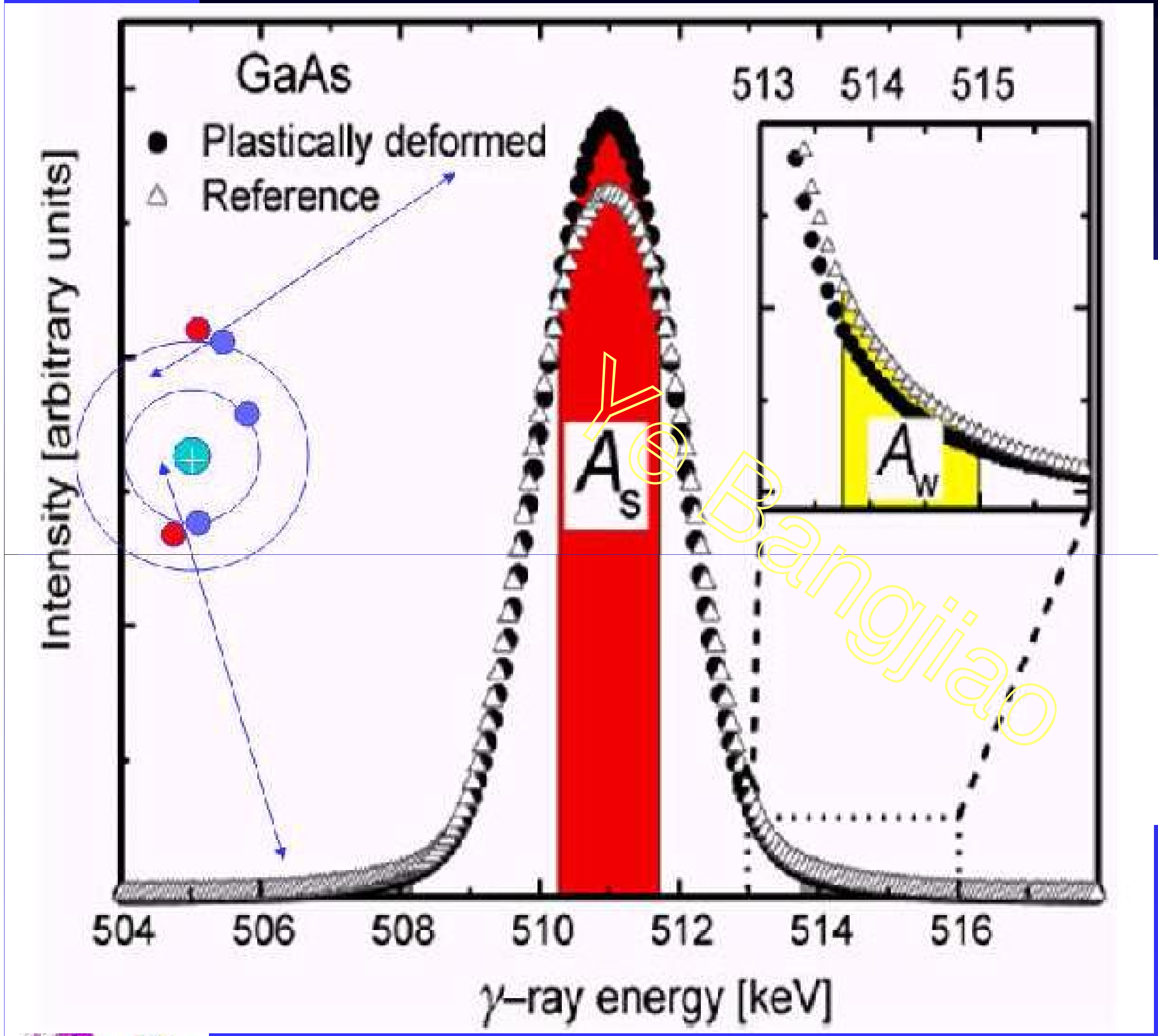

Data Treatment

Line Parameters

- "Shape" parameter

$$S = \frac{A_s}{A_0},\quad A_s = \int_{E_0-E_s}^{E_0+E_s} N_D\, dE$$

- "Wing" parameter

$$W = \frac{A_w}{A_0},\quad A_w = \int_{E_1}^{E_2} N_D\, dE$$

Doppler coincidence spectroscopy

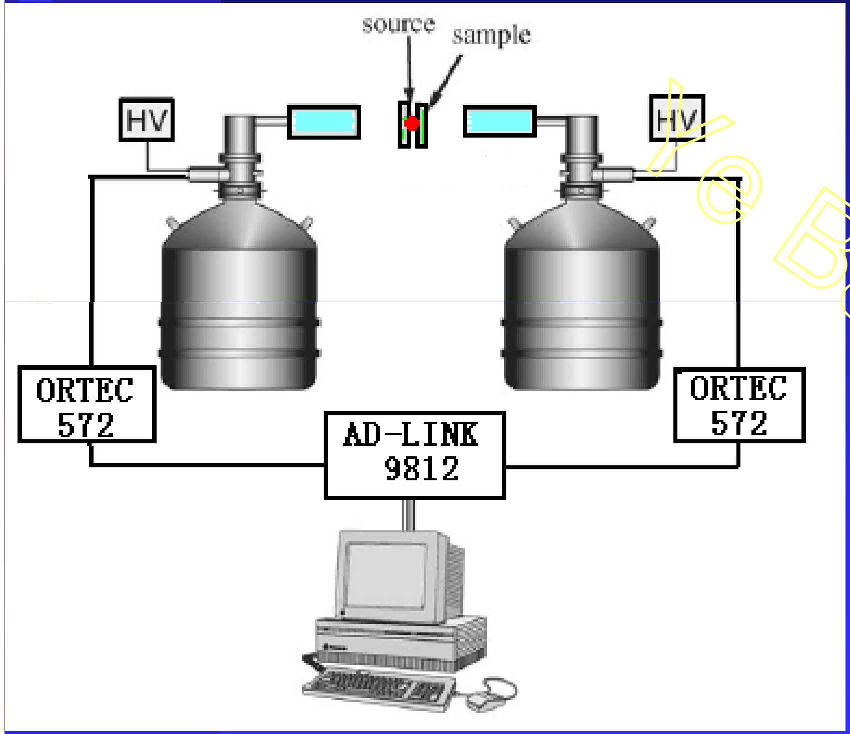

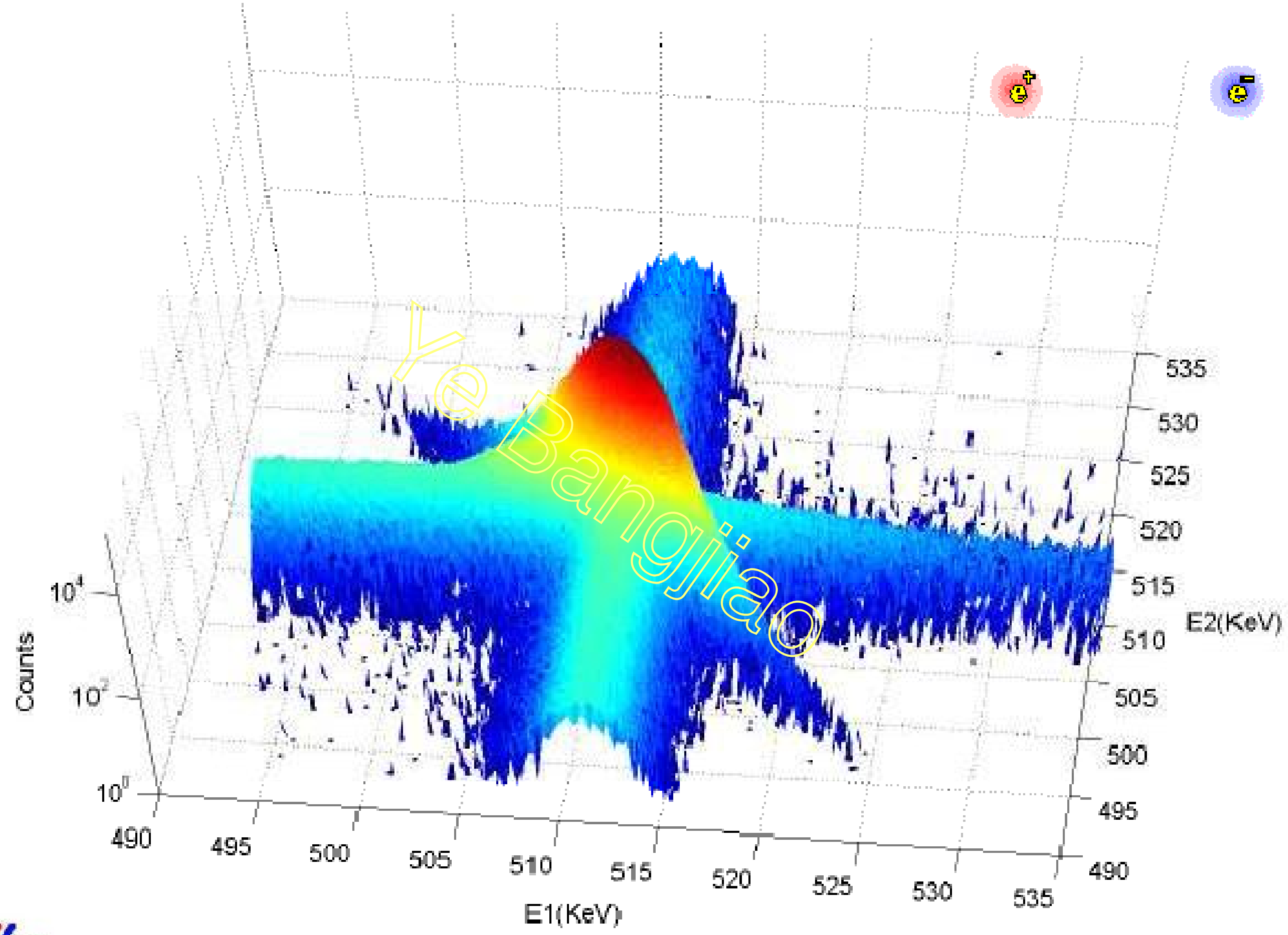
e+
e−
Counts
10^4
10^2
10^0
490
495
500
505
510
515
520
525
530
535
E1(KeV)
535
530
525
520
515
510
505
500
495
490
E2(KeV)

Doppler coincidence spectroscopy

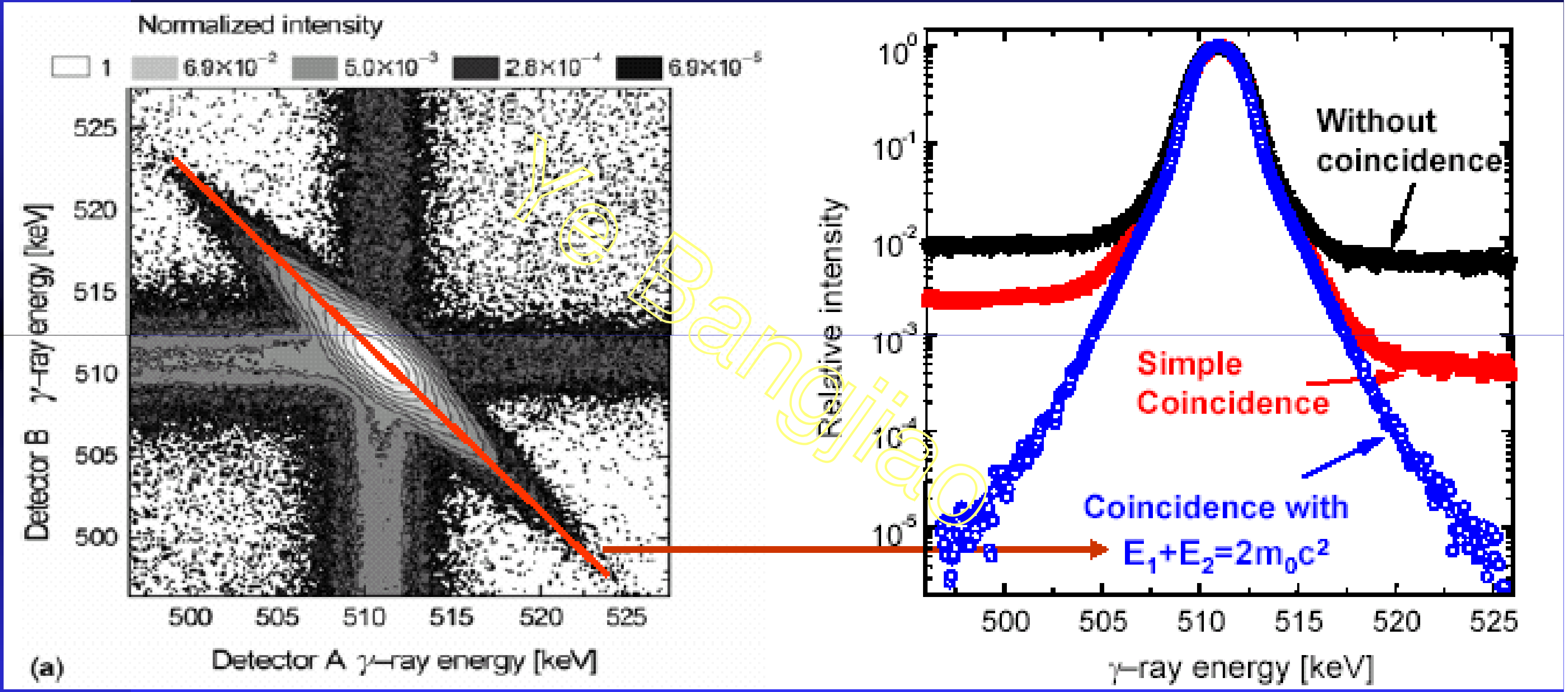

提高峰底比~10^5

- chemical sensitivity of energy spectra

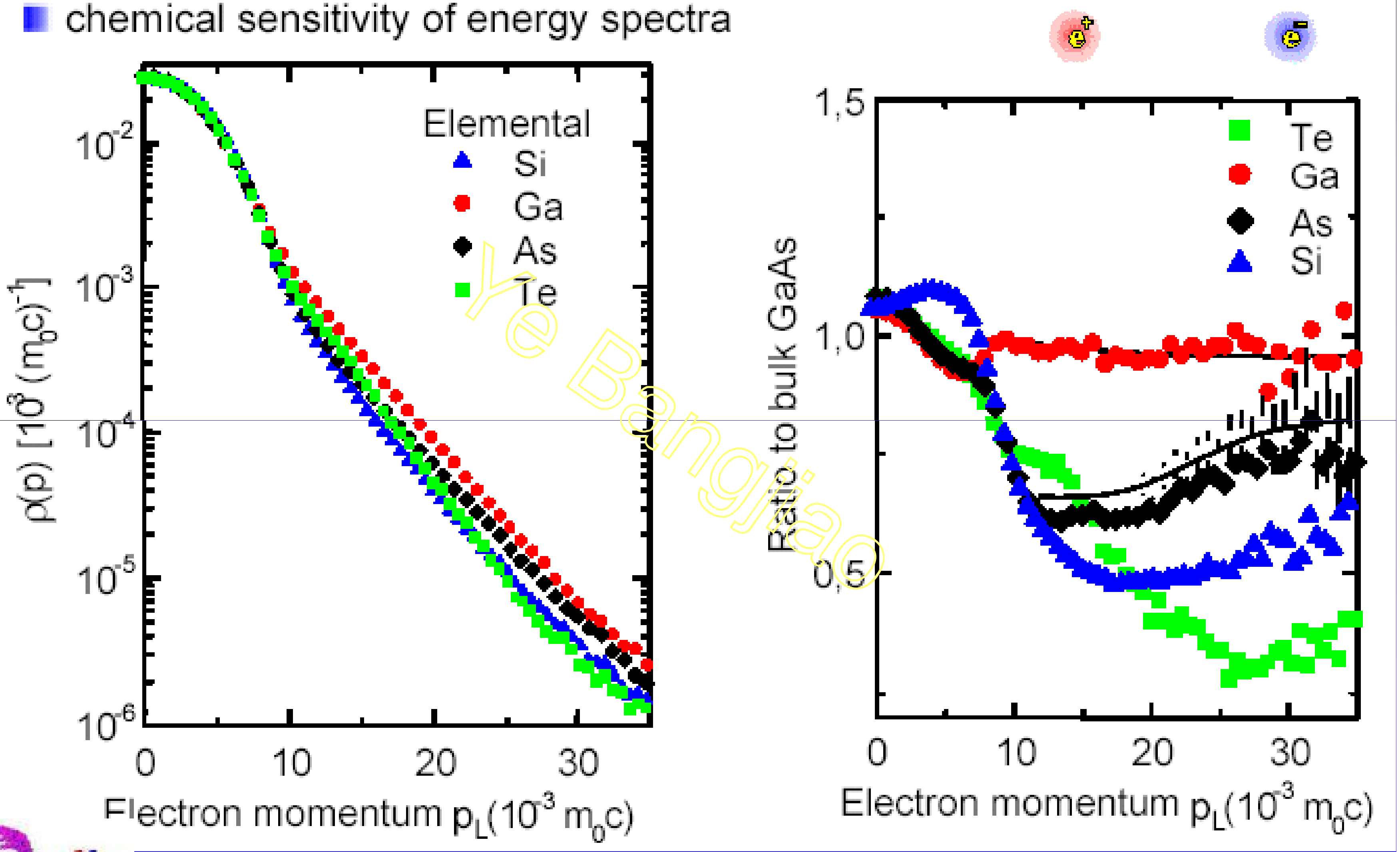

元素的“指纹鉴别”

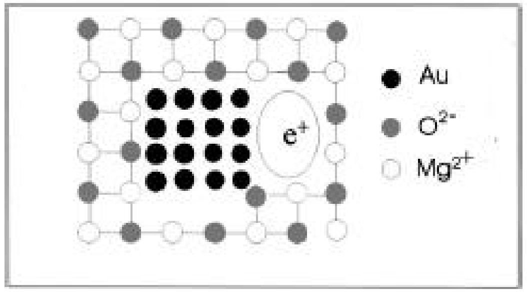
Au
O^{2-}
Mg^{2+}
e^+

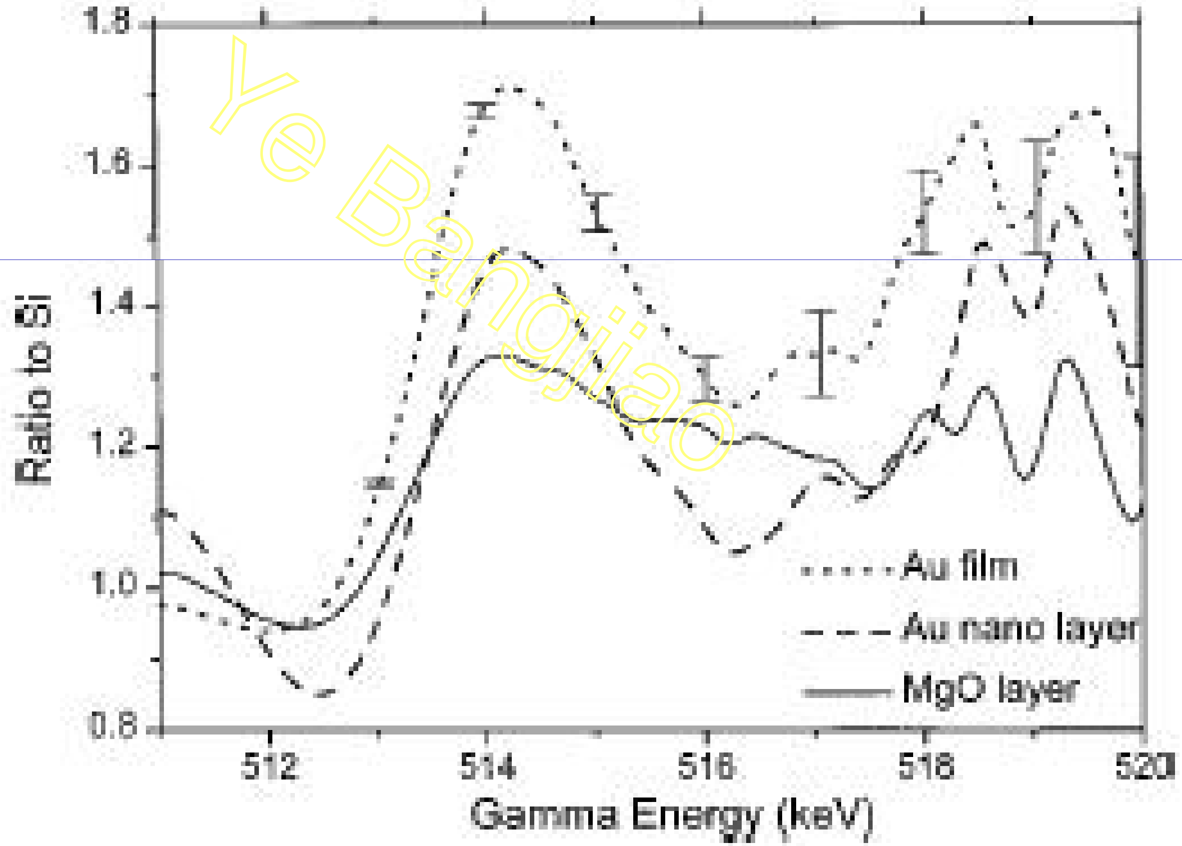
1.8
1.6
1.4
1.2
1.0
0.8
Ratio to Si
512
514
516
518
520
Gamma Energy (keV)
Au film
Au nano layer
MgO layer

	比例	亲和势(eV)	湮灭比例
AlMgCr	97.25/2.5/0.25	-4.41/-6.18/-2.62	69.6/29.8/0.6

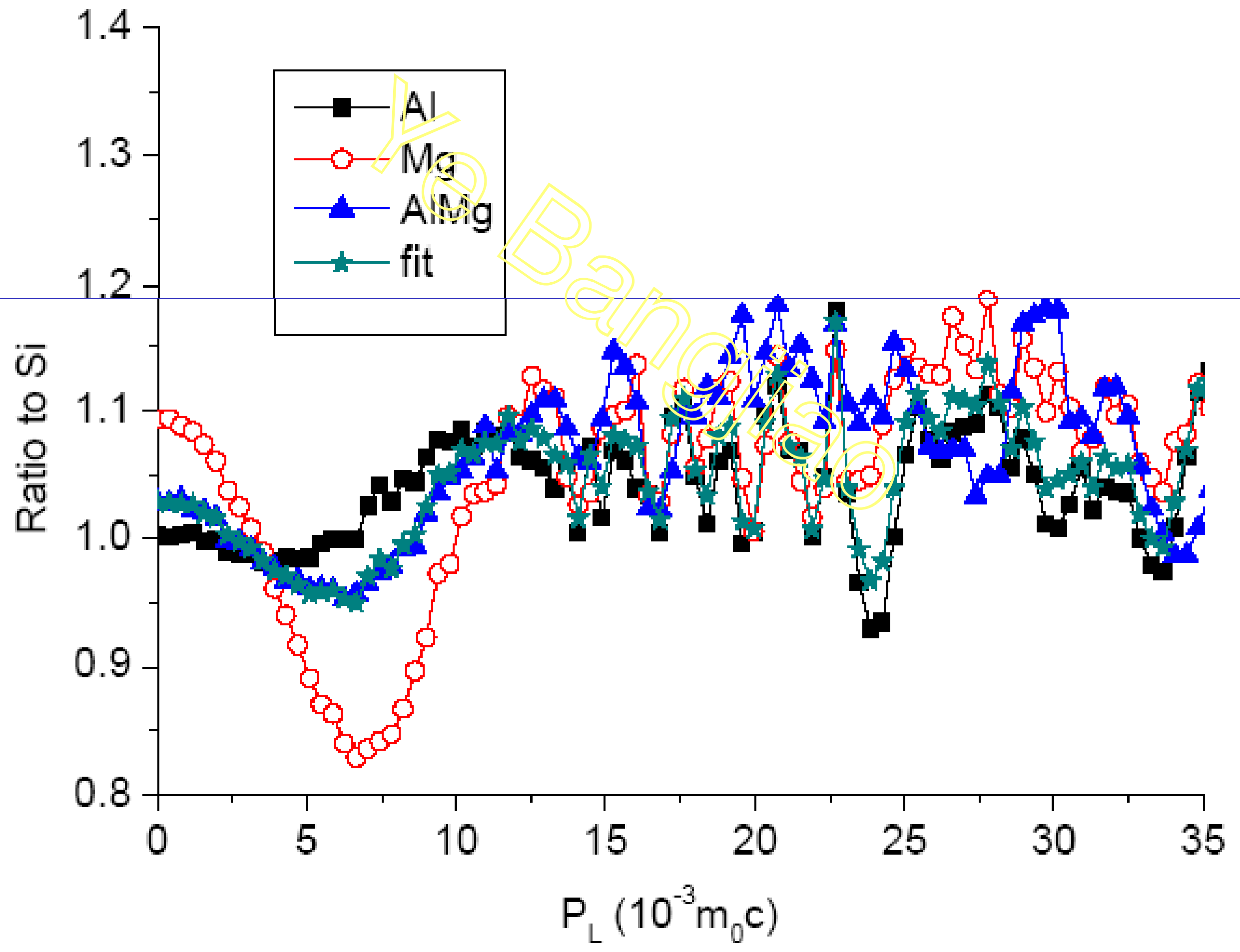

第四周期元素：

Ti: [Ar]$3d^24s^2$

V: [Ar]$3d^34s^2$

Cr: [Ar]$3d^44s^2$

Fe: [Ar]$3d^64s^2$

Co: [Ar]$3d^74s^2$

Ni: [Ar]$3d^84s^2$

Cu: [Ar]$3d^{10}4s^1$

Zn: [Ar]$3d^{10}4s^2$

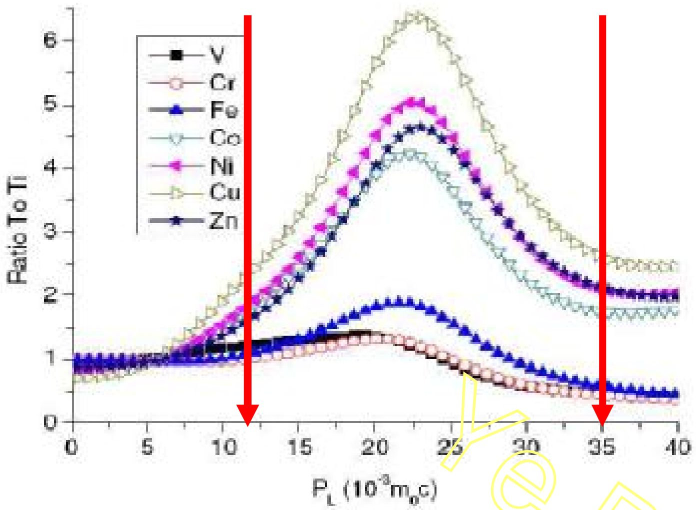

(c) Ti,V,Cr,Fe,Co,Ni,Cu,Zn理论计算结果

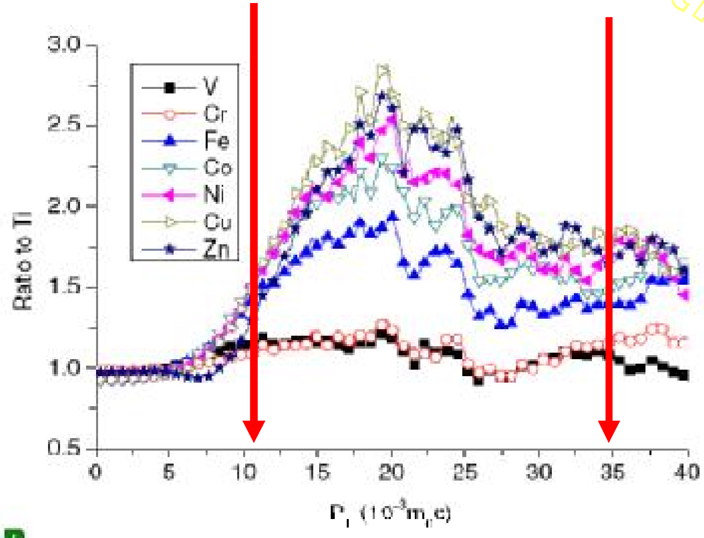

(d) Ti,V,Cr,Fe,Co,Ni,Cu,Zn实验结果

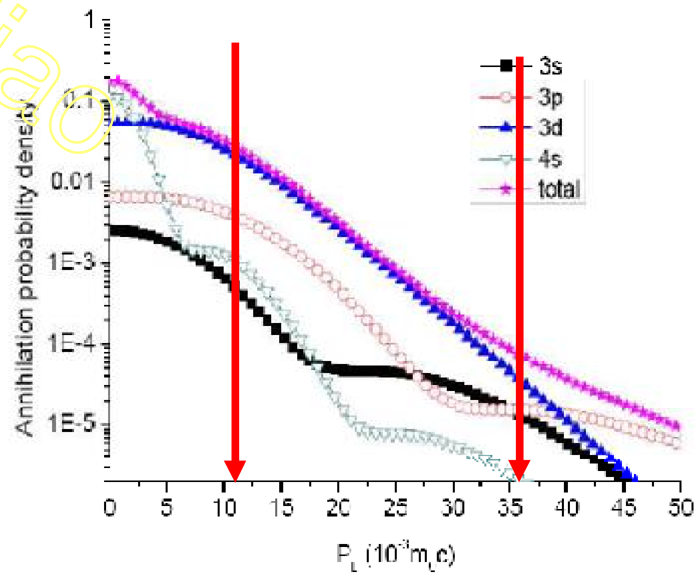

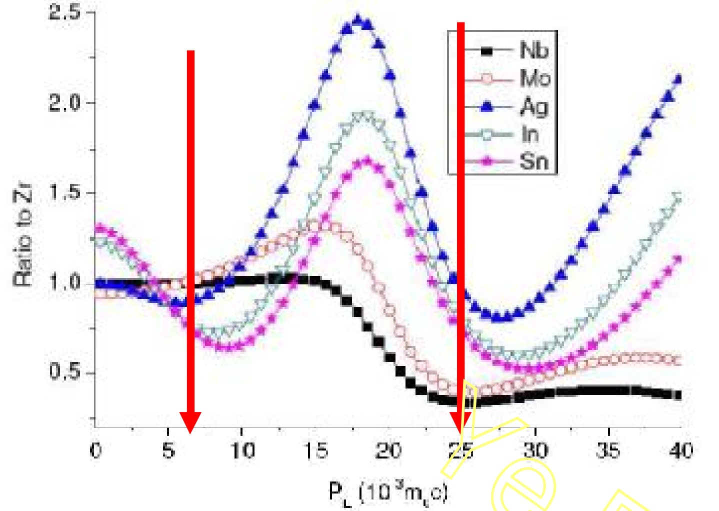

(c) Zr,Nb,Mo,Ag,In,Sn理论计算结果

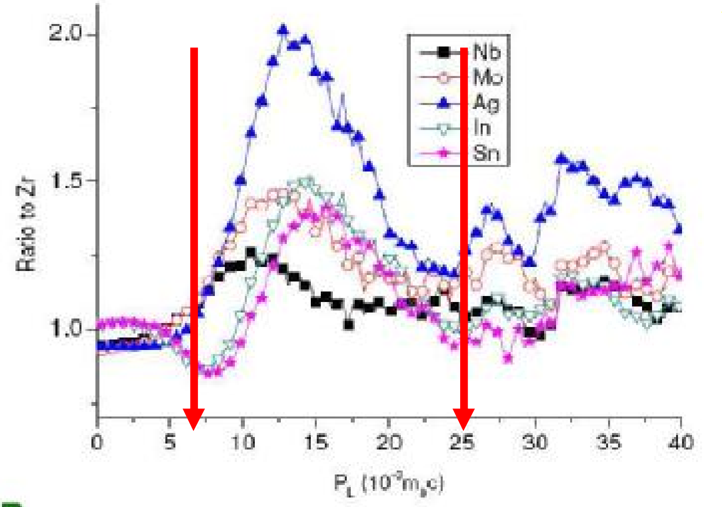

(f) Zr,Nb,Mo,Ag,In,Sn实验结果

第五周期元素：

Zr: [Kr]$4d^{2}5s^{2}$

Nb: [Kr]$4d^{4}5s^{1}$

Mo: [Kr]$4d^{5}5s^{1}$

Ag: [Kr]$4d^{10}5s^{1}$

In: [Kr]$4d^{10}5s^{2}5p^{1}$

Sn: [Kr]$4d^{10}5s^{2}5p^{2}$

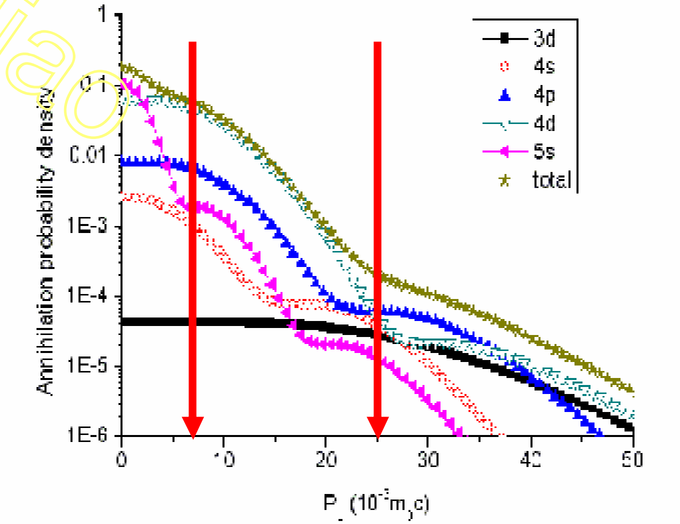

第六周期元素：

Hf: [Xe]$4f^{14}5d^{2}6s^{2}$
Ta: [Xe]$4f^{14}5d^{3}6s^{2}$
W: [Xe]$4f^{14}5d^{4}6s^{2}$
Pb: [Xe]$4f^{14}5d^{10}6s^{2}6p^{2}$

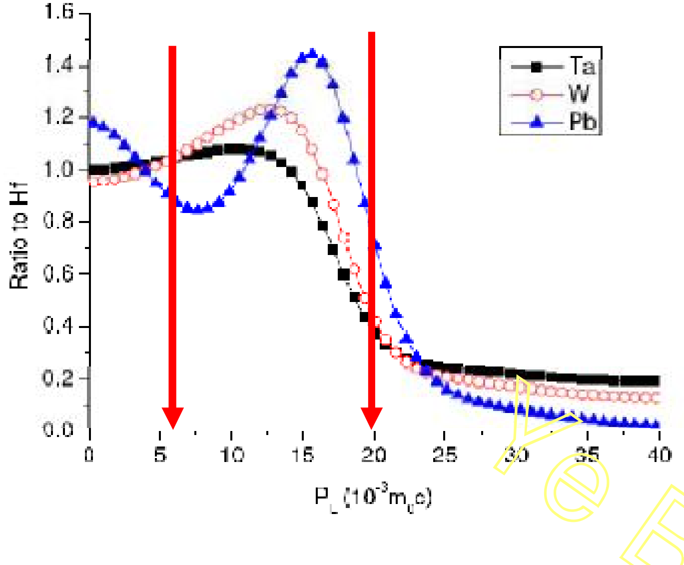

(g) Hf,Ta,W,Pb理论计算结果

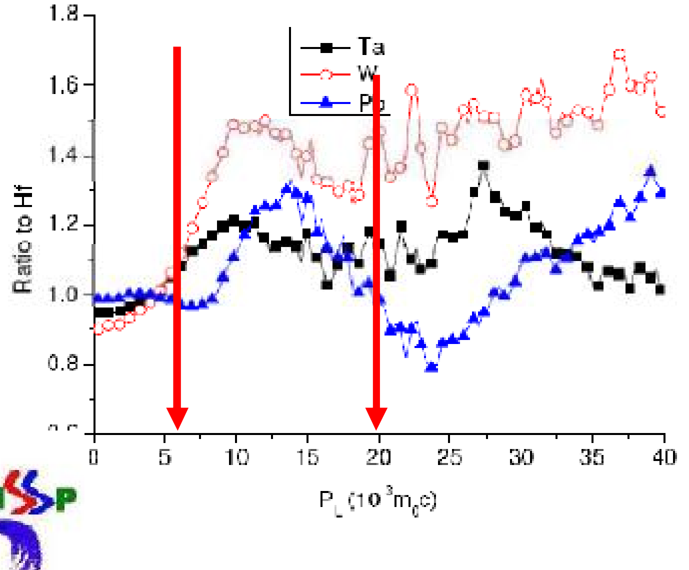

(h) Hf,Ta,W,Pb实验结果

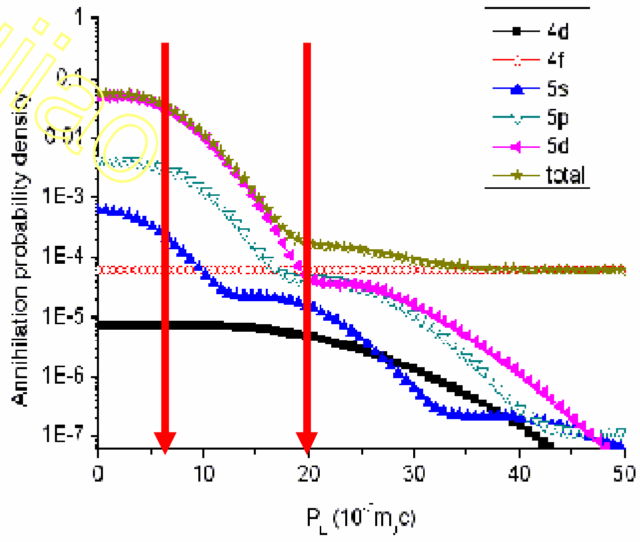

MgAl合金和不锈钢

样品	纯度	尺寸/mm	拟合系数		
			a	b	c
AlMg合金	Al:Mg:Cr=97.25:2.5:0.25	10 × 10 × 0.79	69.6	29.8	0.6
不锈钢	Fe:Cr:Ni=70:19:11	10 × 10 × 0.5	37.5	0.1	60.4

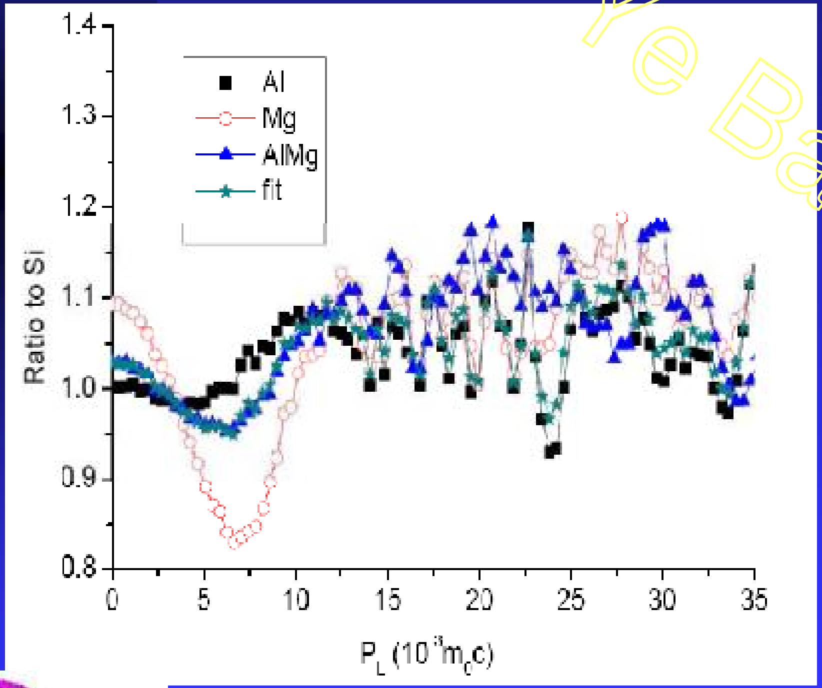

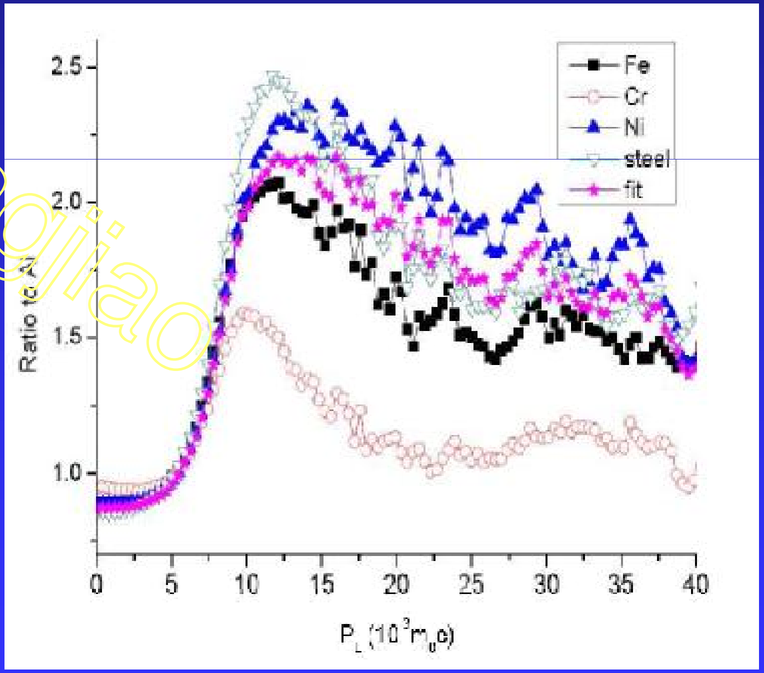

将合金谱拟合成各组分谱的加权和，见下式：

$$S_{alloy} = a \times S_{Al} + b \times S_{Mg} + c \times S_{Cr}$$

样品	纯度	尺寸/mm	拟合系数		
			a	b	c
AlMg合金	Al:Mg:Cr=97.25:2.5:0.25	10 × 10 × 0.79	69.6	29.8	0.6
不锈钢	Fe:Cr:Ni=70:19:11	10 × 10 × 0.5	37.5	0.1	60.4

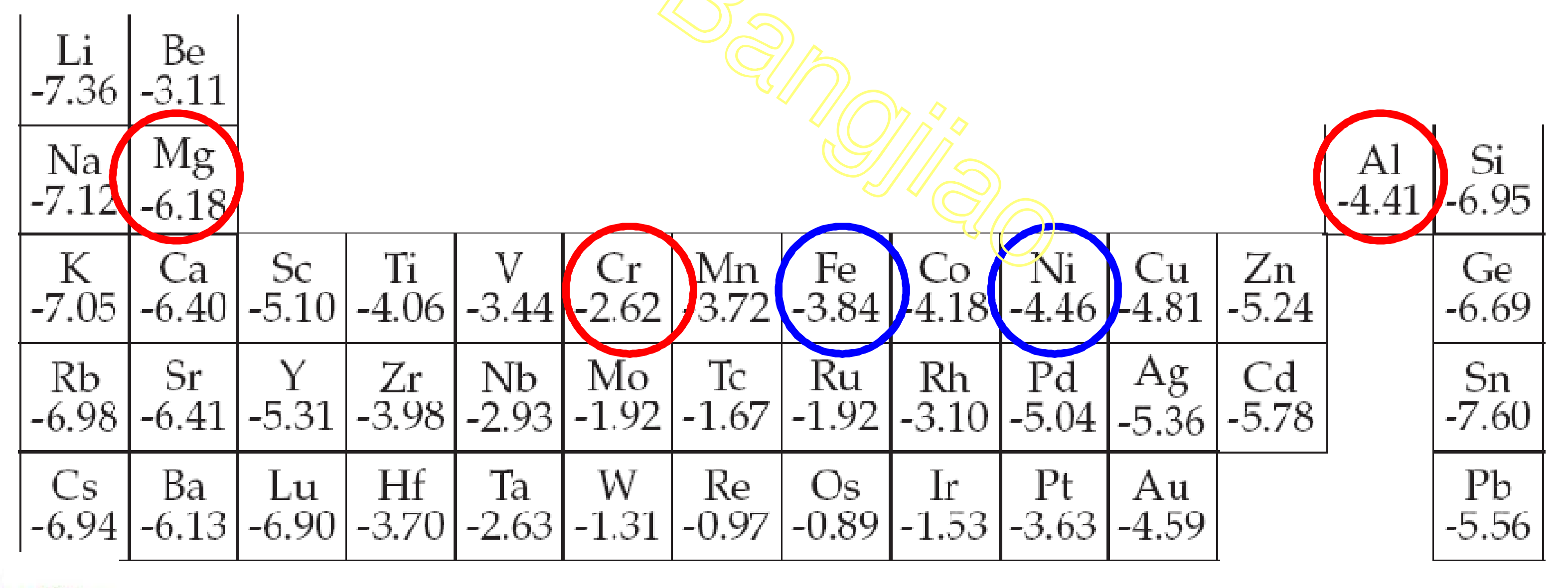

Li -7.36	Be -3.11												
Na -7.12	Mg -6.18											Al -4.41	Si -6.95
K -7.05	Ca -6.40	Sc -5.10	Ti -4.06	V -3.44	Cr -2.62	Mn -3.72	Fe -3.84	Co -4.18	Ni -4.46	Cu -4.81	Zn -5.24		Ge -6.69
Rb -6.98	Sr -6.41	Y -5.31	Zr -3.98	Nb -2.93	Mo -1.92	Tc -1.67	Ru -1.92	Rh -3.10	Pd -5.04	Ag -5.36	Cd -5.78		Sn -7.60
Cs -6.94	Ba -6.13	Lu -6.90	Hf -3.70	Ta -2.63	W -1.31	Re -0.97	Os -0.89	Ir -1.53	Pt -3.63	Au -4.59			Pb -5.56

正电子看到的元素比例 = $f(A_+) \times$ 合金中元素的质量百分比

●二维角关联

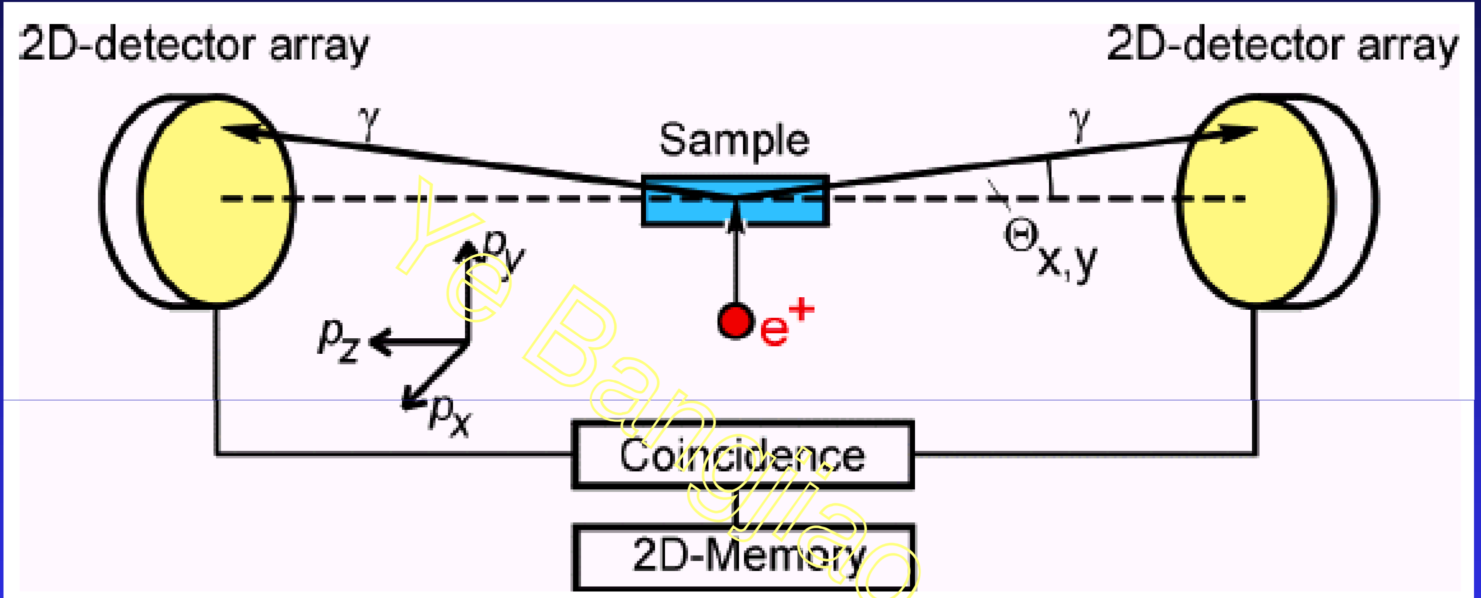

Coincidence counting rate N_c:

$$N_c(\Theta_x,\Theta_y) = A_c \int \sigma(\Theta_x m_0 c,\ \Theta_y m_0 c,\ p_z)\,dp_z$$

$$\Theta_{x,y} = p_{x,y}/m_o c$$

Resolution: 0.2~5mrad (0.05~1.2keV)

- e+e-湮没产生的2γ的夹角与180° 有一微小的偏离。实验同时测量e+e-湮没产生的2γ关联信号，可以获得电子动量分布信息，并且可进一步得到费米面形貌，研究能带结构等。
- 同CDB相似, 二维角关联（2D-ACAR）可以由e+-e-湮灭的动量分布来获得电子结构的信息，特别对单晶材料。

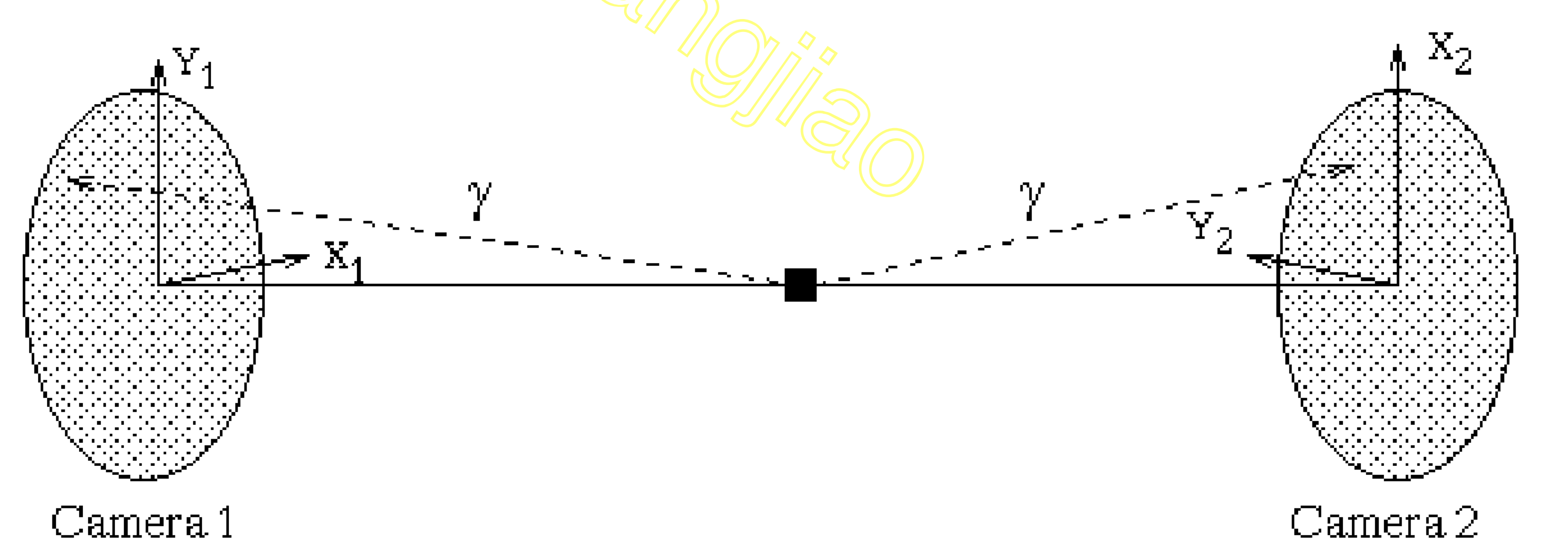

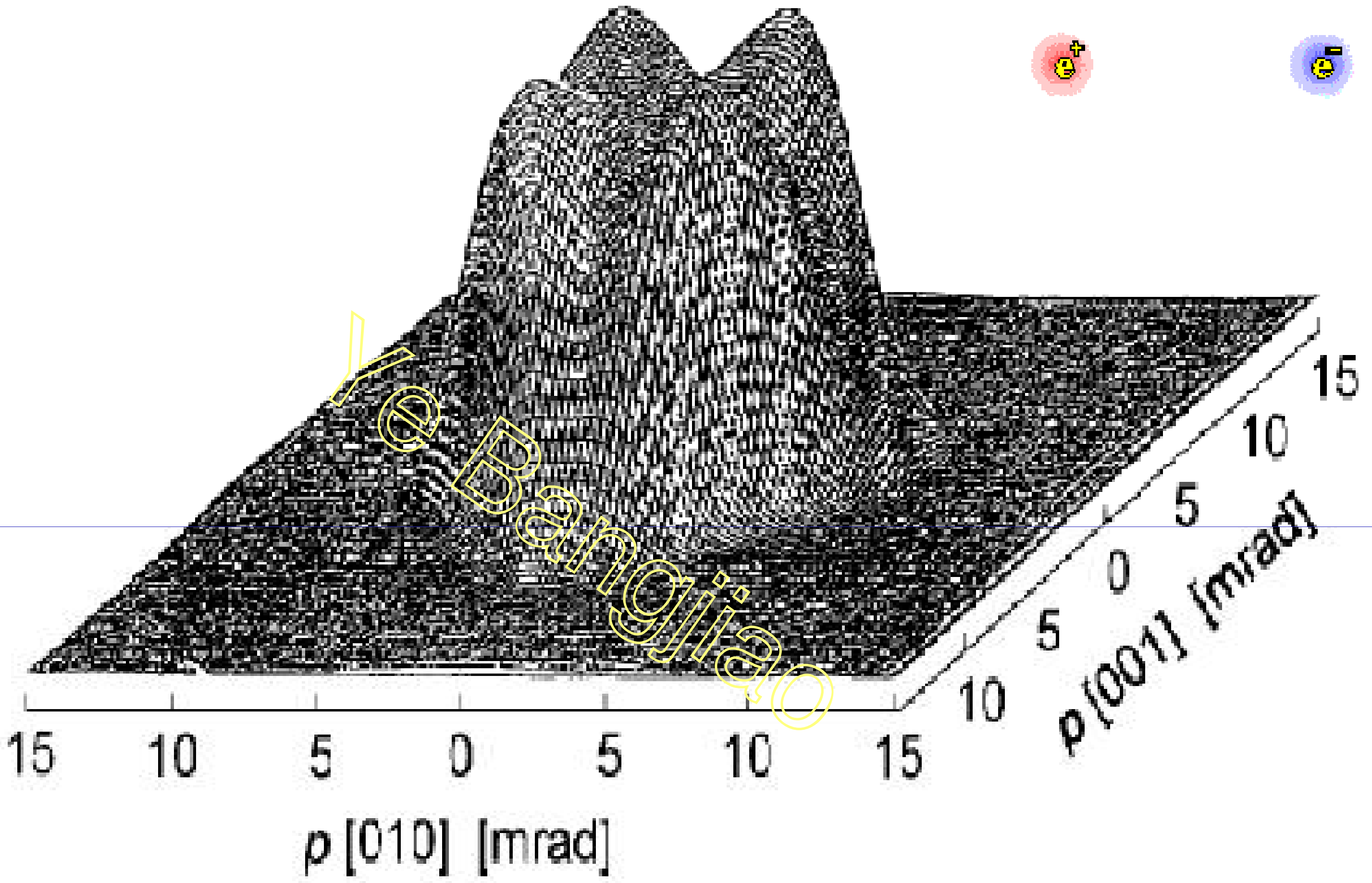

(Tanigawa et al., 1995) 3D-Fermi surface can be reconstructed from measurements in several directions of a single crystal

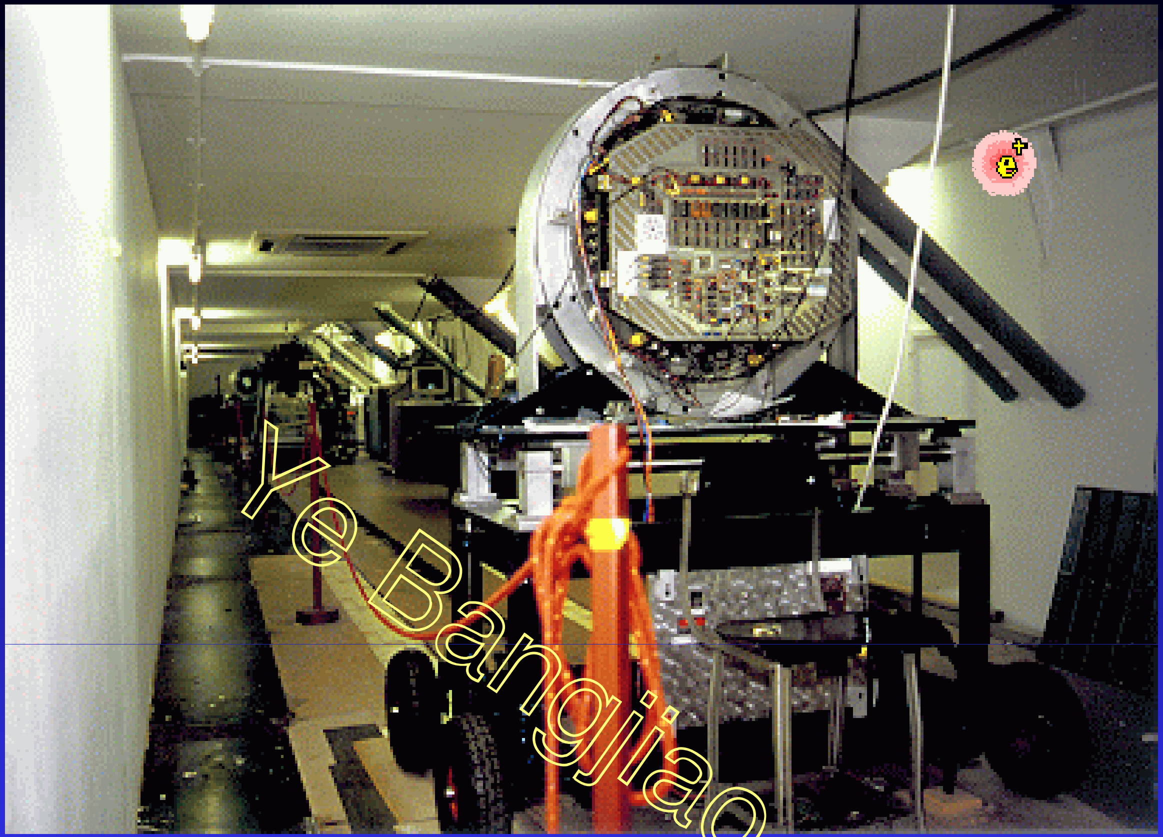

The ‘long laboratory’

- A 2D-ACAR setup coupled to the intense ($8*10^7 e+/s$) monochromatic slow *e*+ beam POSH (POSitrons from the HOR reactor) is used for depth-selective research.

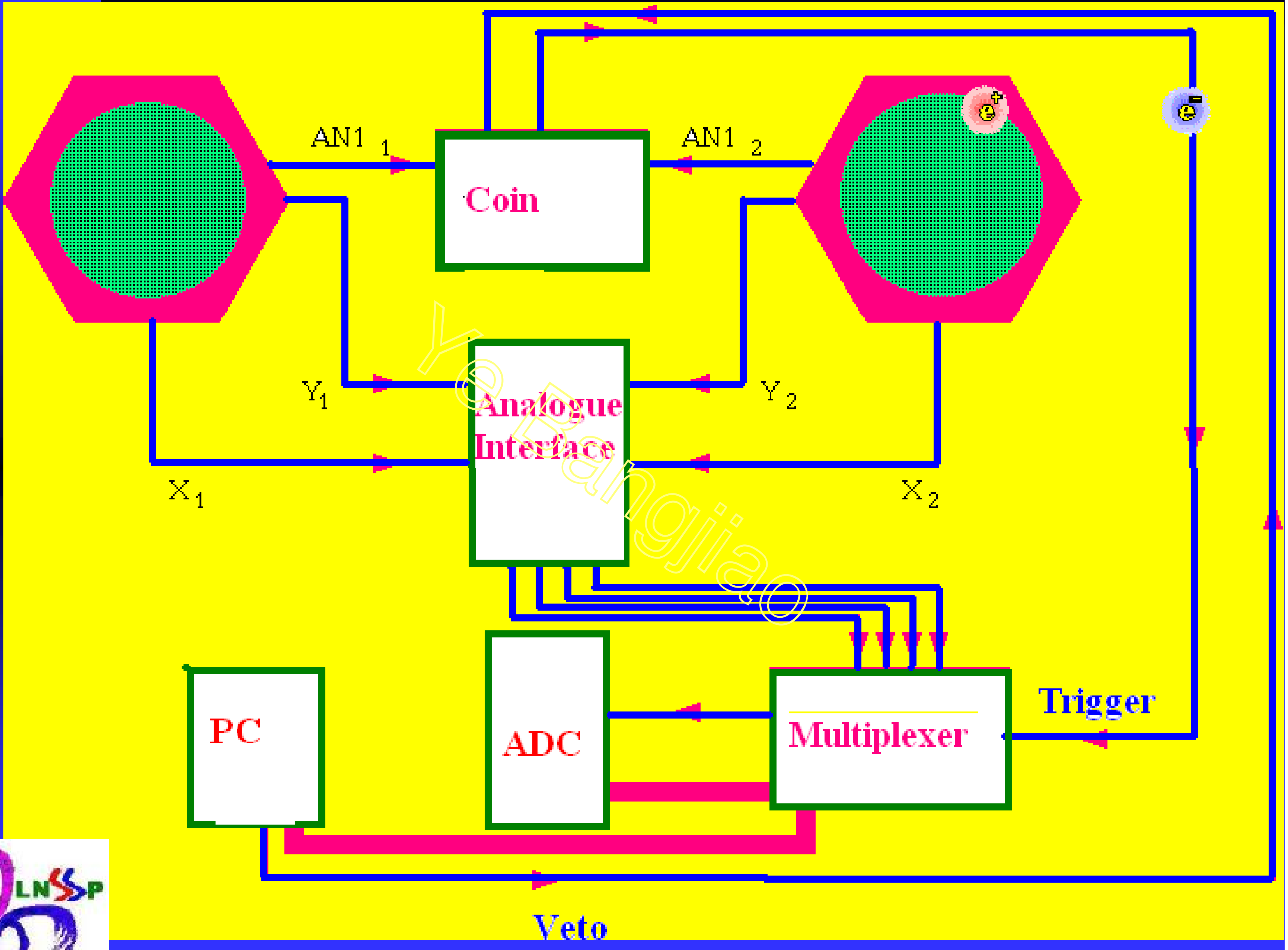

$AN1_1$

$AN1_2$

Coin

Y_1

Y_2

Analogue Interface

X_1

X_2

PC

ADC

Multiplexer

Trigger

Veto

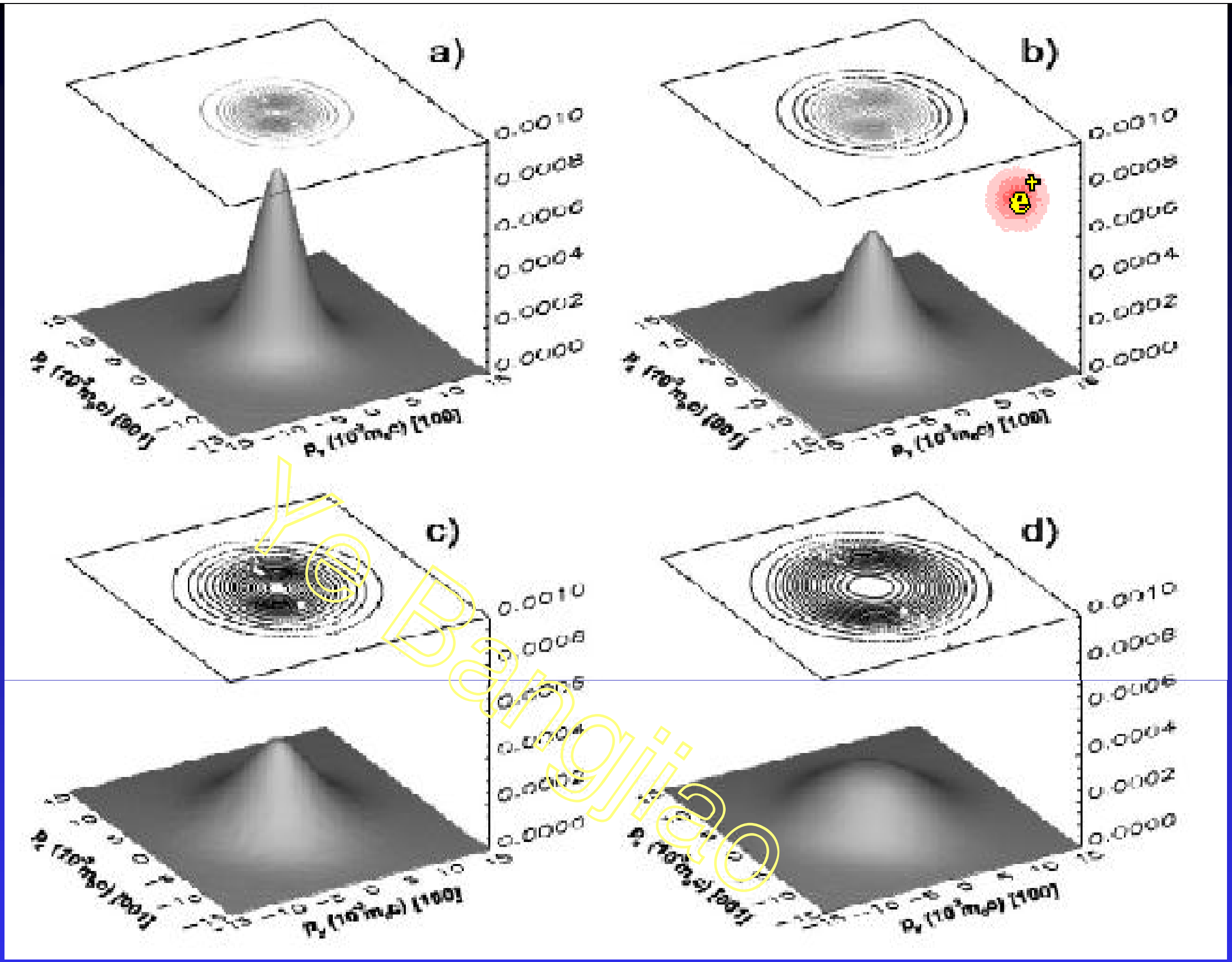

2D-ACAR distributions for Li implanted MgO(100) at positron energies of(a)4 keV, (b) 7.5 keV, and(c) 11.5 keV; (d) 2D-ACAR spectrum for bulk MgO(100). The distributions are normalized to equal total numbers of counts..

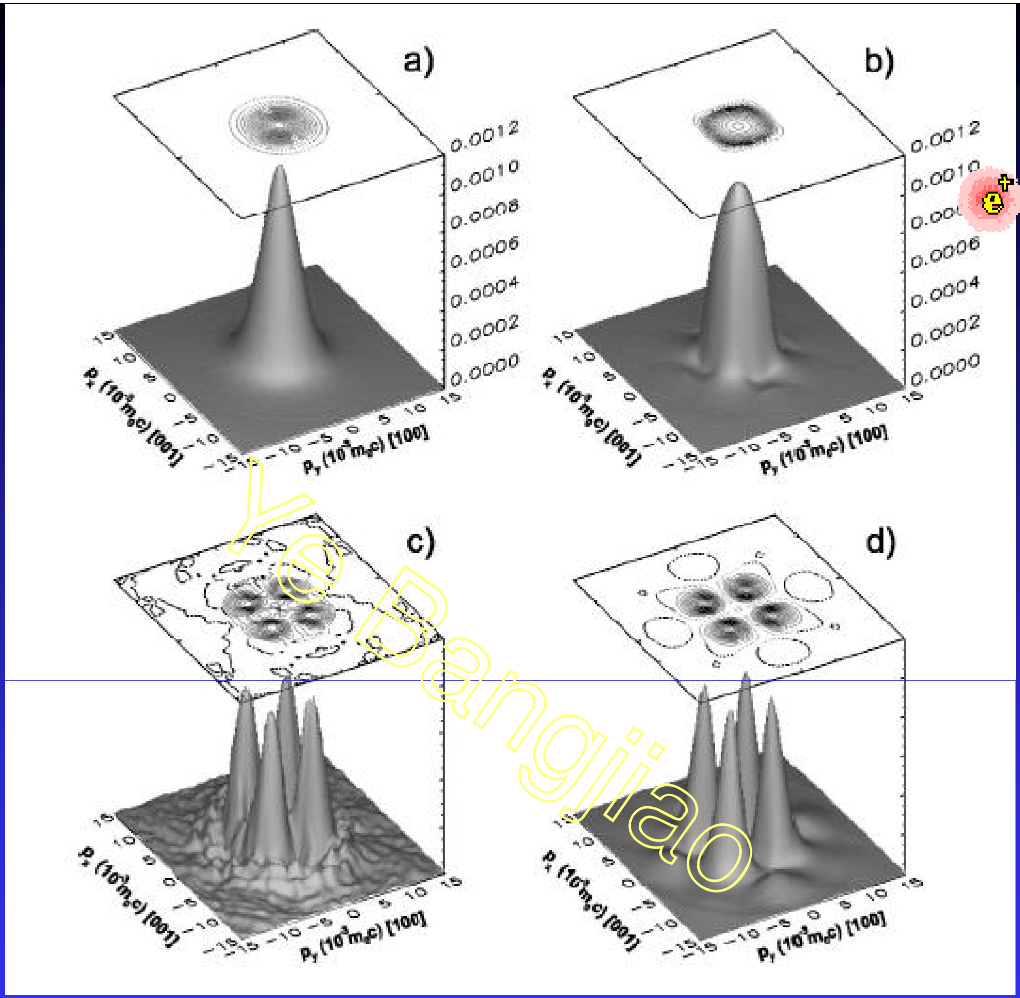

(a) Experimental 2D-ACAR distribution after subtracting the bulk MgO(100) contribution (43%); (b) theoretical spectrum of fcc Li(100); (c) and (d) anisotropies of the istributions in (a) and (b). The distributions are normalized ith respect to the total number of counts.

●寿命-动量关联

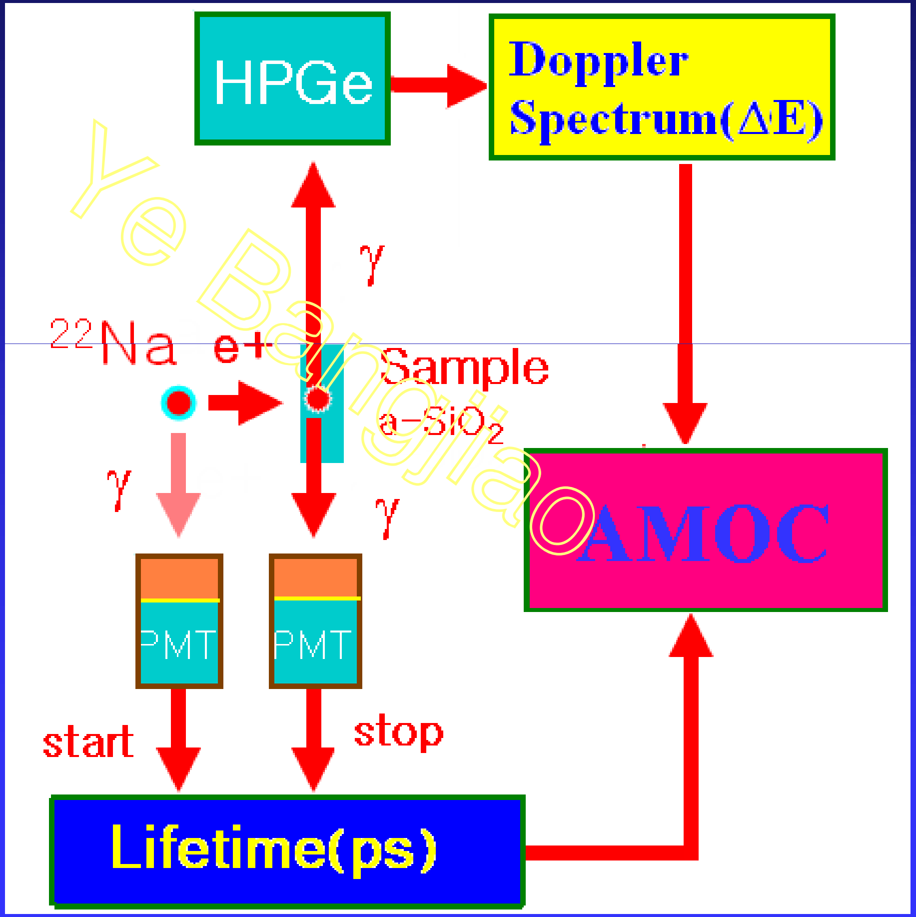
HPGe
Doppler Spectrum(ΔE)
γ
^{22}Na
e+
Sample
a-SiO$_2$
γ
γ
AMOC
PMT
PMT
start
stop
Lifetime(ps)

AMOC技术按测量寿命的起始触发信号分，主要有两种：

- 采用触发γ（1.28MeV）作起始信号，即所谓的AMOC-γγΔEγ技术；
- 采用正电子作起始信号，即AMOC-β^+γΔEγ技术。

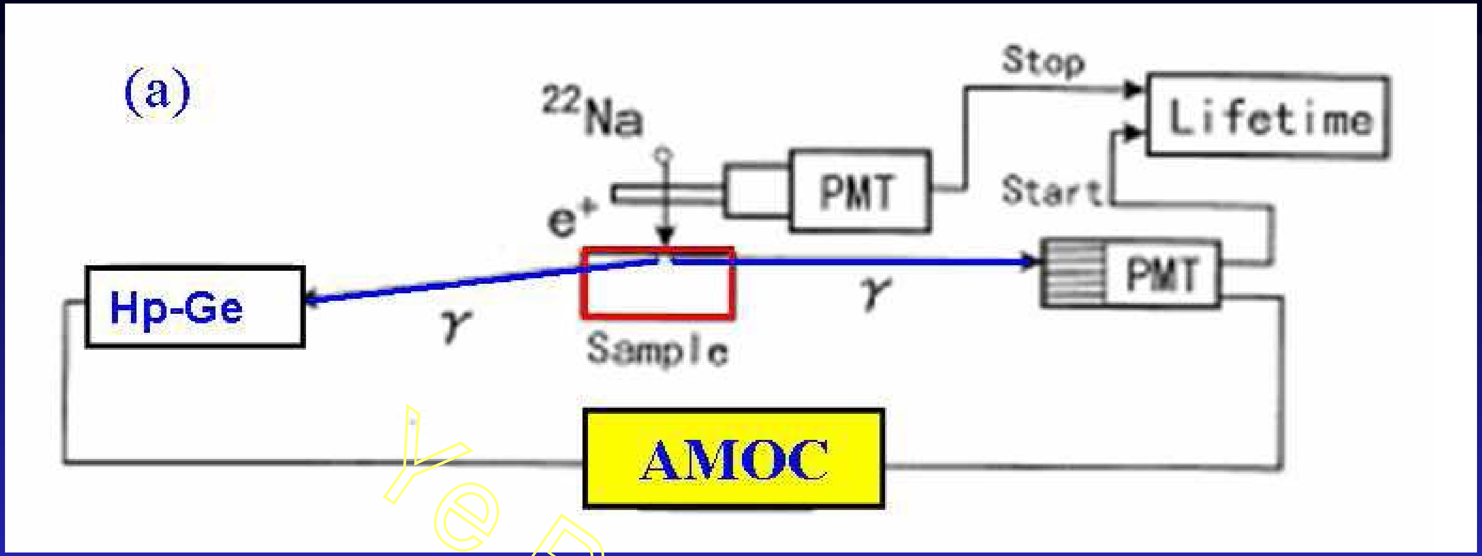
(a)
^{22}Na
e$^+$
PMT
Stop
Start
Lifetime
PMT
Hp-Ge
γ
γ
Sample
AMOC

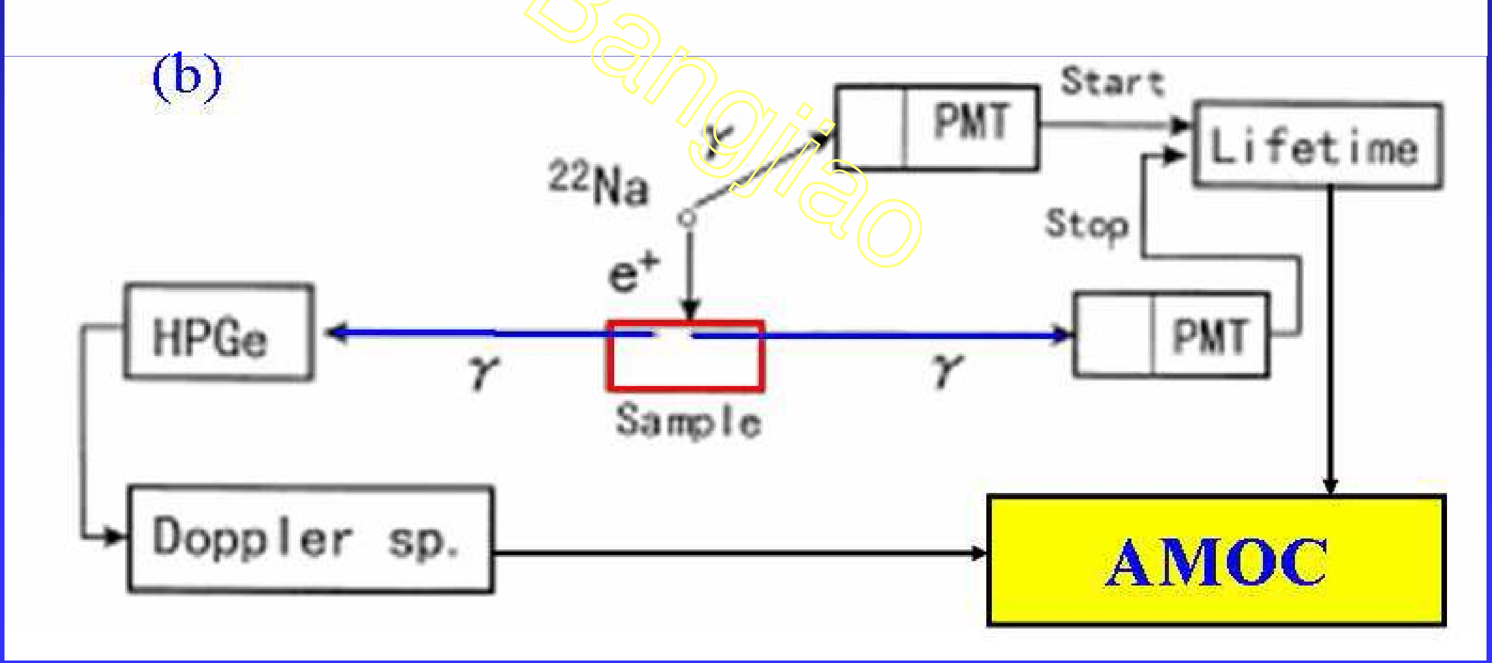
(b)
PMT
Start
Lifetime
^{22}Na
γ
e$^+$
Stop
HPGe
γ
γ
PMT
Sample
Doppler sp.
AMOC

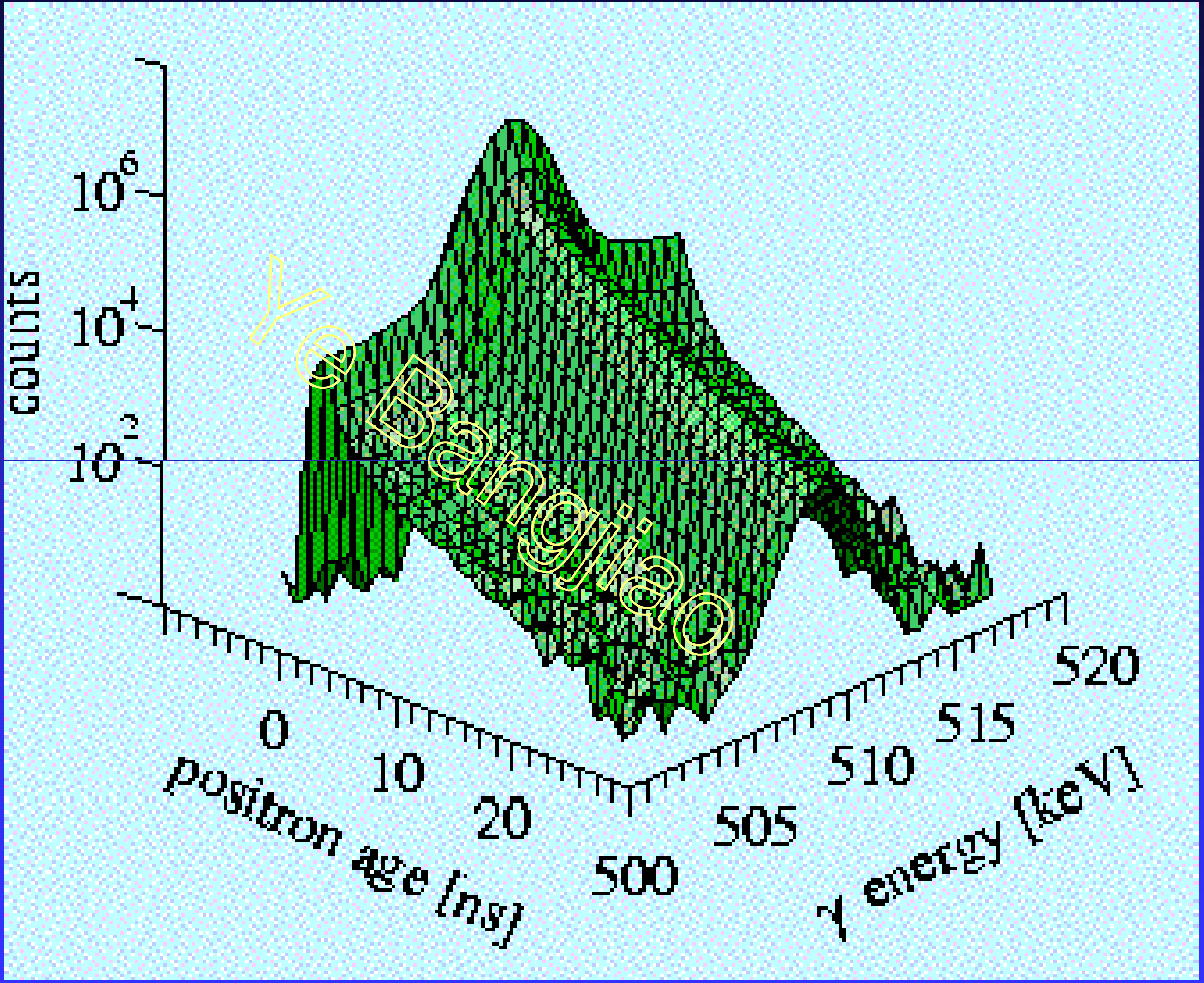
counts
10^6
10^4
10^2
0
10
20
positron age [ns]
500
505
510
515
520
γ energy [keV]

S_t分析

- AMOC二维谱是正电子湮灭时间和湮灭光子的多普勒展宽的关联。通常的正电子寿命谱可对所有正电子能谱积分得到，通常的多普勒展宽可对不同的寿命积分得到。
- 此外，还可以获得多普勒展宽的S参数随寿命的变化（即计算不同寿命下的S参数）称S_t线性函数：

$$S^t(t)=\frac{\int_{\pm\Delta p}N(p,t)dp}{\int N(p,t)dp}=\frac{\int_{\pm\Delta p}N(p,t)dp}{L(t)}$$

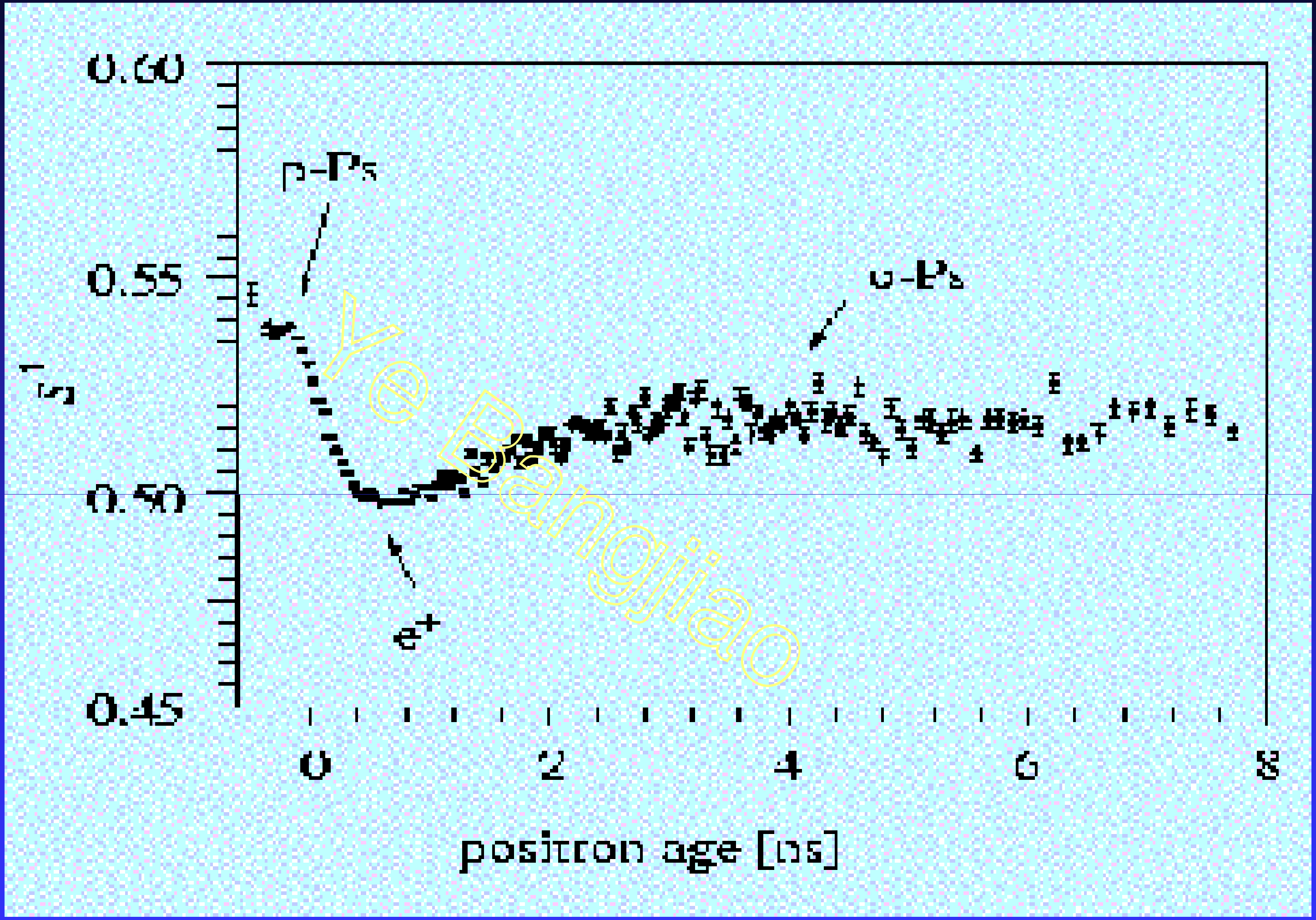
0.60
0.55
0.50
0.45
S
p-Ps
o-Ps
e+
0
2
4
6
8
positron age [ns]

Tsukuba分析

- 从AMOC二维谱中抽取正电子平均寿命随正电子的能量的变化称**Tsukuba**（筑波）分析

- 平均寿命是以**511keV**对称分布的，在**511keV**处是一个谷。

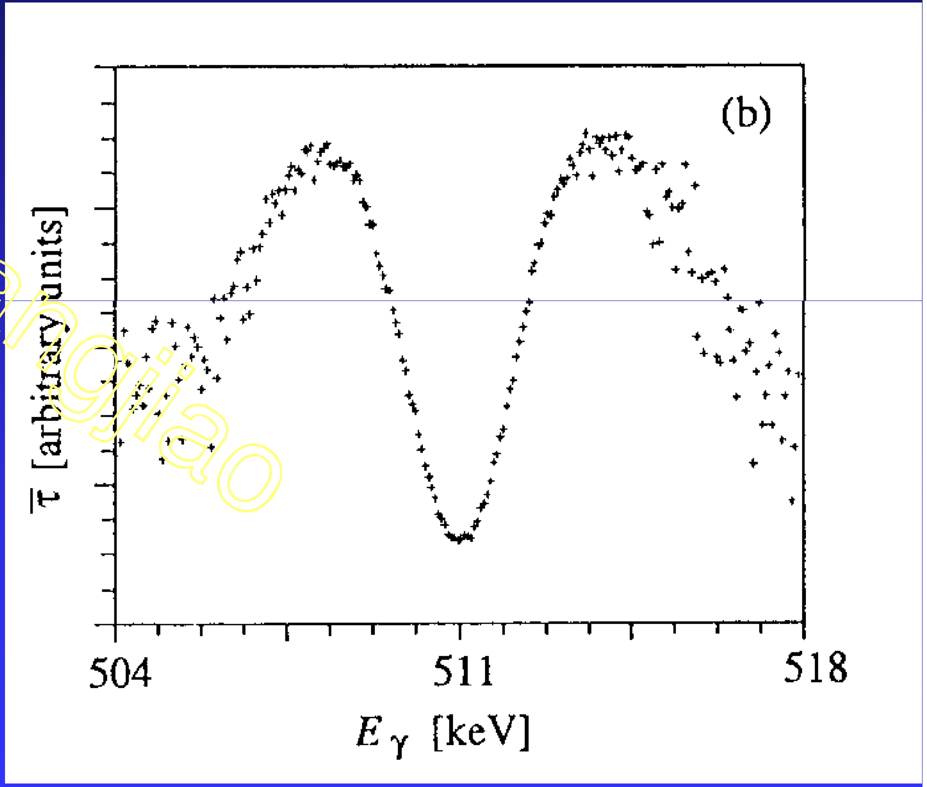

● 3γ measurement

$$N(3\gamma/2\gamma) = \frac{\sum_{341keV}^{490keV} N(E)}{\sum_{490keV}^{540keV} N(E)}$$

$$npPs = \sum_{510.25keV}^{511.75keV} N(E)$$

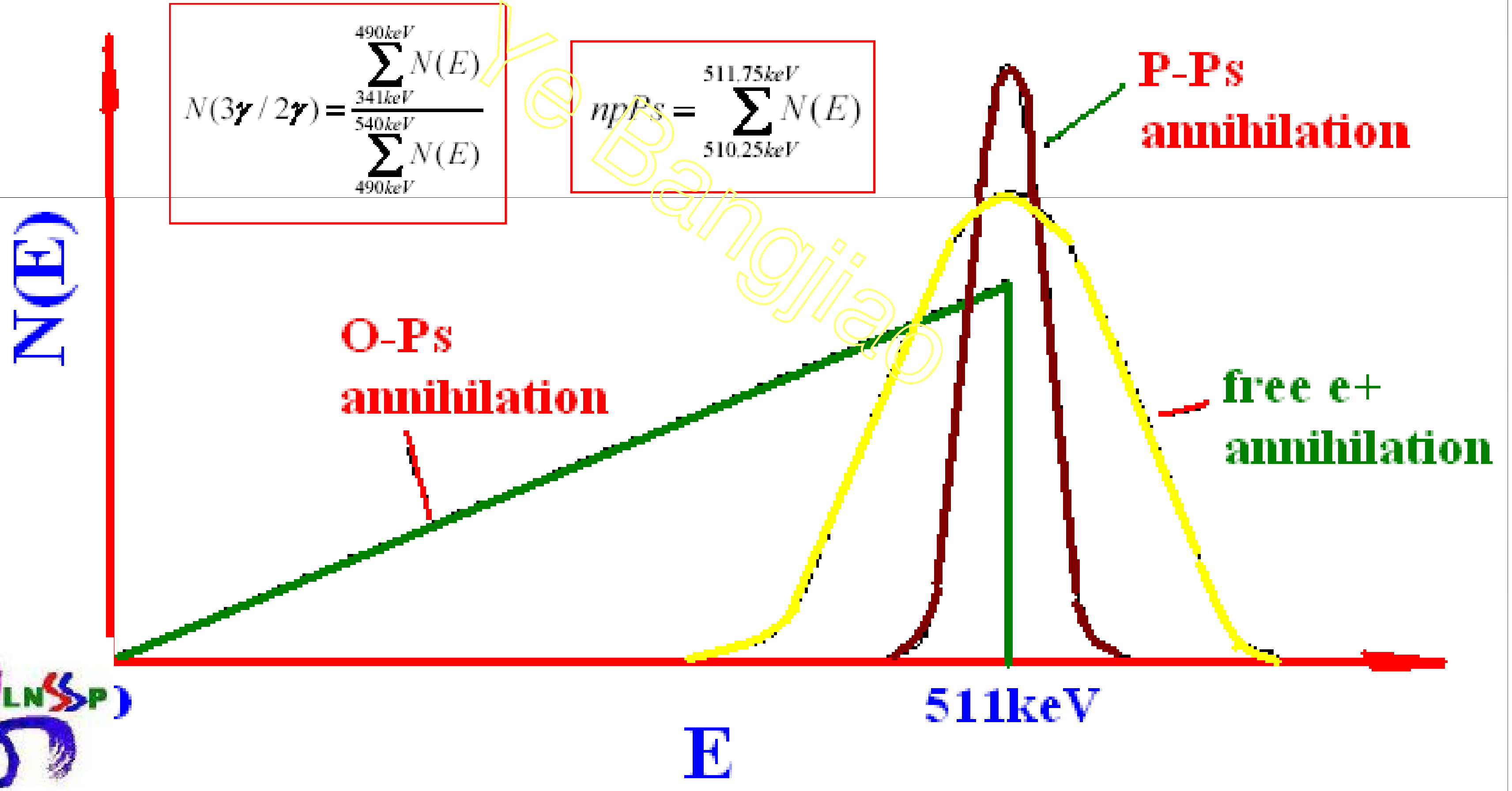

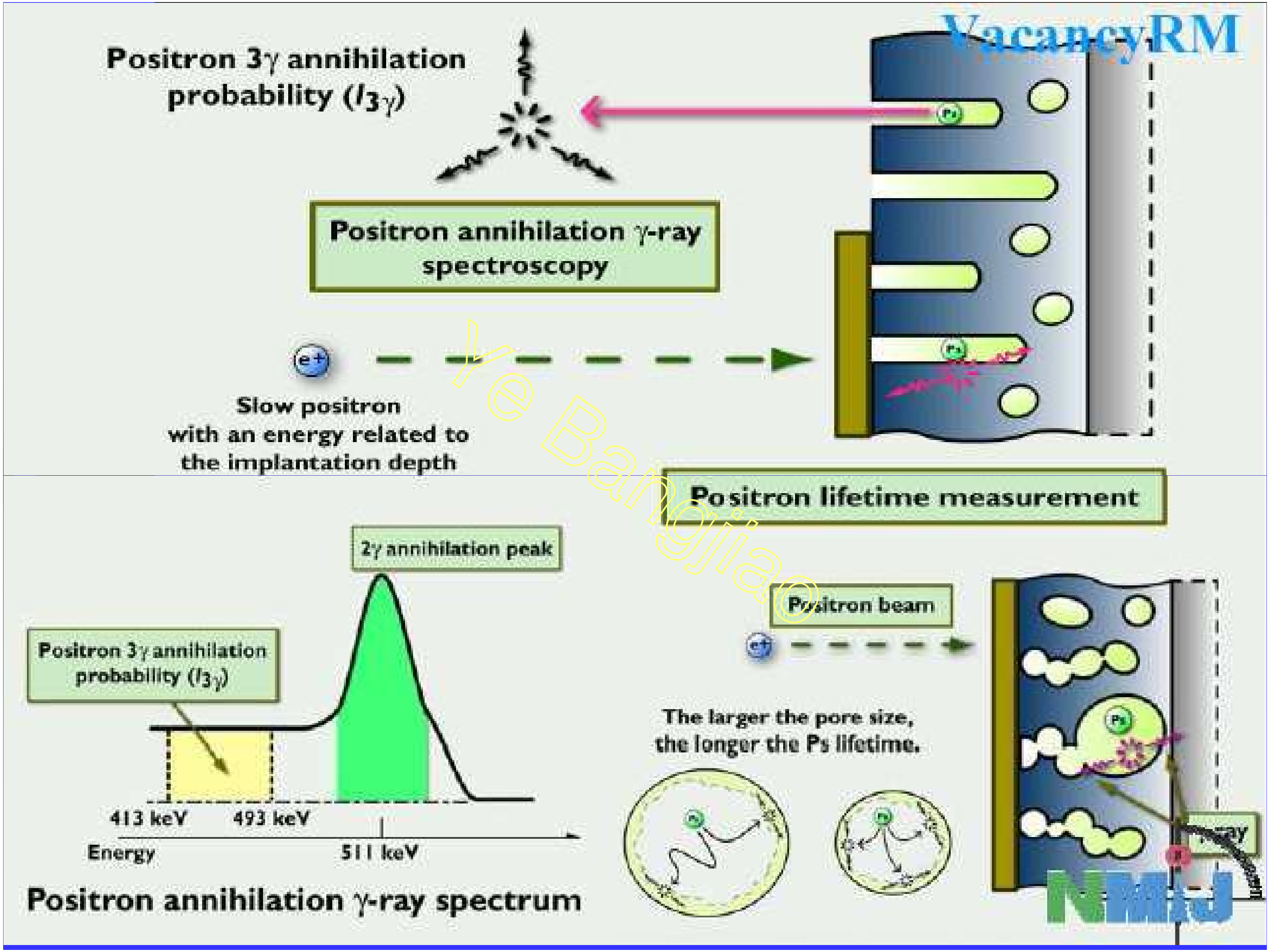
VacancyRM
Positron 3γ annihilation probability (I3γ)
Positron annihilation γ-ray spectroscopy
e+
Ps
Slow positron with an energy related to the implantation depth
Positron lifetime measurement
2γ annihilation peak
Positron 3γ annihilation probability (I3γ)
413 keV
493 keV
511 keV
Energy
Positron annihilation γ-ray spectrum
Positron beam
The larger the pore size, the longer the Ps lifetime.
γ-ray
NMIJ

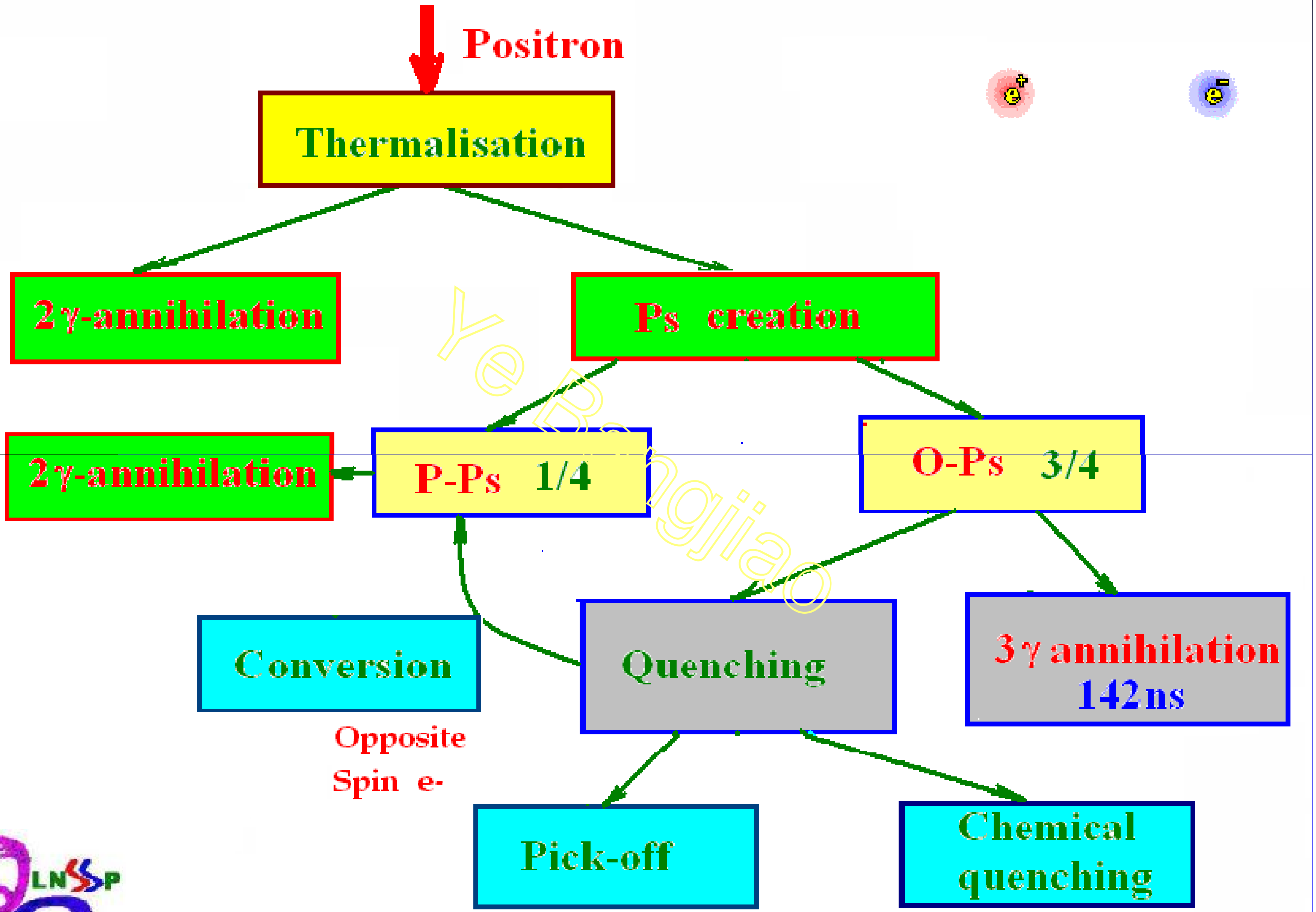

Positron

Thermalisation

2γ-annihilation

Ps creation

2γ-annihilation

P-Ps 1/4

O-Ps 3/4

Conversion

Opposite
Spin e-

Quenching

3γ annihilation
142ns

Pick-off

Chemical
quenching

相 变

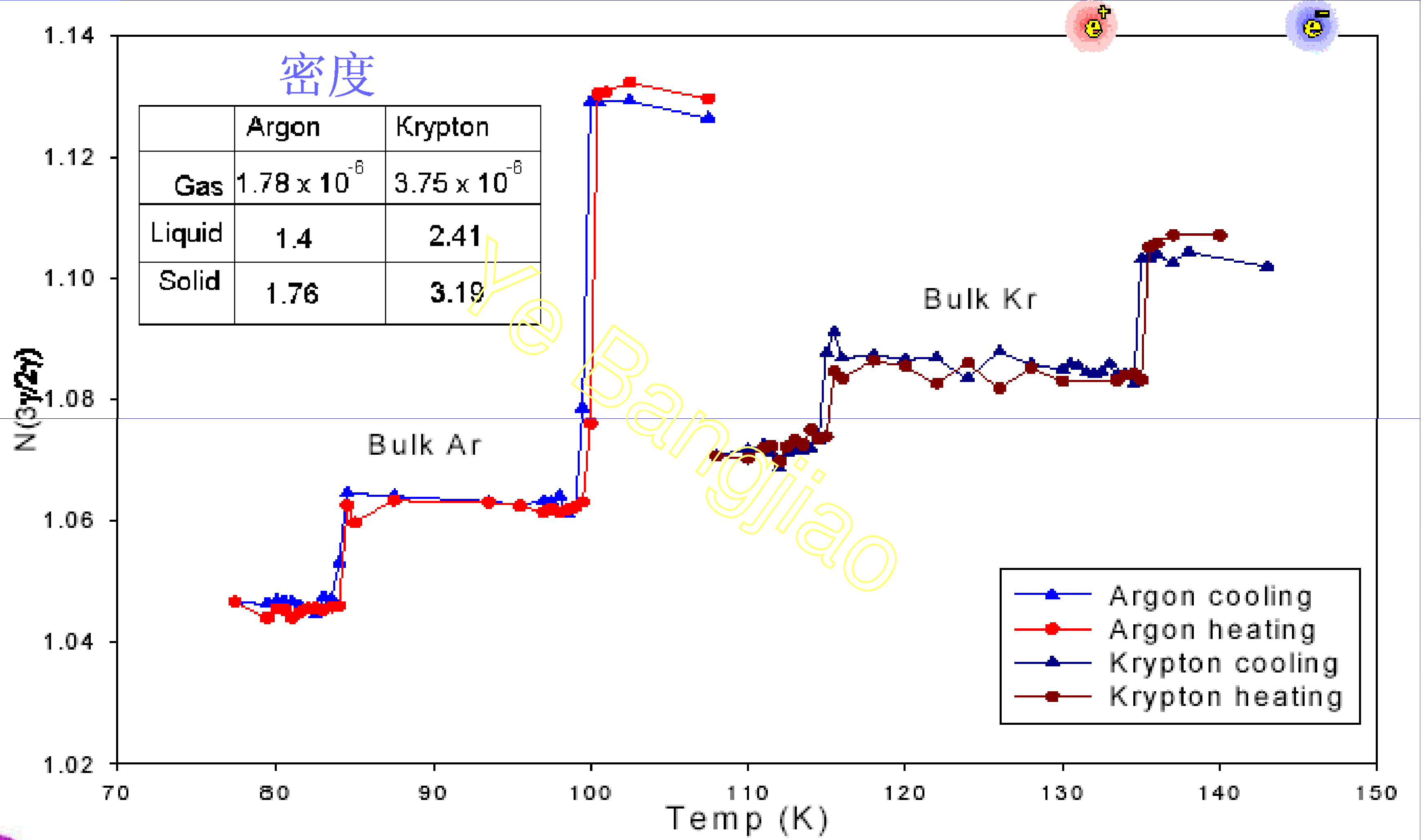

	Argon	Krypton
Gas	1.78×10^{-6}	3.75×10^{-6}
Liquid	1.4	2.41
Solid	1.76	3.19

he $N(3\gamma / 2\gamma)$ parameter for bulk argon and krypton at a constant pressure of 3 bar.

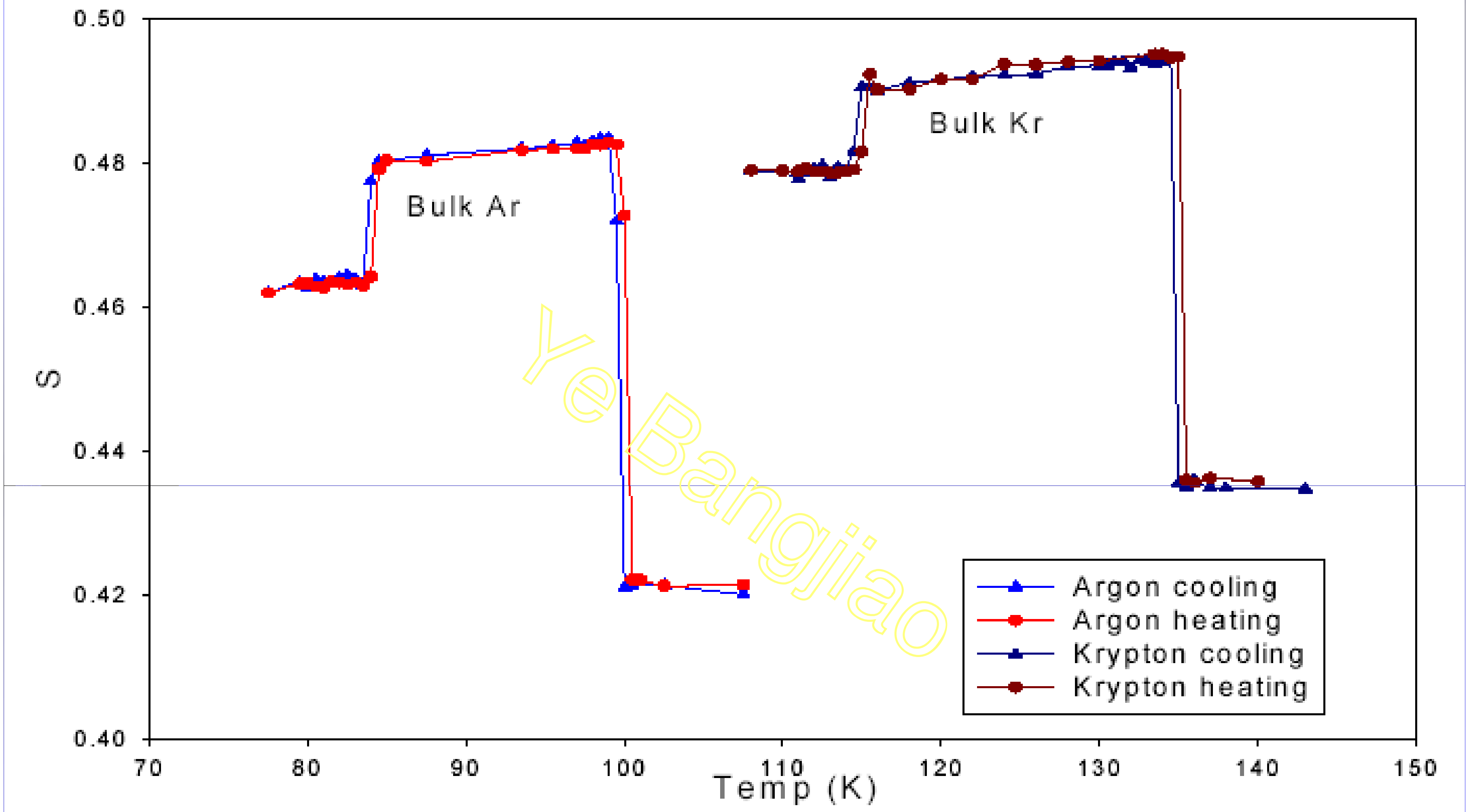

The S parameter for bulk argon and krypton at a constant pressure of 3 bar.

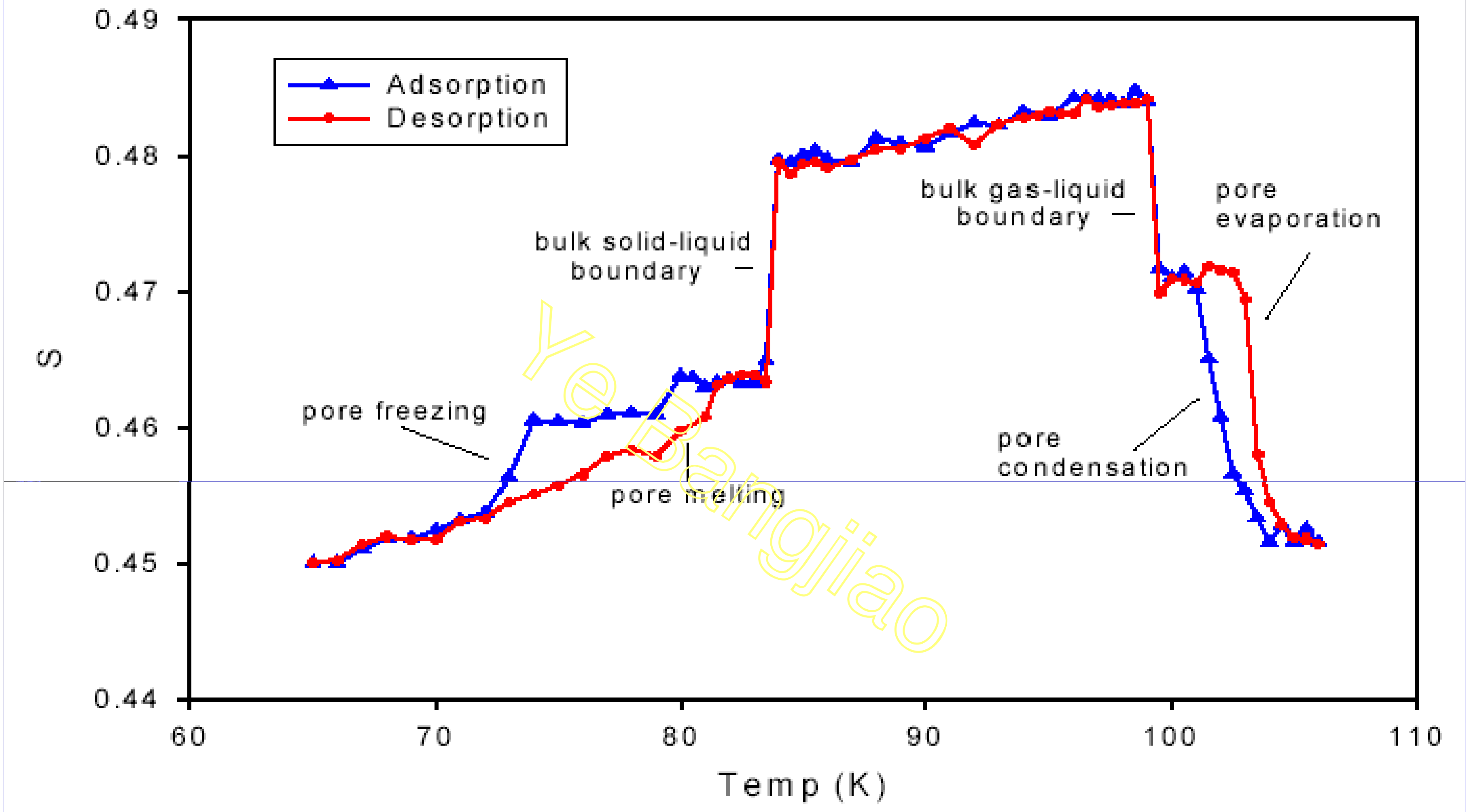

The S parameter for an isobaric argon experiment at 3bar.

2D-PALS

Ye Bangjiao

porous materials

Long-lived o-Ps 3γ annihilation

Age - **Pulse Height**

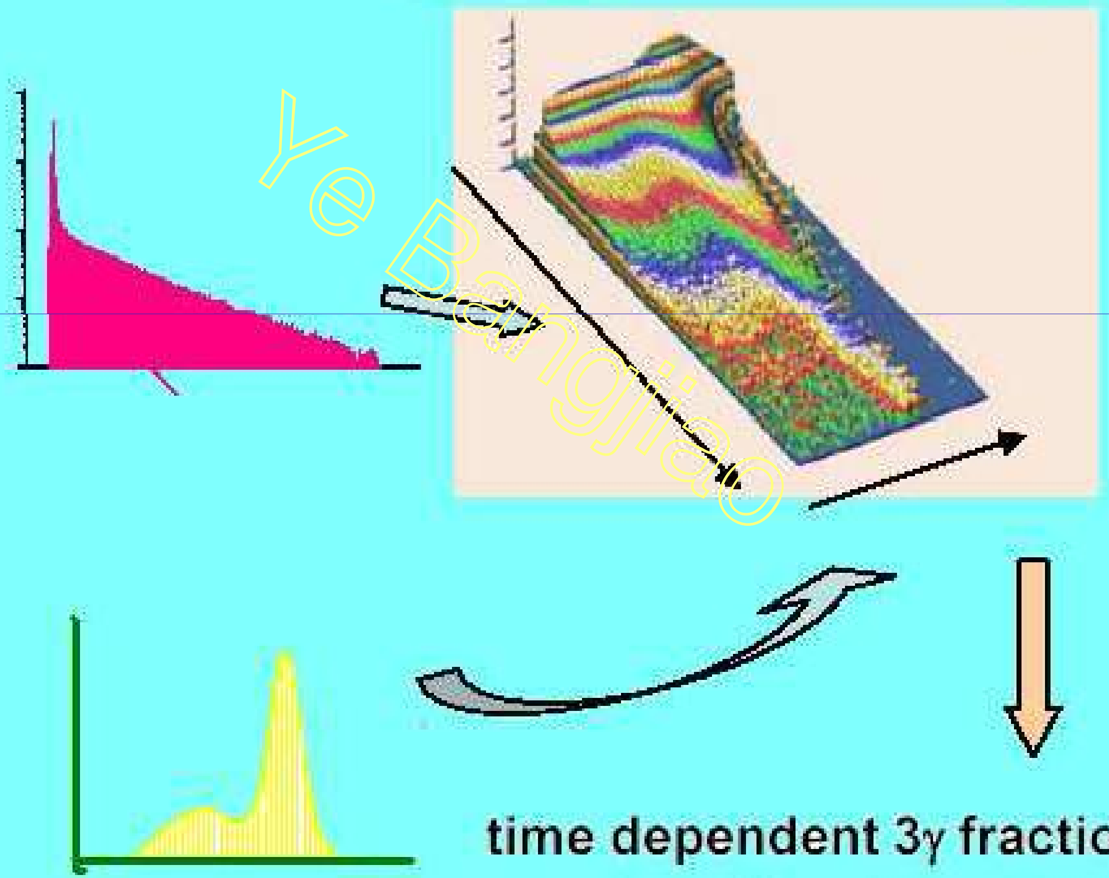

time dependent 3γ fraction

$F_{3\gamma}(t)$

Pulse Height

without Cap

with Cap

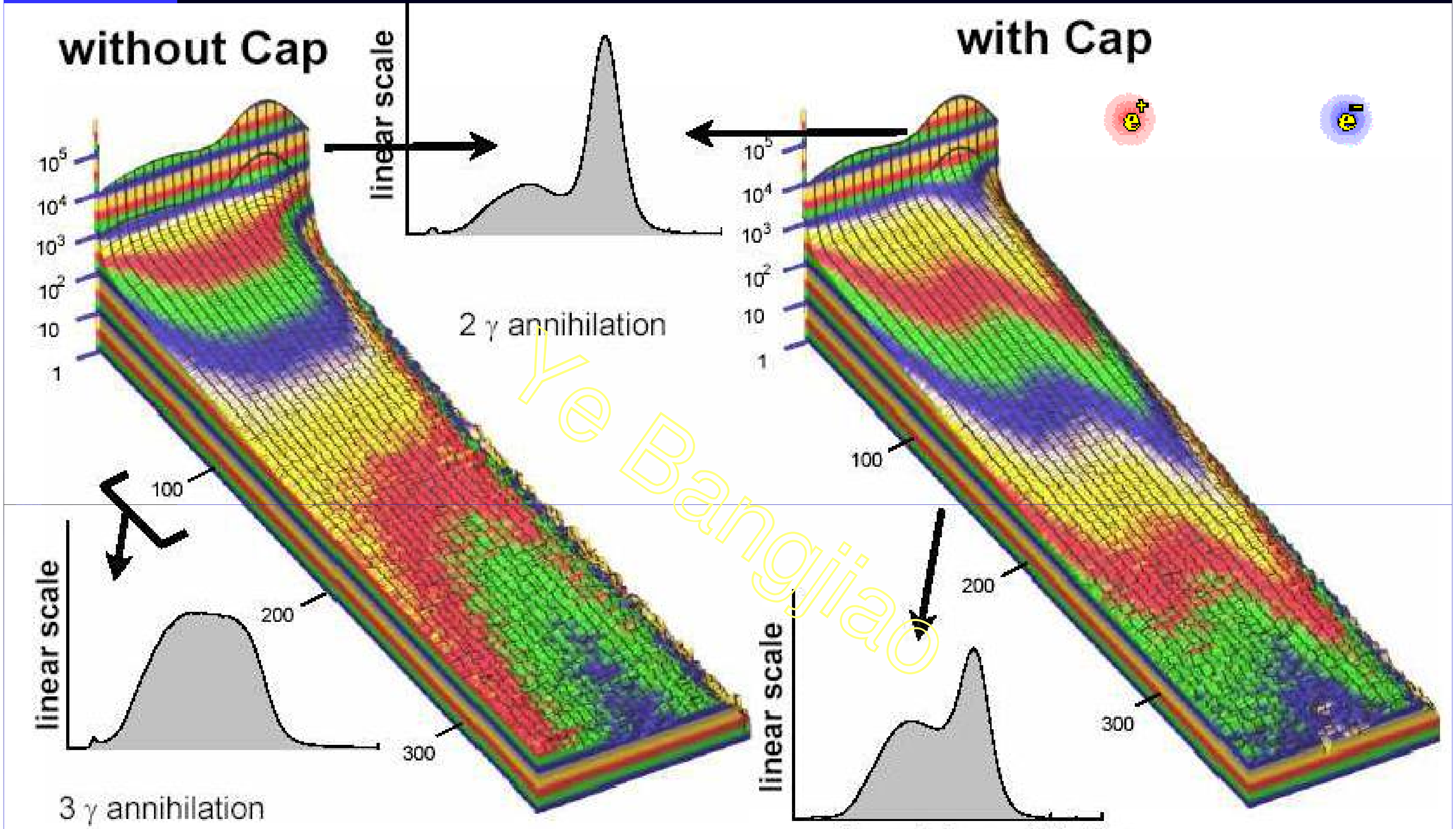

in vacuum

in pores

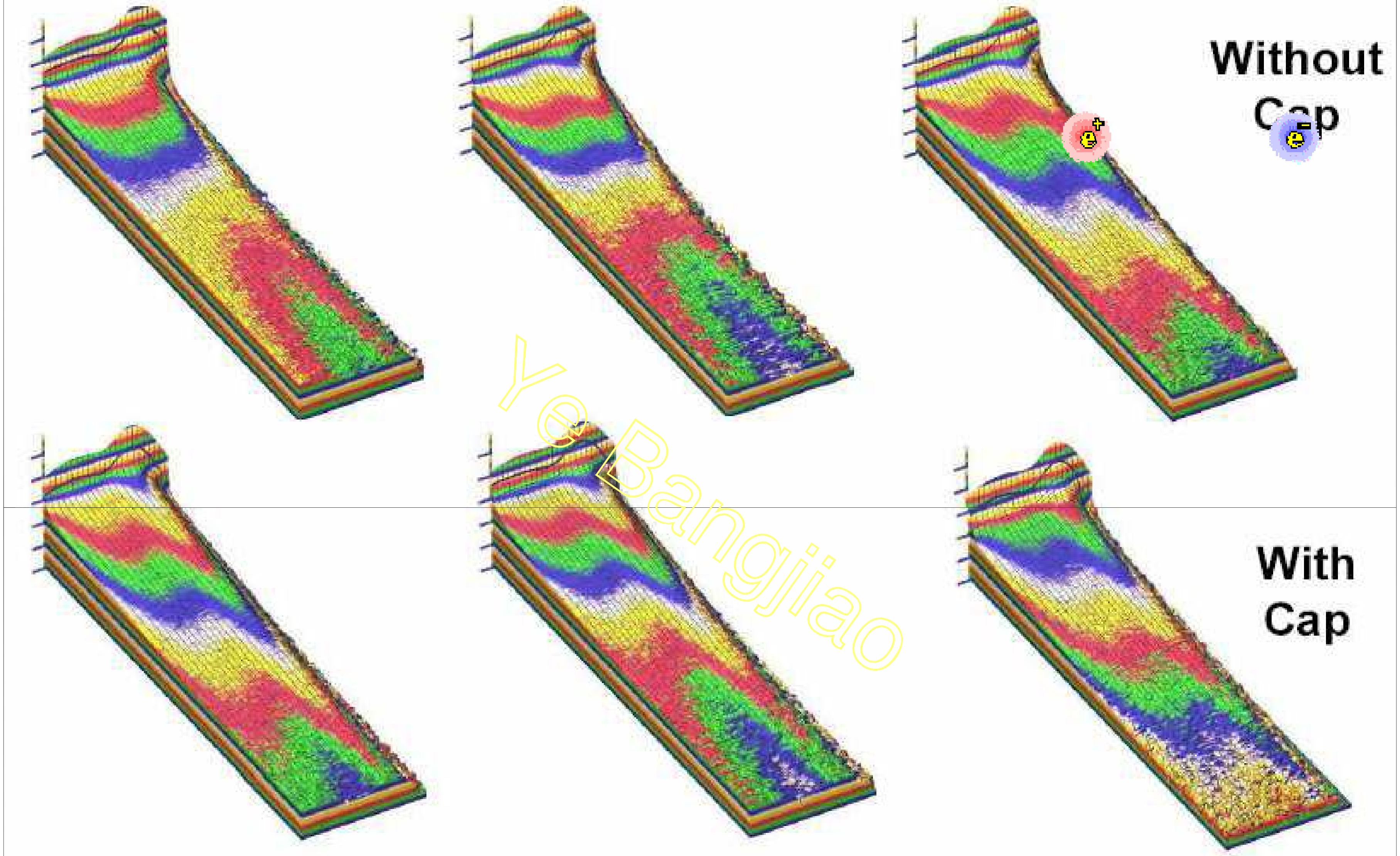

Sample A

andom, large

Sample B

random, small

Sample C

periodic

Calculation of 3γ fraction f(t)

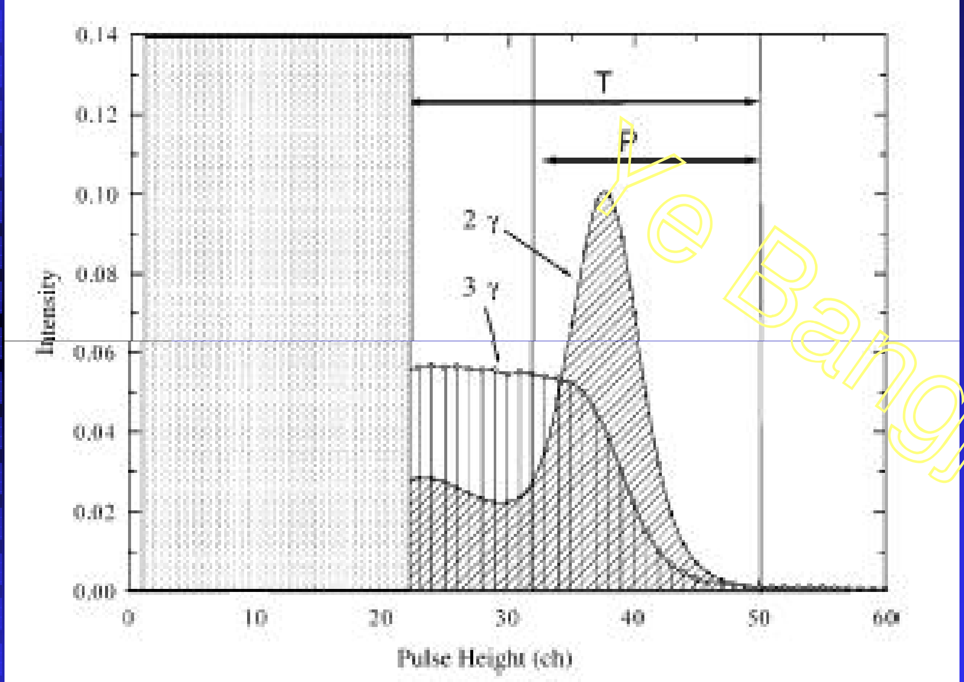

$$T_f = f\,T_{3\gamma} + (1-f)\;T_{2\gamma}$$

$$P_f = f\,P_{3\gamma} + (1-f)\;P_{2\gamma}$$

↓

$2\gamma : f=0, \quad 3\gamma : f=1$

$$R = P_f \,/\, T_f$$

↓

$$f(t) = \left[1 + (T_{3\gamma} / T_{2\gamma})(R(t) - R_{3\gamma})(R_{2\gamma} - R(t))^{-1}\right]^{-1}$$

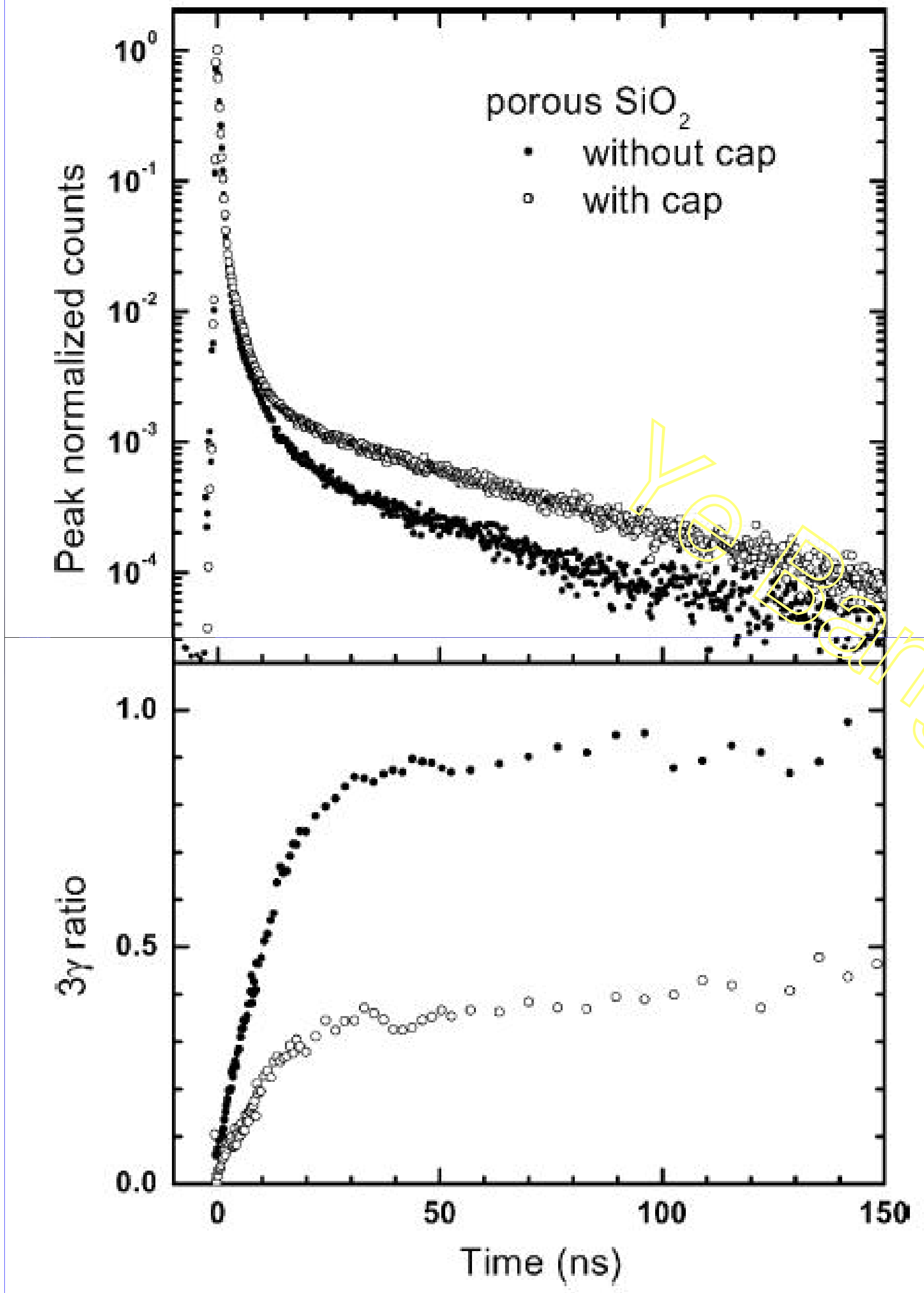

Positron lifetime spectra (upper) and three-gamma ratio (lower) as a function of annihilation time for capped (○) and noncapped (•) porous SiO_2 films.

慢正电子束技术

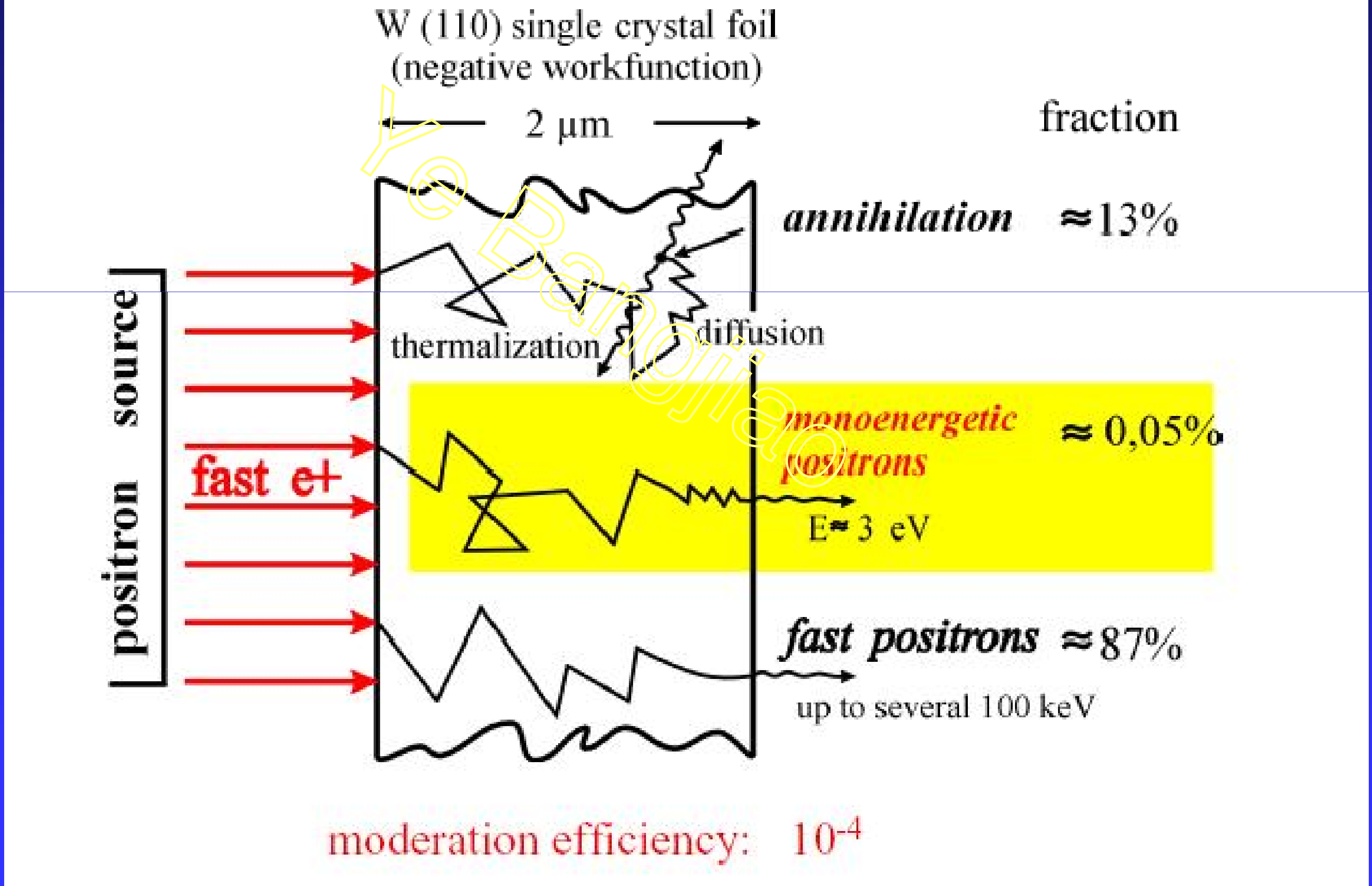

moderation efficiency: 10^{-4}

e^+ e^-

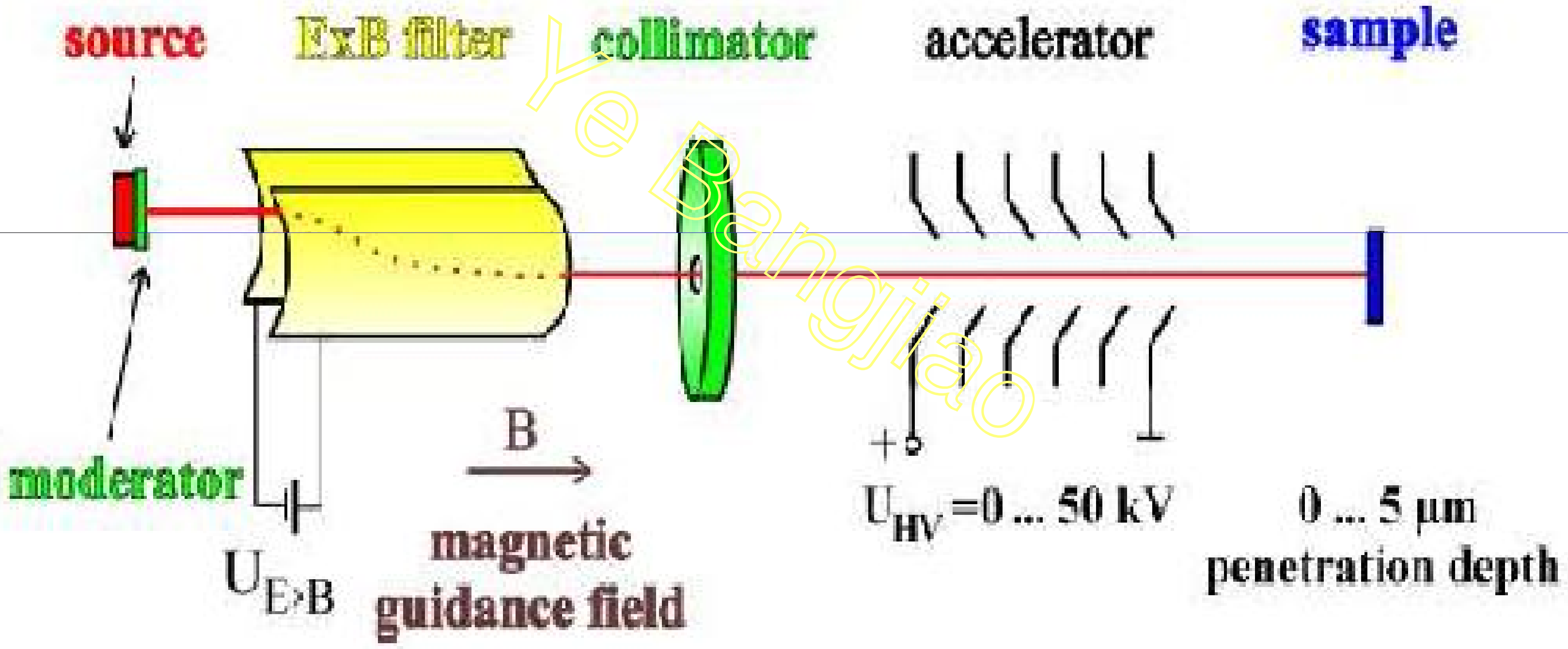
source
ExB filter
collimator
accelerator
sample
moderator
$U_{E\times B}$
B
magnetic guidance field
+
U_{HV} =0 ... 50 kV
0 ... 5 µm penetration depth

我国第一个慢正电子束装置

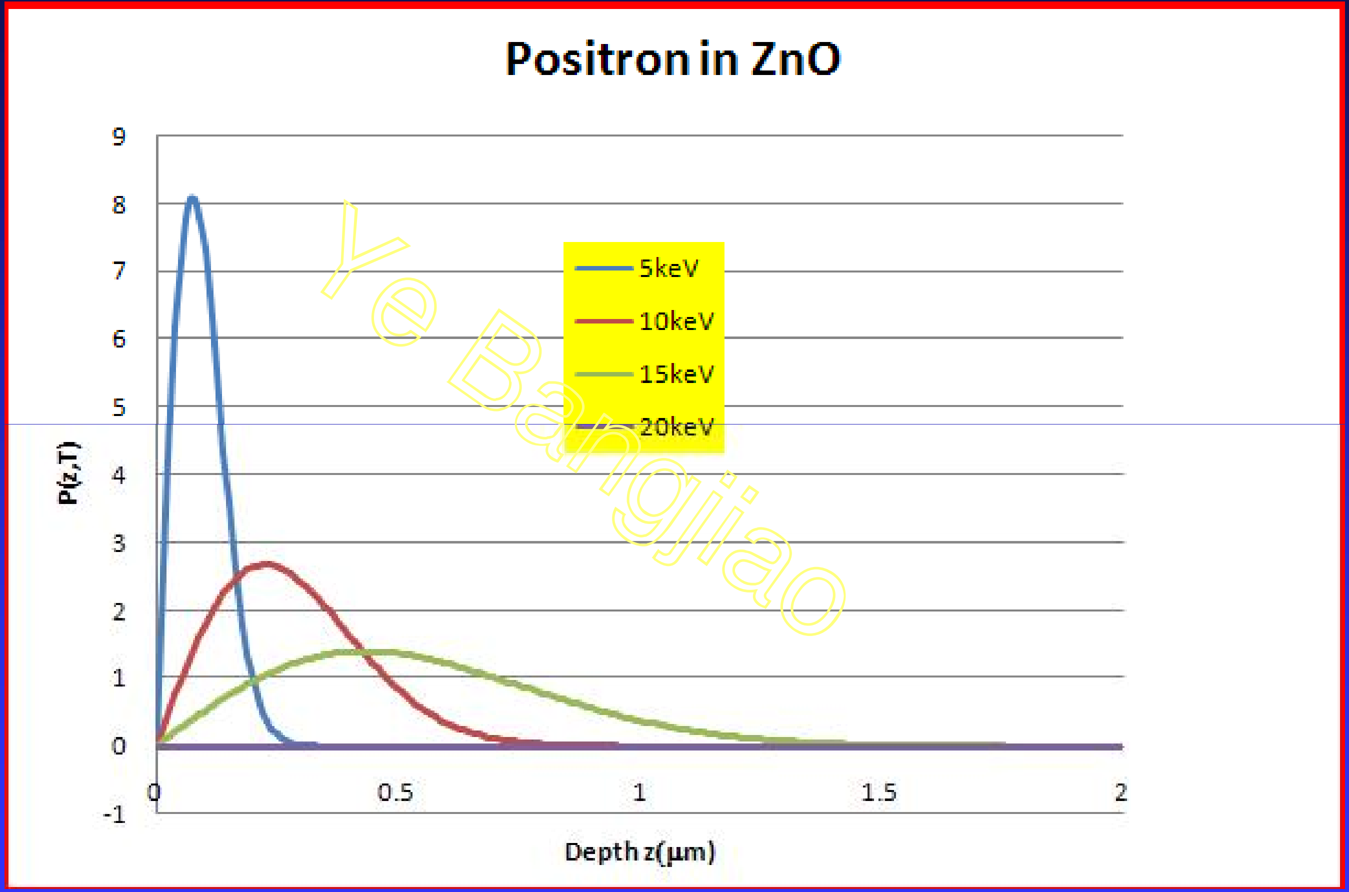
Positron in ZnO
9
8
7
6
5
4
3
2
1
0
-1
P(z,T)
0
0.5
1
1.5
2
Depth z(μm)
5keV
10keV
15keV
20keV

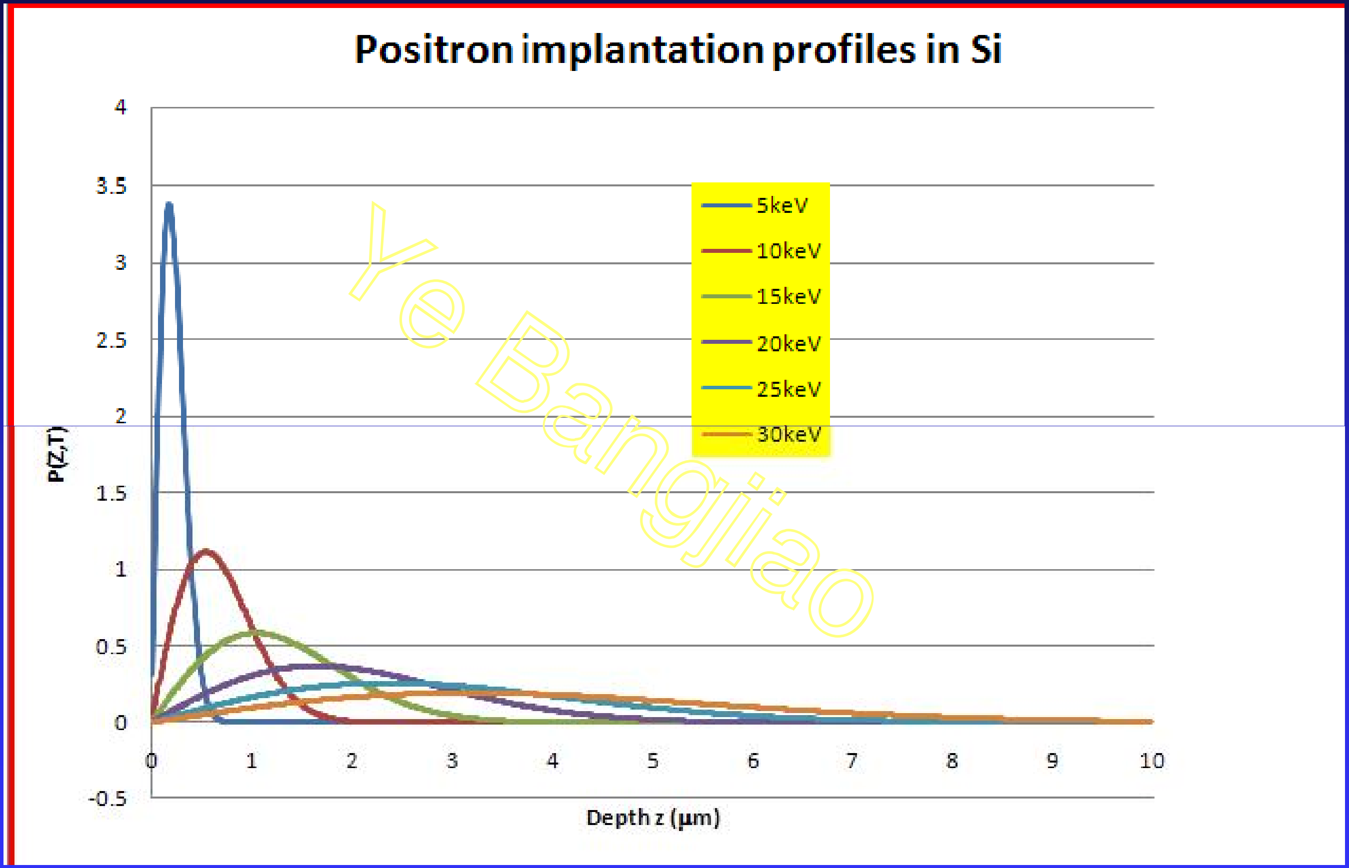
Positron implantation profiles in Si
P(Z,T)
4
3.5
3
2.5
2
1.5
1
0.5
0
-0.5
0
1
2
3
4
5
6
7
8
9
10
Depth z (µm)
5keV
10keV
15keV
20keV
25keV
30keV

S-E and S-W plots

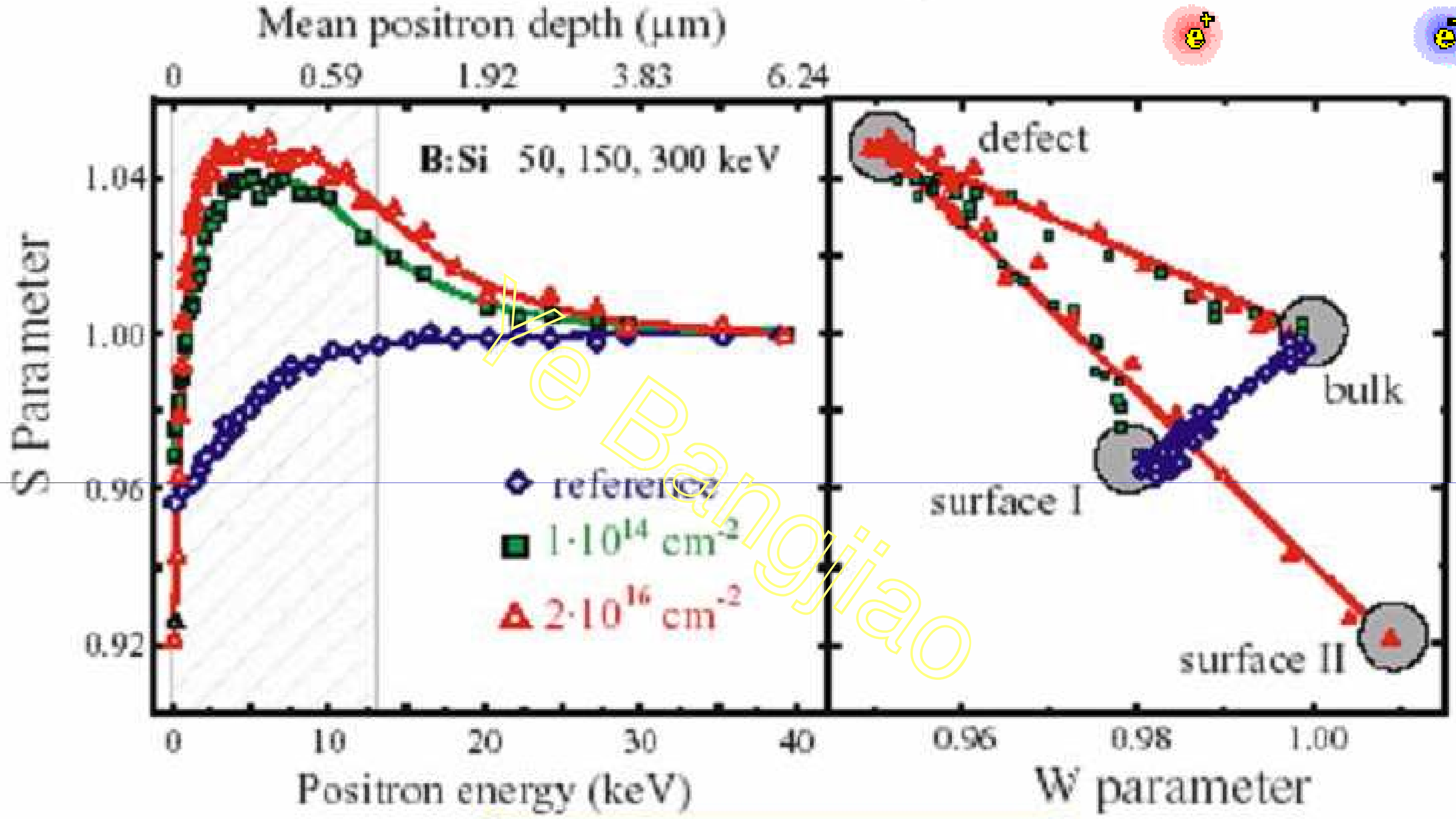

Ion implantation in Si

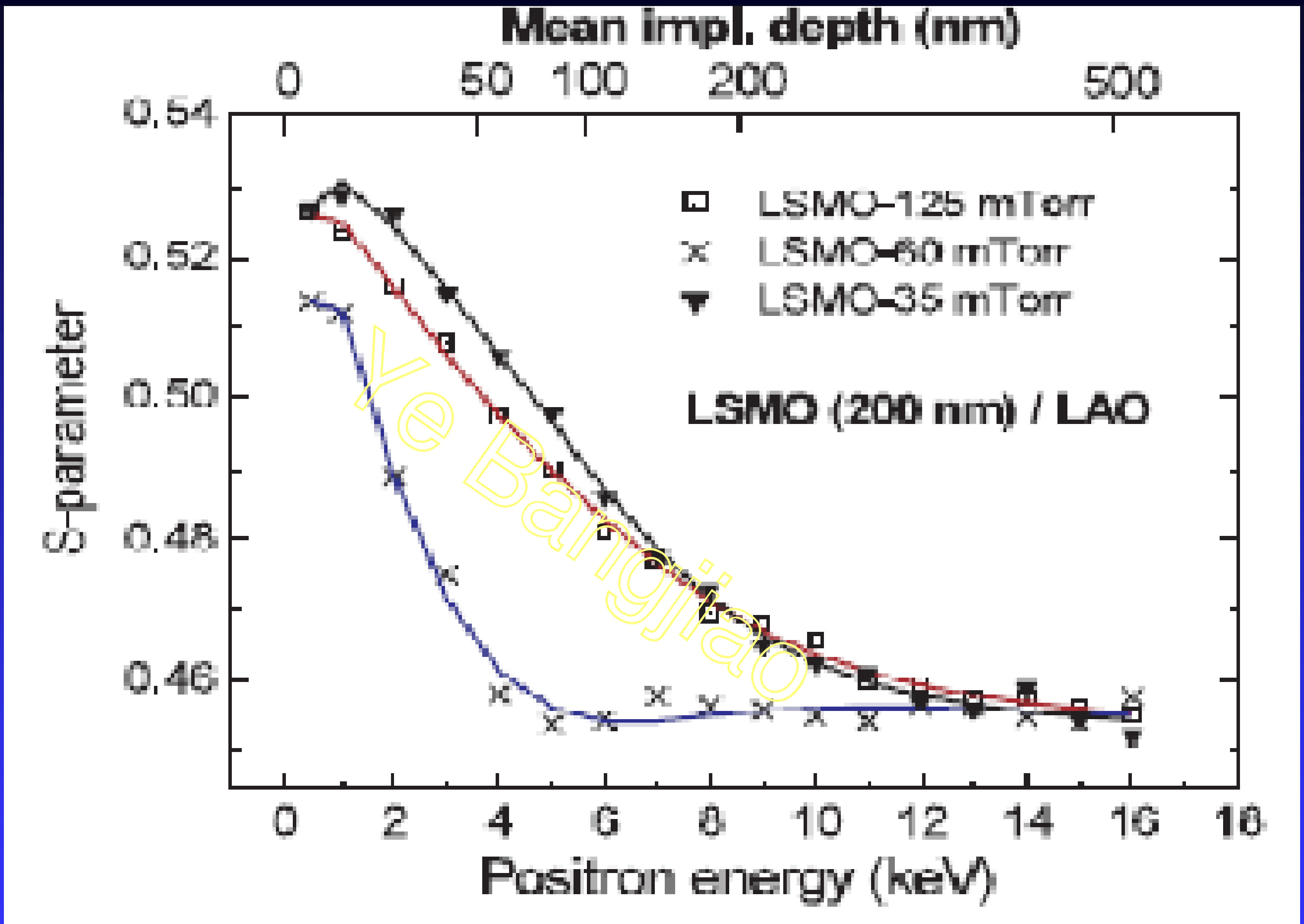

$La_{0.7}Sr_{0.3}MnO_3$外延膜缺陷的研究

SiC 单晶在不同条件件退火后缺陷的变化

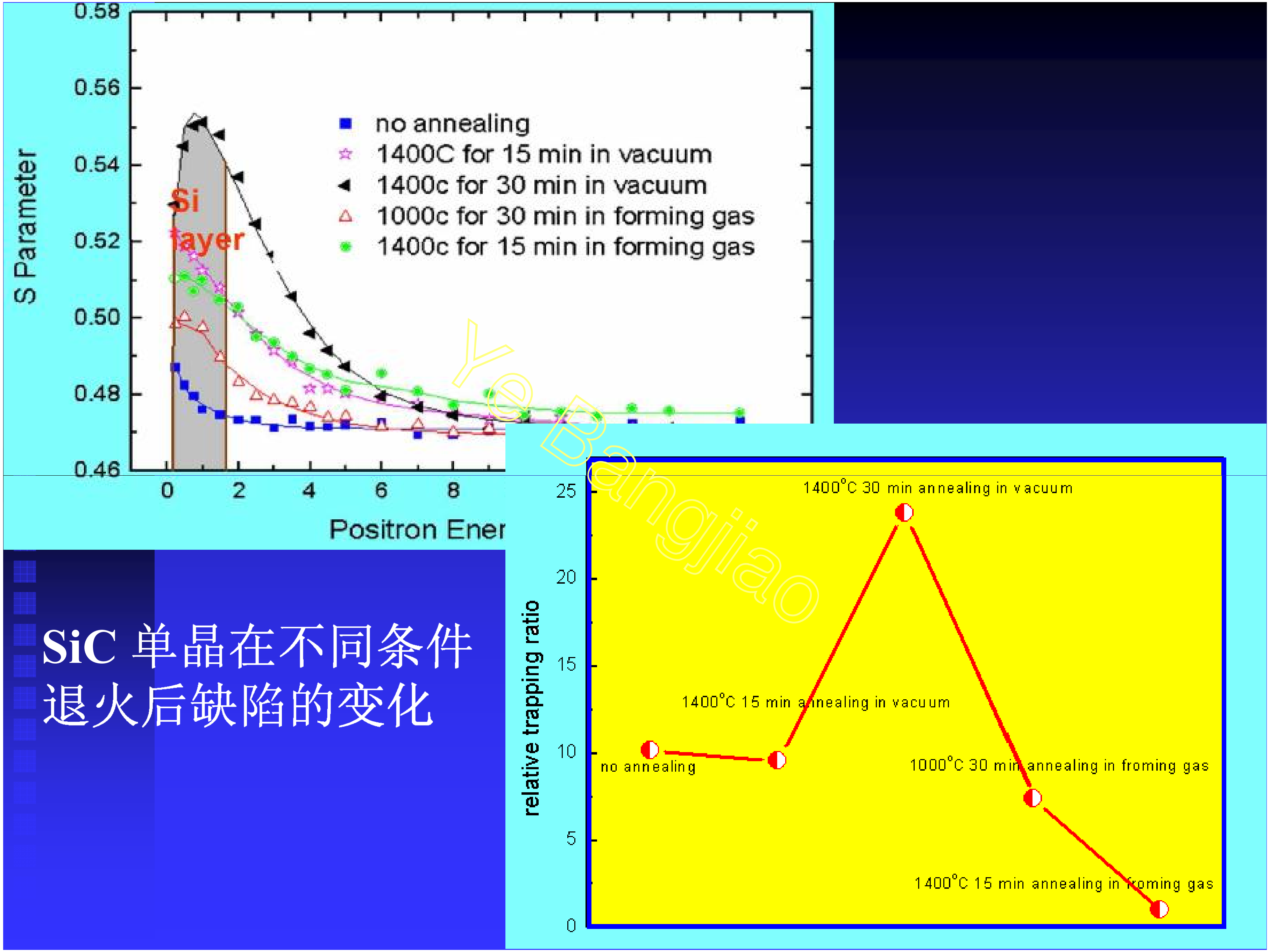

正电子表面研究技术

- 正电子衍射（低能和高能）
- PAES技术

几十多年以来，科学家们致力于寻找最合适的研究固体表面的探针，电子、正电子、光子、原子和离子都可作为研究表面的探针，然而，一个理想的表面结构探针应该具有以下的2个基本特性：

- 粒子必须要有小的平均自由程(<30A°)，即要对表面灵敏；
- 粒子与表面的相互作用应该较弱，以使测量结构可以被精确地模拟计算。

正电子最合适作为表面探针的理想粒子：

- 因为它在固体中的平均自由程很短 e^+ 事实上 e^- 对能量低于200eV的正电子，其平均自由程比电子平均自由程要短；对能量大于200eV的正电子，平均自由程与电子类似。因此正电子对最初的3-4层原子层特别灵敏。

- 正电子的散射因子与X-射线和电子基本类似。而电子的散射因子有尖锐的各向异性角分布，而正电子的角分布圆滑变化，如图为微分角分布。

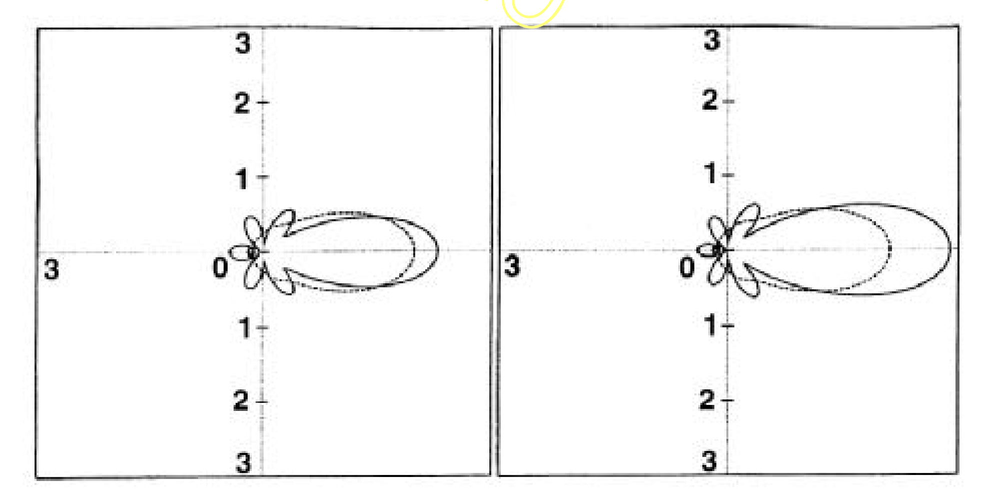

Messenger	Spectroscopy
Positron	LEPD RHEPD Positron work function measurement Positron re-emission spectroscopy and microscopy Re-emitted positron energy loss spectroscopy (REPELS) Positron tunnelling spectroscopy Positron backscattering
Ps	Ps emission/formation spectroscopies Inverse Ps formation spectroscopy* Ps diffraction*
Gamma photon	Surface ACAR Positron-annihilation microscopy
Electron	PAES Positron-induced secondary electron emission

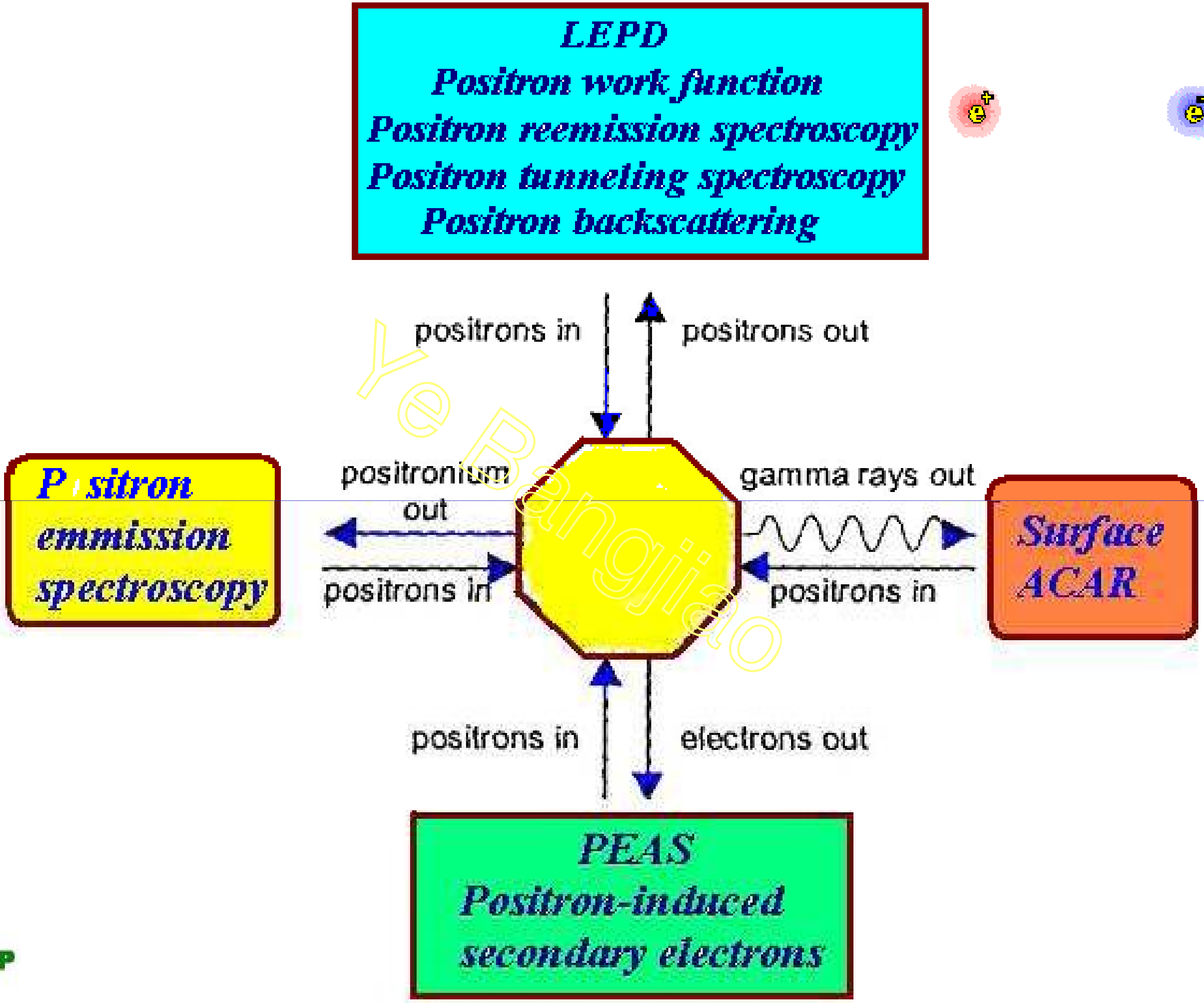

LEPD
Positron work function
Positron reemission spectroscopy
Positron tunneling spectroscopy
Positron backscattering

Positron emmission spectroscopy

Surface ACAR

PEAS
Positron-induced secondary electrons

●正电子衍射

■低能正电子衍射LEPD

Positron Diffraction Experiments

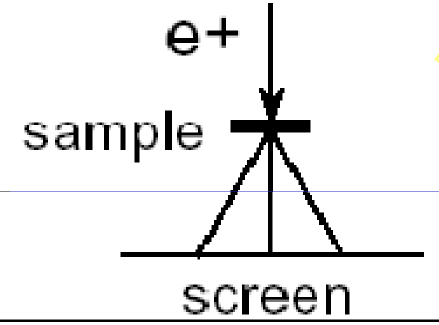	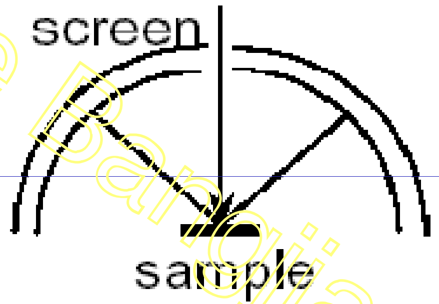	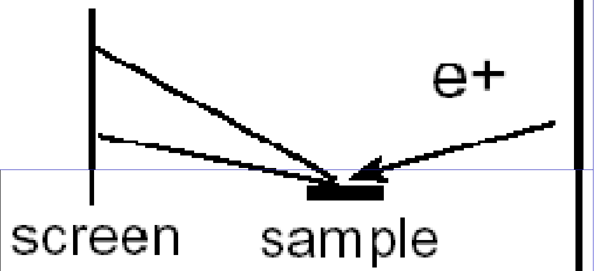
TPD Transmission Positron Diffraction	LEPD Low Energy Positron Diffraction	**RHEPD** Reflection High Energy Positron Diffraction
100keV ▪ 1MeV	10 ▪ 500eV	10 ▪ 100keV
Bulk ▪ Study	**▪ Surface ▪ Study ▪**	

LEPD

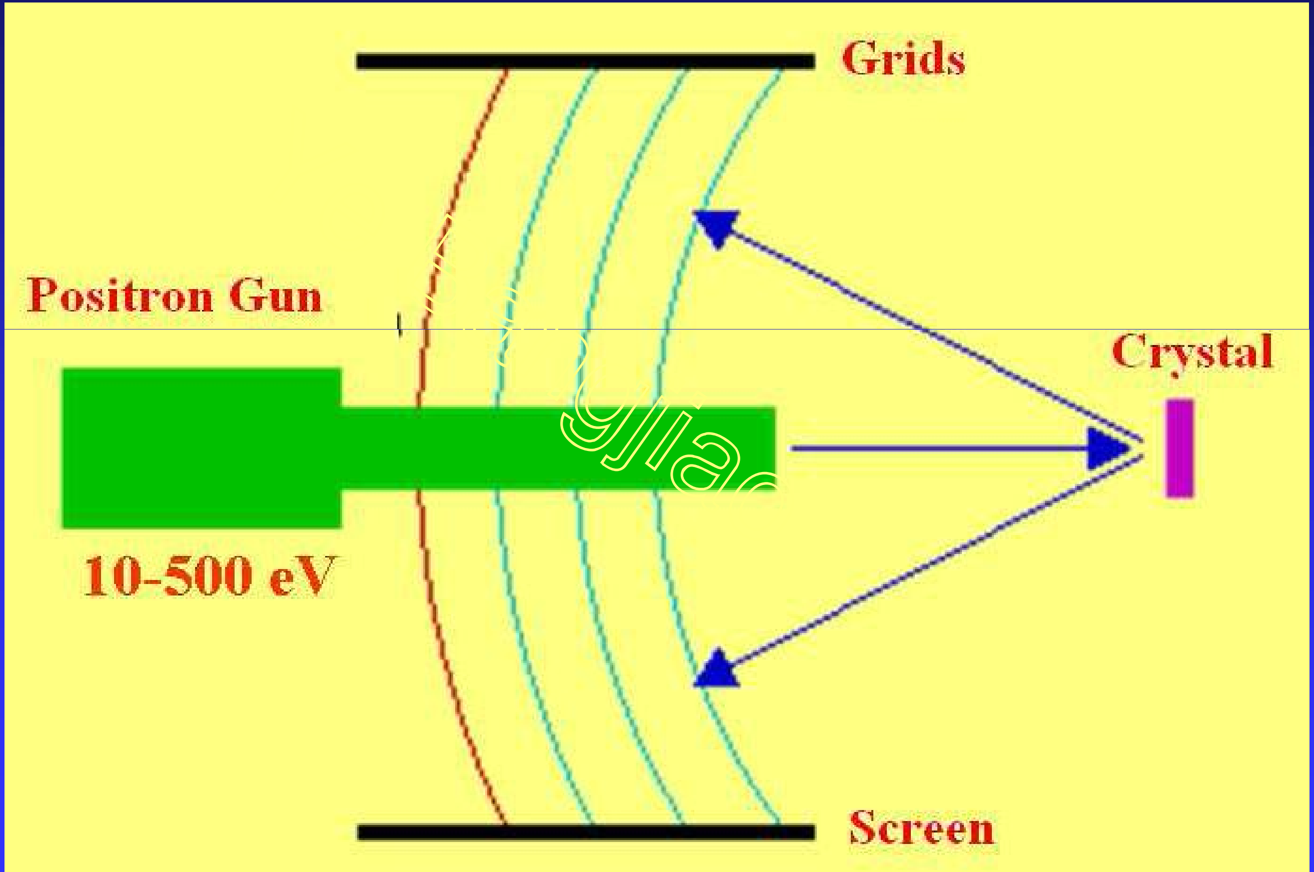

Grids

Positron Gun

Crystal

10-500 eV

Screen

Derive LEED equation using Bragg's Law for X-ray diffraction, where appropriate angles are substituted and λ is for the electron wavelength.

X-ray Diffraction

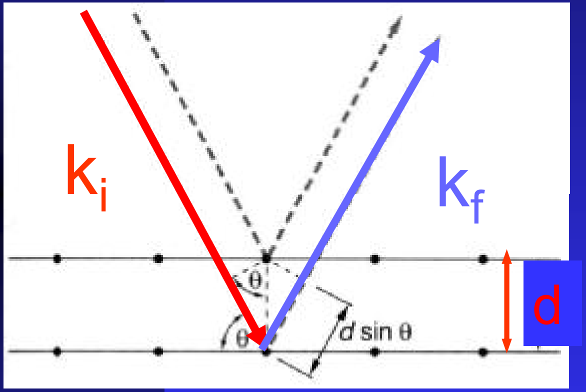

$$n\lambda_{\text{xray}} = 2d\sin\theta$$

$$n\lambda = 2(D\sin\alpha)(\cos\alpha)$$

$$\lambda = D\sin 2\alpha$$

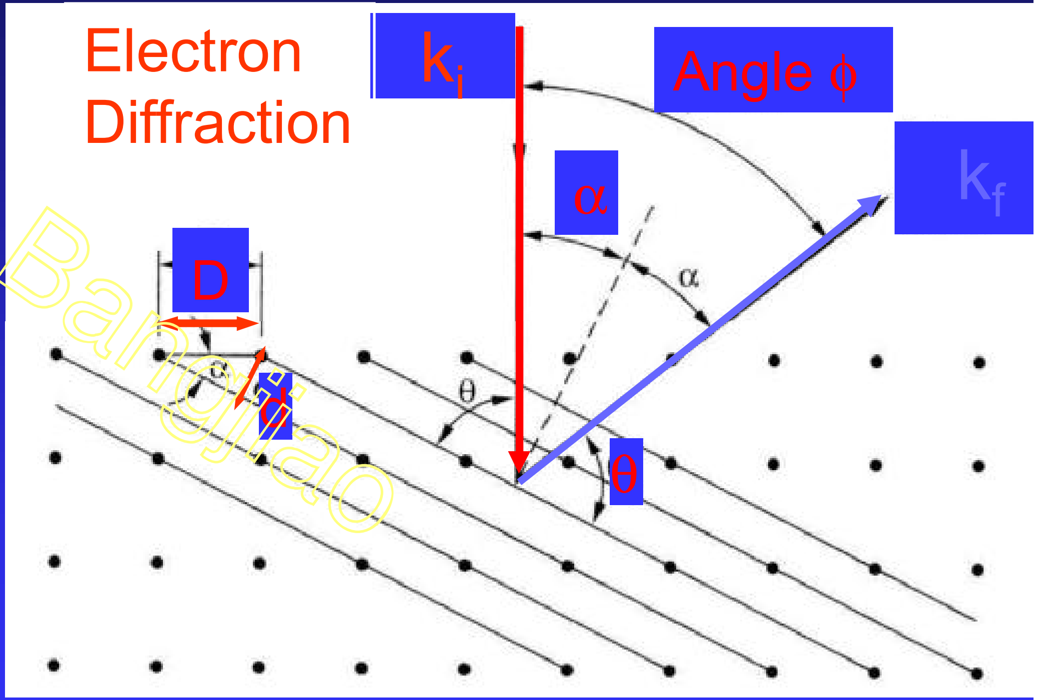

$$n\lambda_{\text{elec}} = D\sin\phi$$

LEPD的优点

- 正电子散射的相移与原子序数Z的依赖不如电子散射灵敏；因而LEPD在多成分系统对结构参数更加灵敏。
- LEPD的非弹截面大，意味着LEPD的平均自由程比LEED短，而平均自由程与扩散深度直接有关，因而，LEPD比LEED在表面有更大的灵敏度。
- 使用在LEPD I-V轮郭理论计算中的正电子-电子相互作用关联项的不确定比之在LEED中等价的项要弱。
- 由于正电子接近离子芯时减速，因而对从高Z材料表面的散射电子其相对论效应如自旋-轨道耦合将减少。

美国Brookhaven实验室和 Bell实验室及其它研究中心也已经开始发展LEPD测量技术。

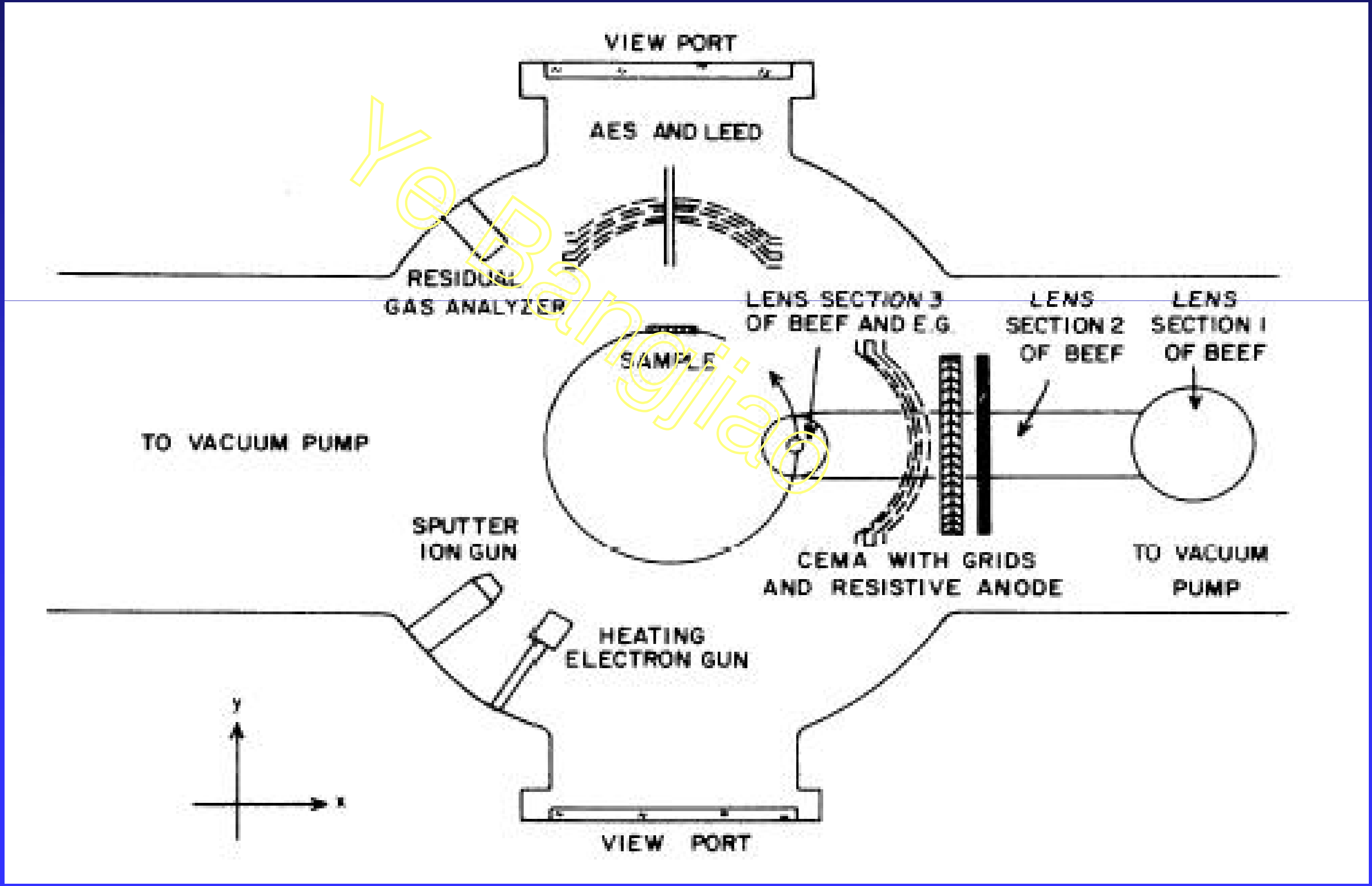

■高能正电子衍射(RHEPD)

Reflection high-energy positron diffraction

KAWASUSO, A., (JAERI)

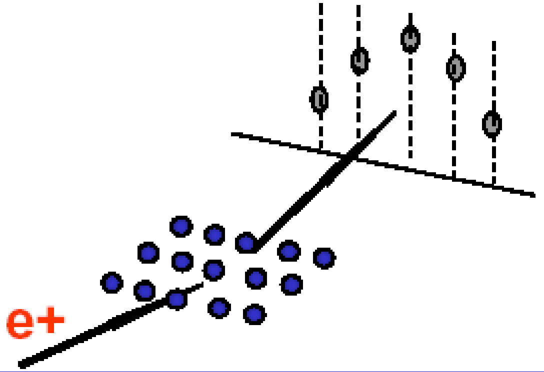

- Primary Bragg Reflection
- Total Reflection

Negative Inner Potential

Positive Inner Potential

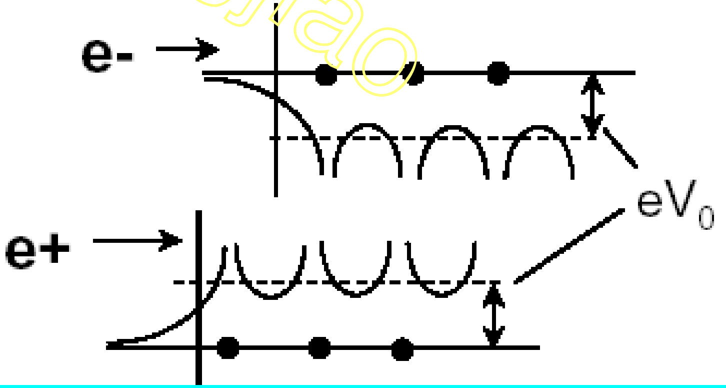

Bragg condition: $\underline{E\sin^2\theta = 37.5\, n^2/d^2 + eV_0}$

Present RHEPD apparatus at JAERI

Key elements	
•Positron beam	10 -20 keV
•Low angular divergence	<1°
•Small beam diameter	<1mm

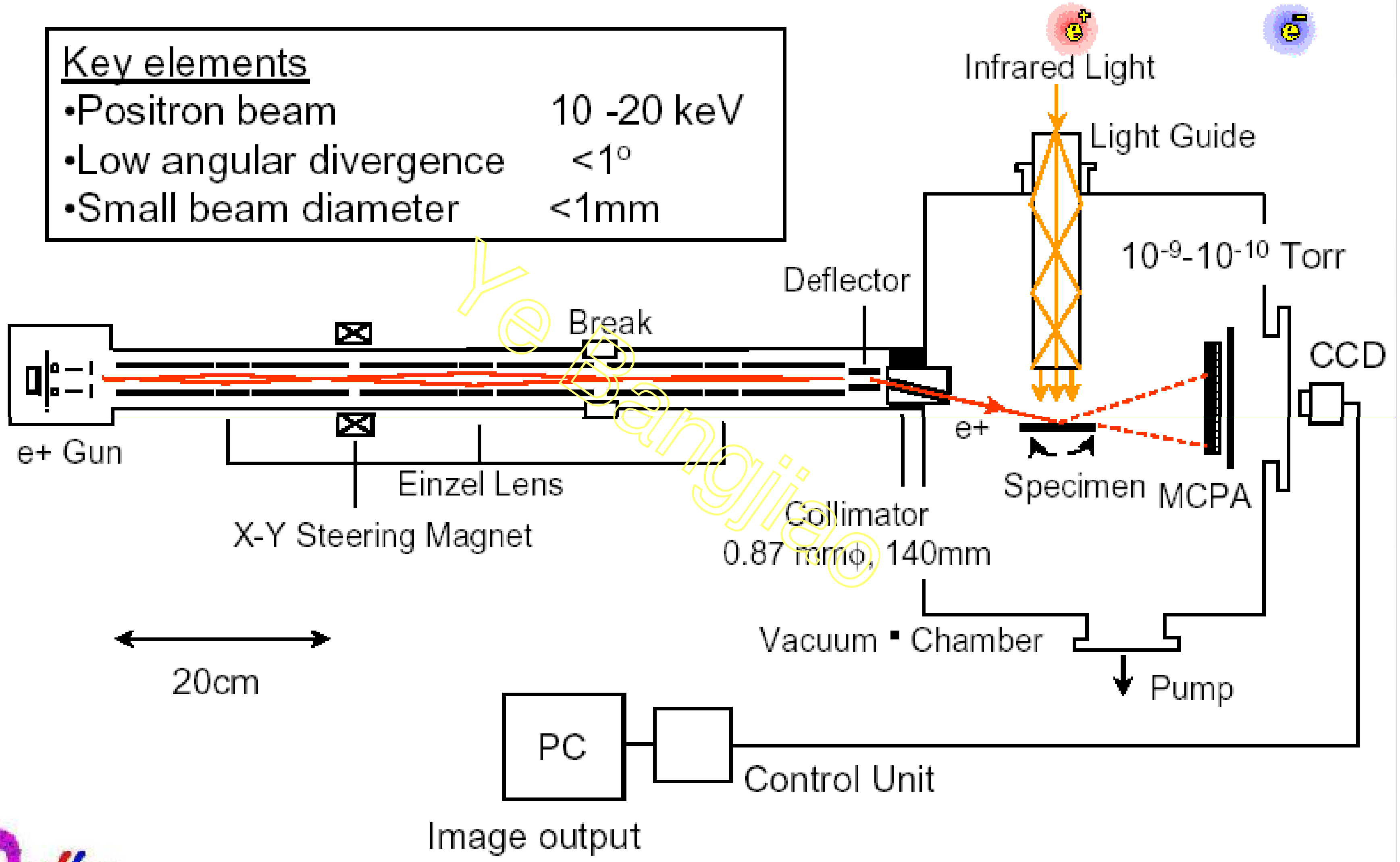

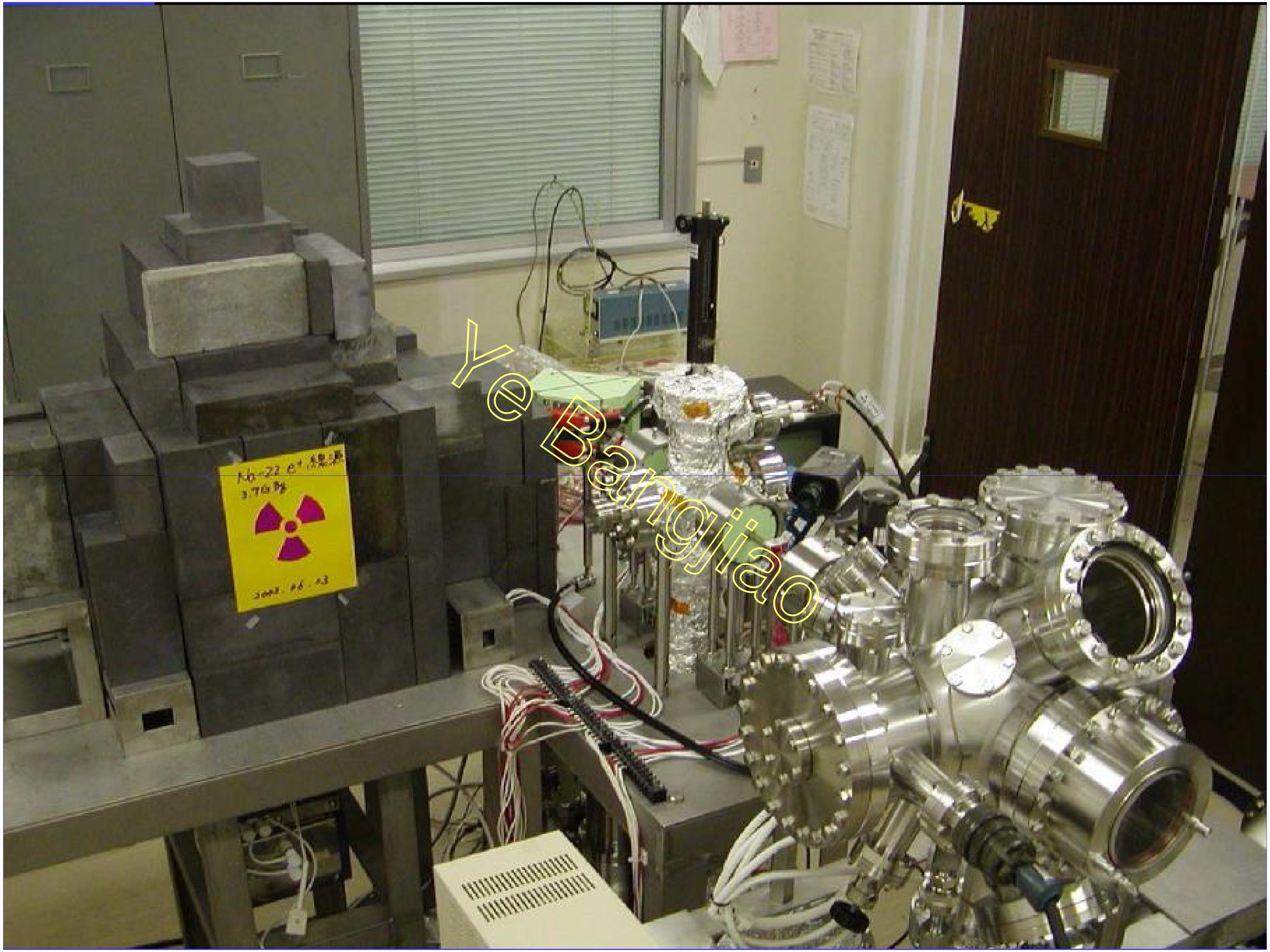
Na-22 e+ 線源
3.7GBq
2003. 06. 13

First RHEPD pattern from Si(111)H

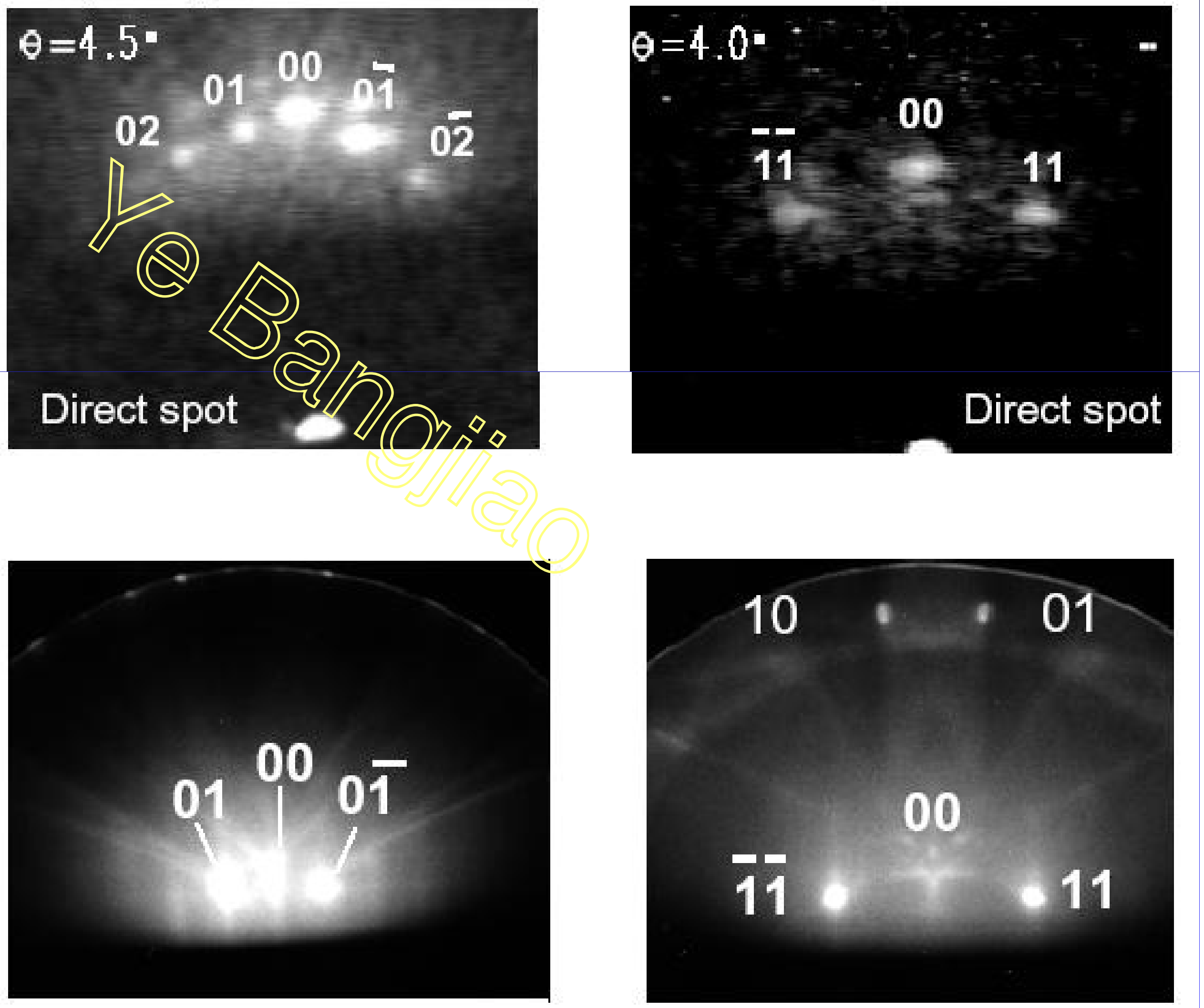

$[11\bar{2}]$ incidence

$[1\bar{1}0]$ incidence

RHEPD

RHEED

● PAES

Positron-annihilation induced AES (PAES)

Core holes are created by annihilation of the core electrons with positrons trapped by the surface state.

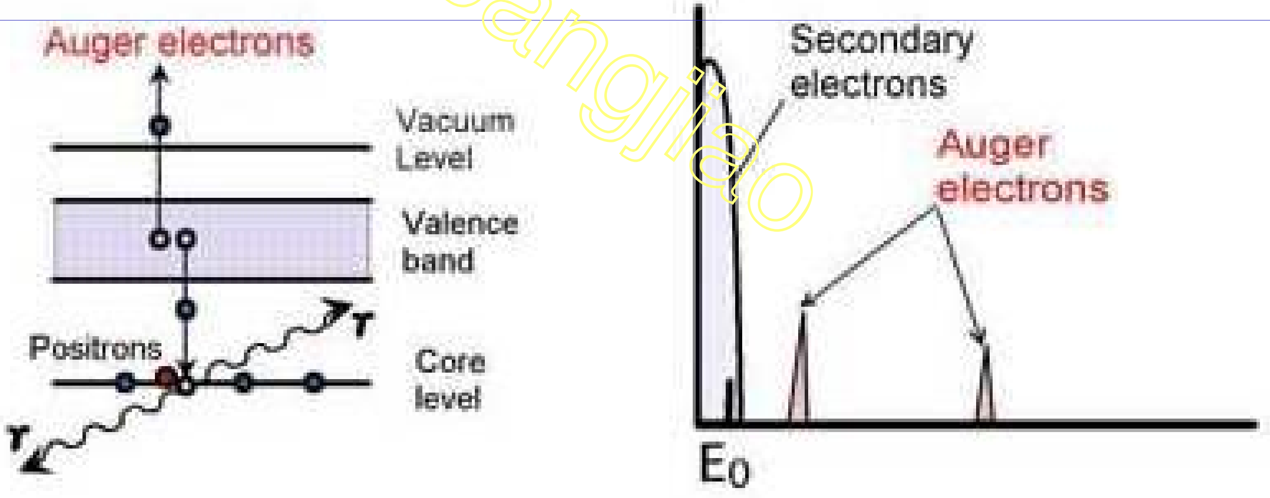

俄歇电子发射的基本原理是：低能正电子注入固体表面时，相当一部分扩散回到表面，被近表面或表面态捕获，一部分被捕获的正电子与芯电子湮没，产生芯空位，因而产生俄歇电子发射

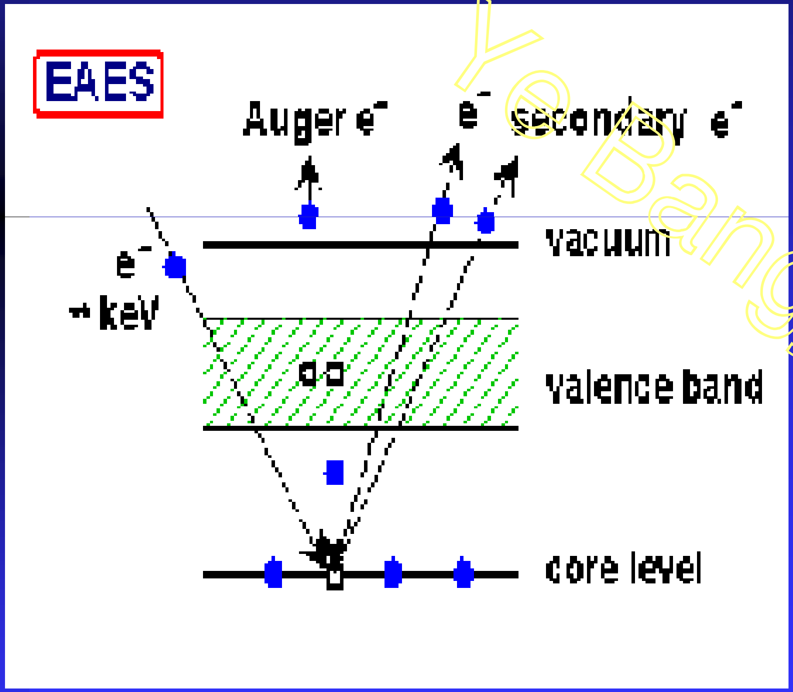

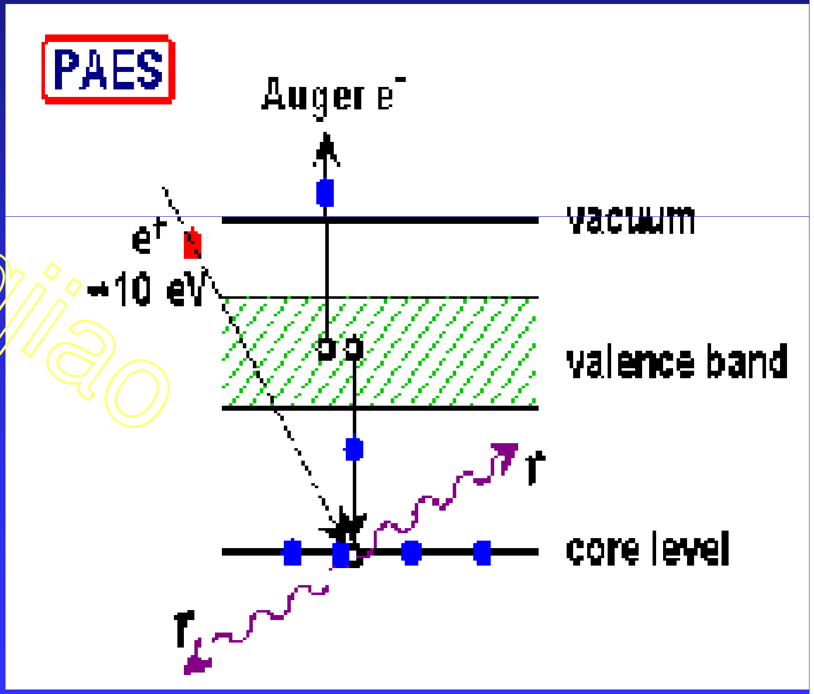

Weiss等人在**1988**年首先发展了正电子湮没诱发的俄歇电子谱仪（**PAES**），该技术的主要优点有：

（1）对表面灵敏，可以分析最表面的原子层；

（2）在非常低的能量损失下（大约比电子俄歇谱**EAES**的能量损失低5个量级）得到**PAES**谱；

（3）可以大大消除的二次电子本底。因而**PAES**技术特别适宜于俄歇线型分析。

(a) Electron induced AES (EAES)

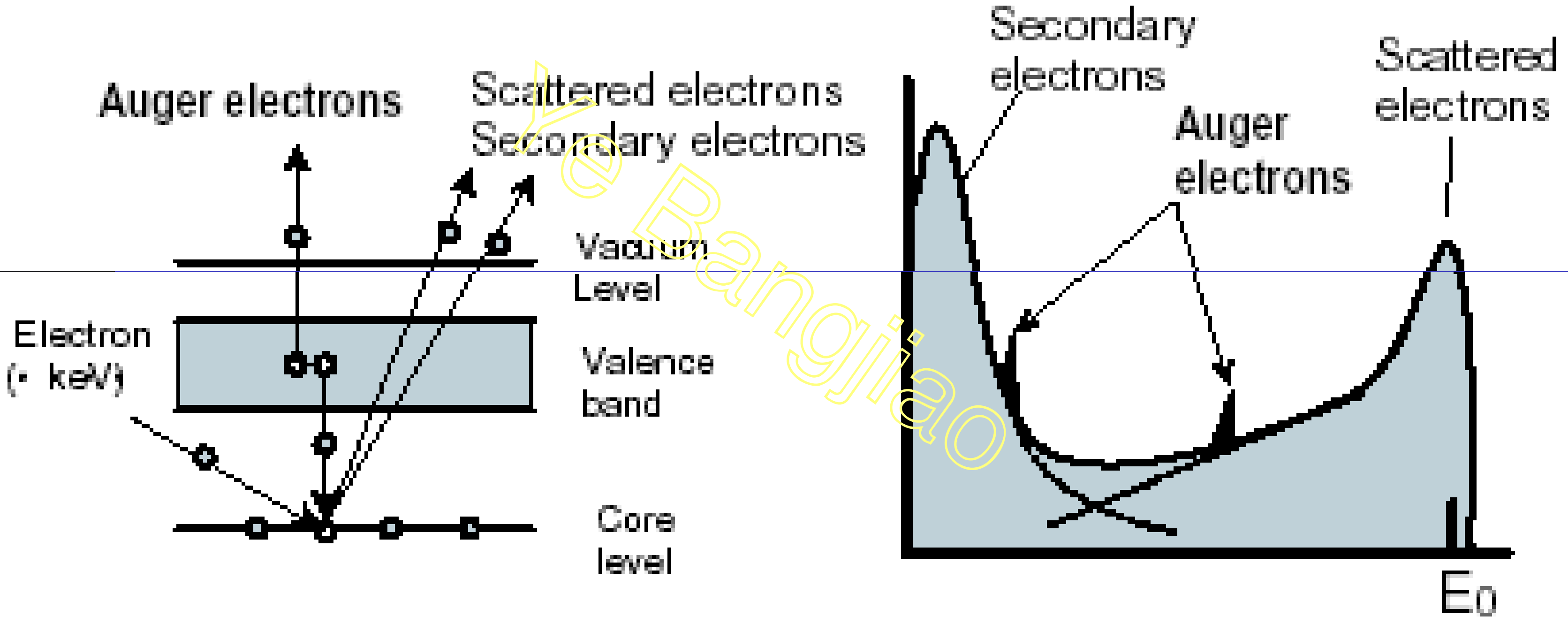

TOF-PAES

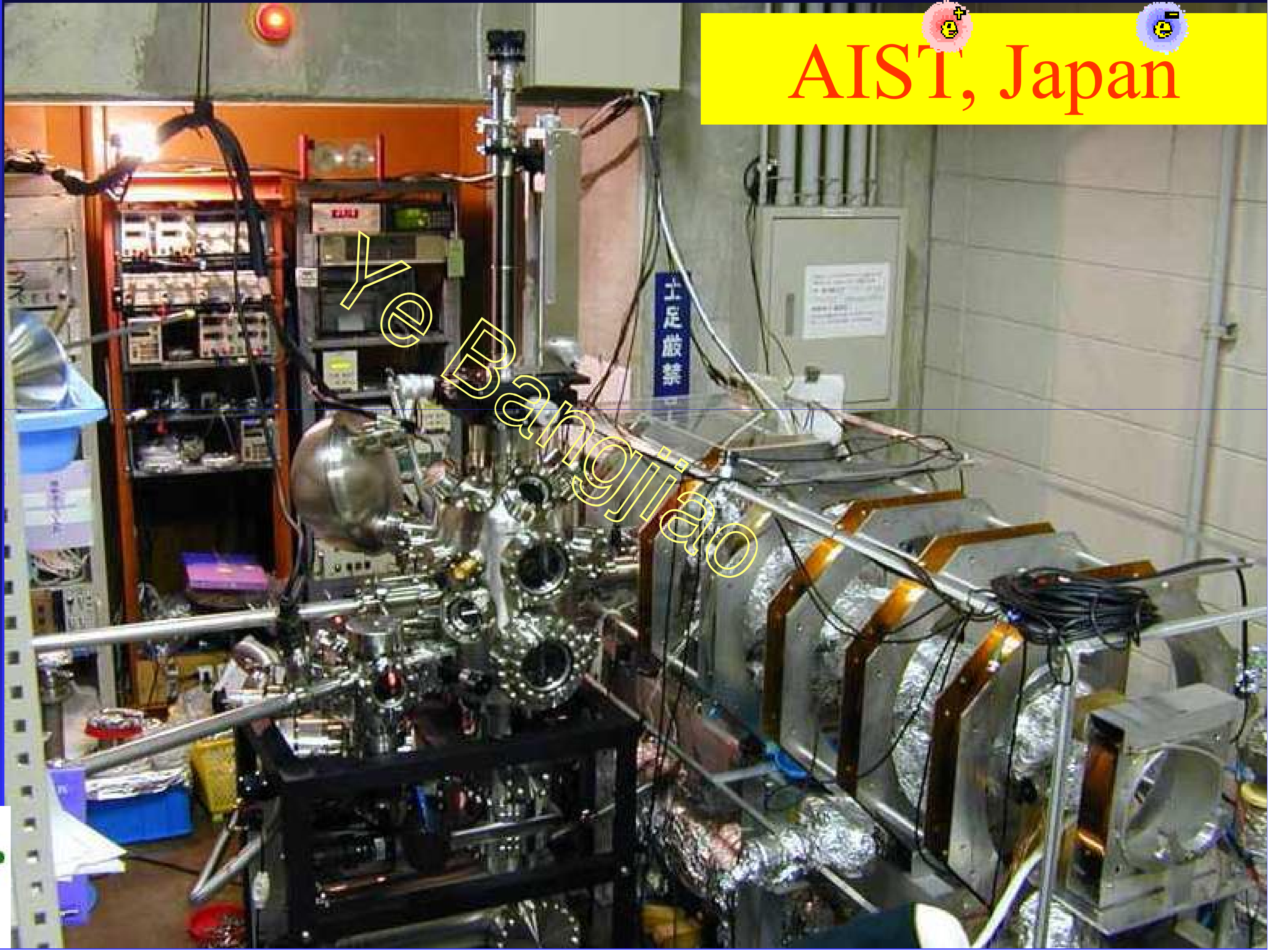

AIST, Japan

TOF-PAES apparatus

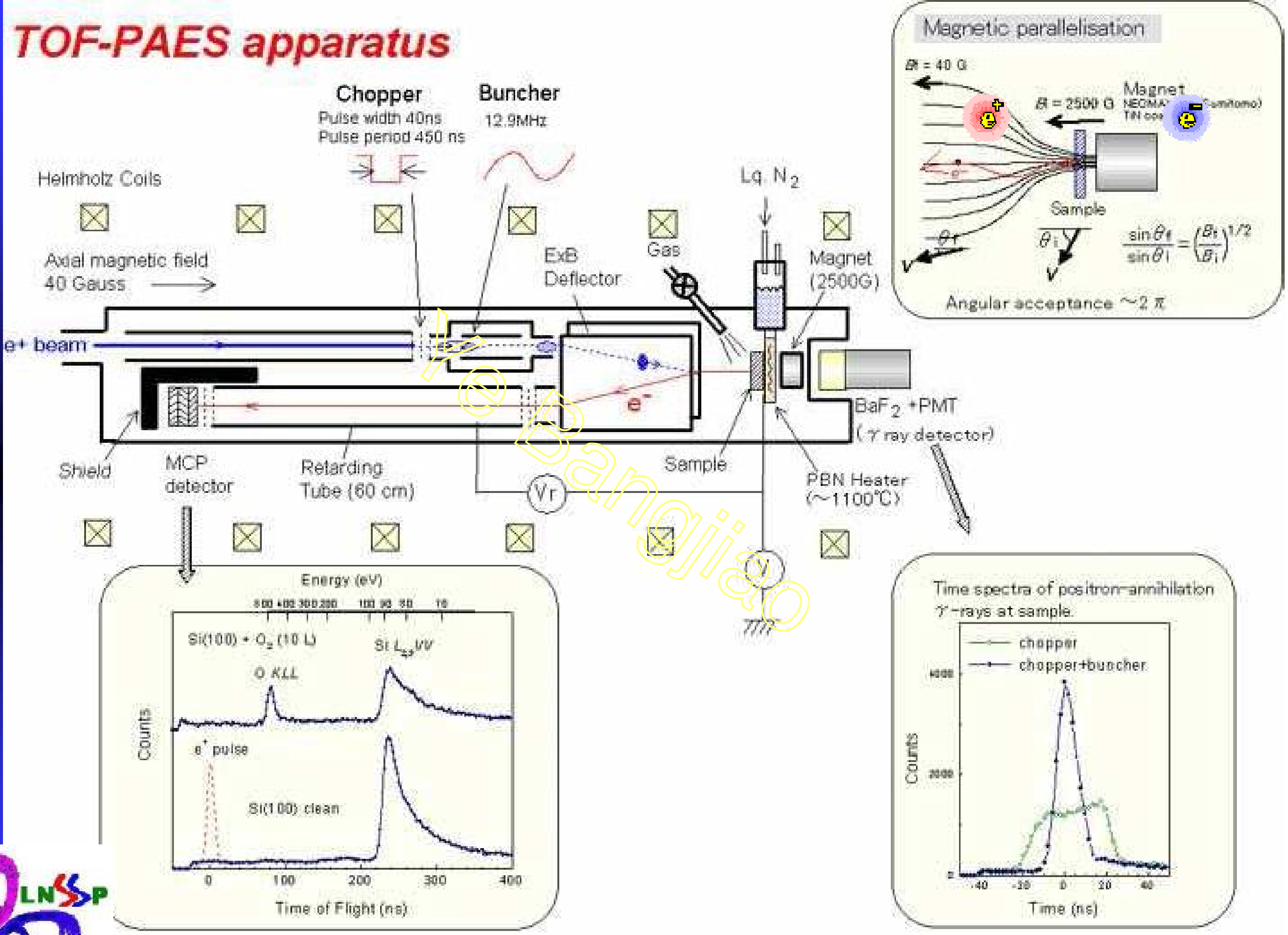

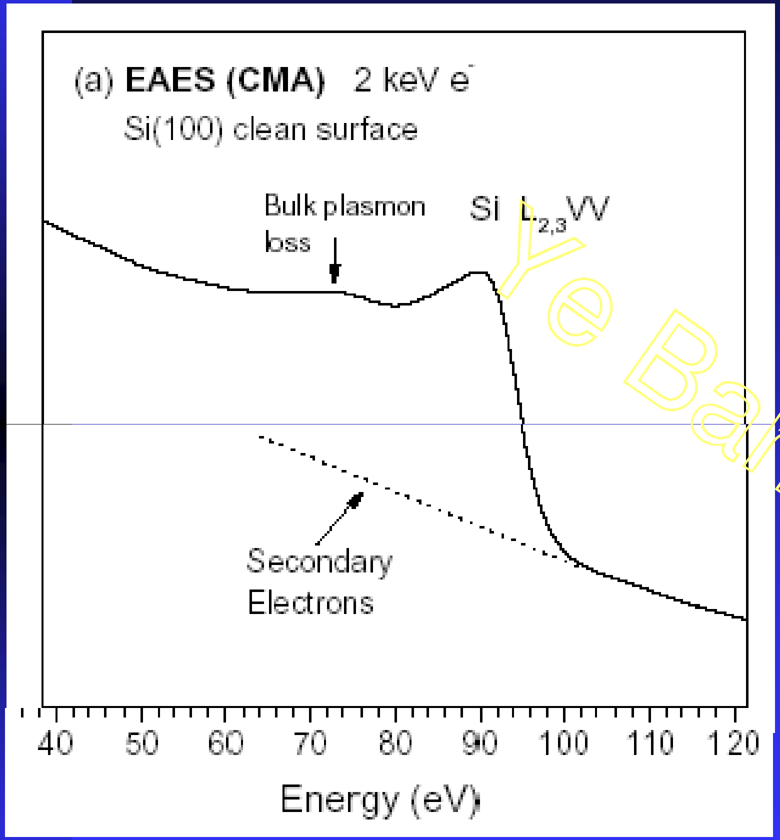
(a) **EAES (CMA)** 2 keV e$^-$
Si(100) clean surface
Bulk plasmon loss
Si $L_{2,3}VV$
Secondary Electrons
40
50
60
70
80
90
100
110
120
Energy (eV)

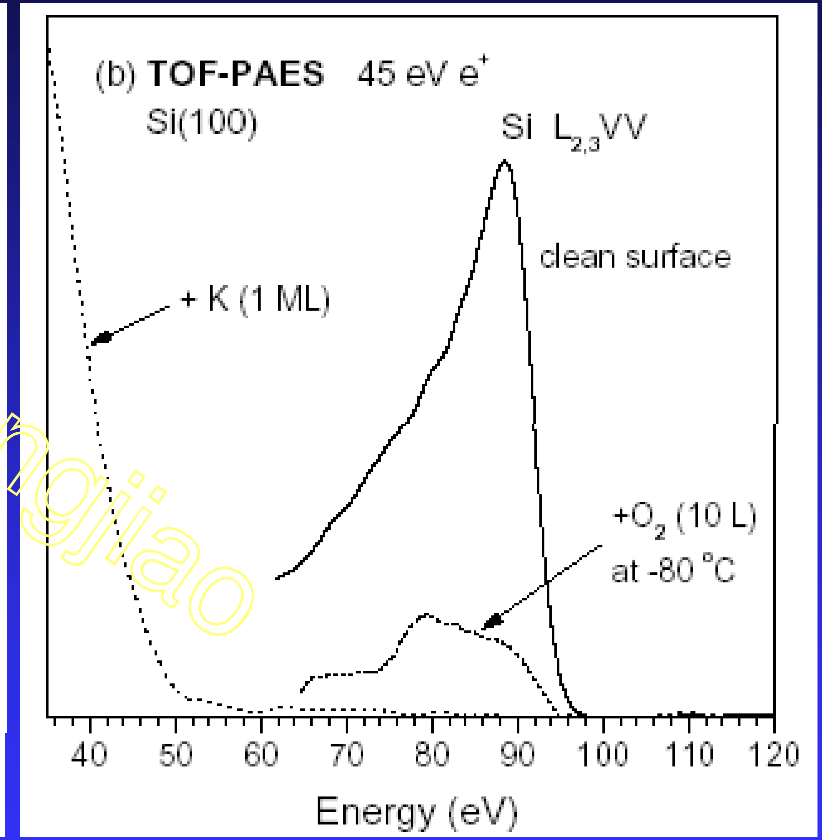
(b) **TOF-PAES** 45 eV e$^+$
Si(100)
Si $L_{2,3}VV$
clean surface
+ K (1 ML)
+O_2 (10 L) at -80 °C
40
50
60
70
80
90
100
110
120
Energy (eV)

美国Texas大学PAES

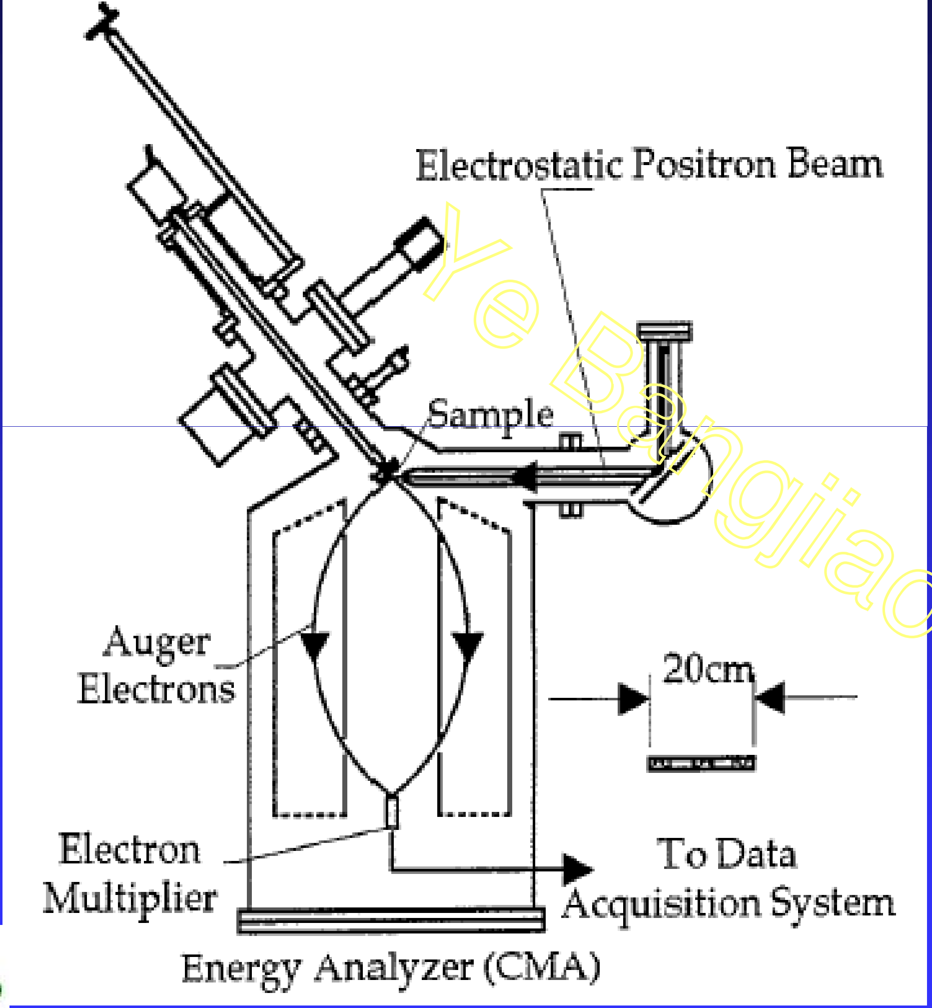

美国Texas大学Arlington分校的Weiss在1995年建立了一台能量分辨为2%的高分辨PAES谱仪，配备60mCi的^{22}Na，可获得~8×10^{4} e^{+}/s束流强度。

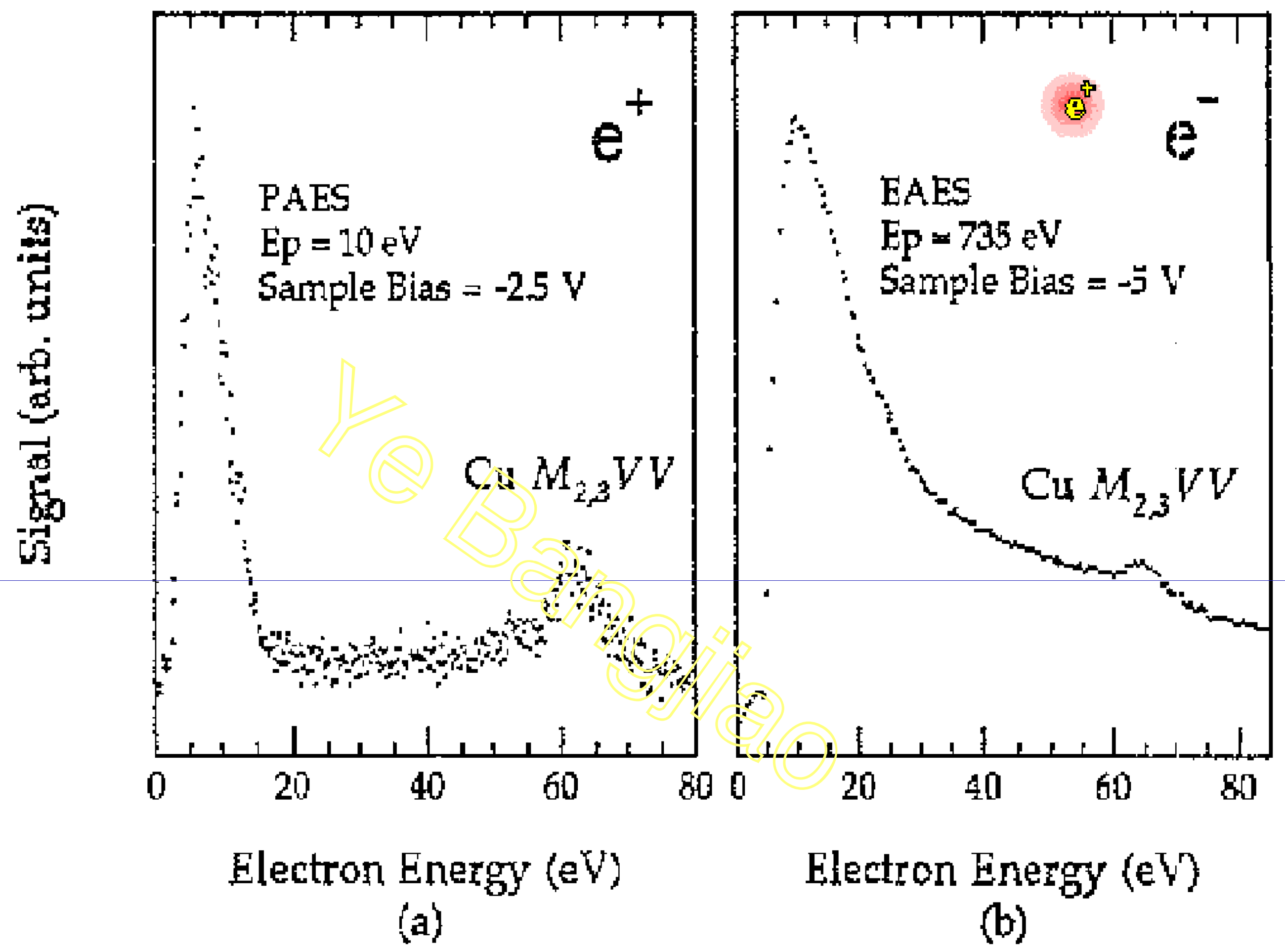

正电子和电子在多晶铜表面引起的俄歇电子发射。

（a）正电子能量10eV，（b）电子能量735eV。

Brookhaven National Lab.
PAES

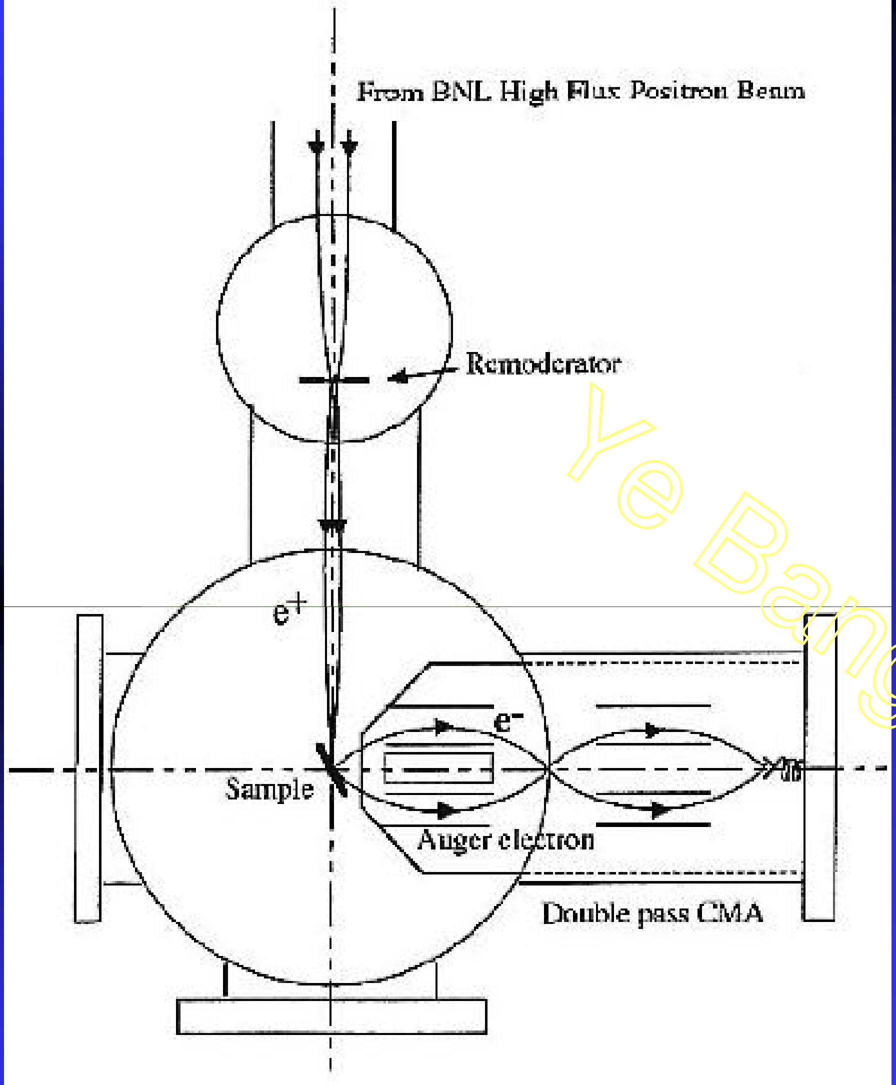

eamline at the BNL High Flux Positron Beam

这个装置可产生比通常的PAES要大100倍的正电子束流强度，这样可以使测量时间从原来的几小时减少到几分钟，因此可用来对薄膜生长动力学和不稳定的多成份表层系统进行高分辨测量研究。

●微　　束

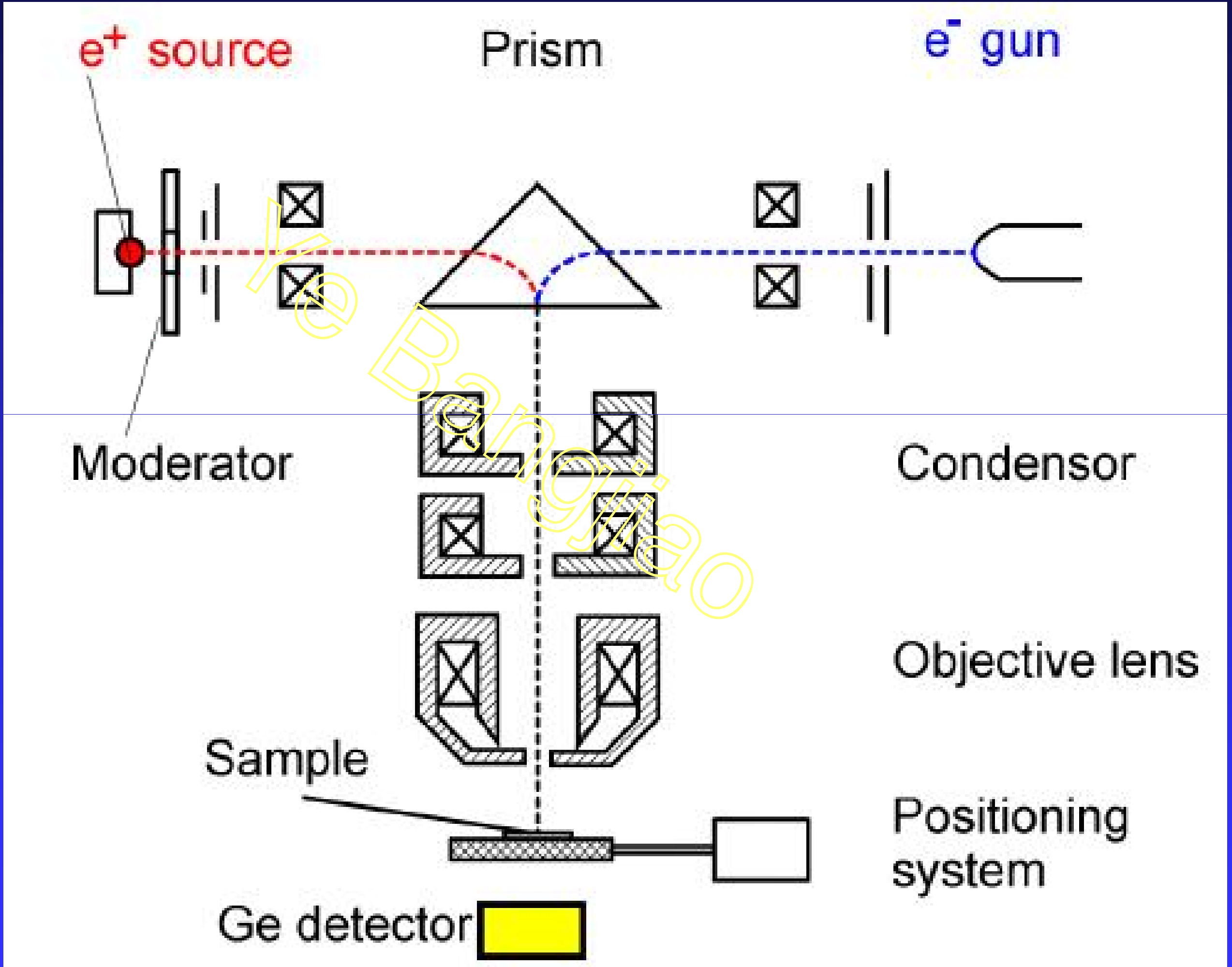

The Positron Microscope at Bonn University

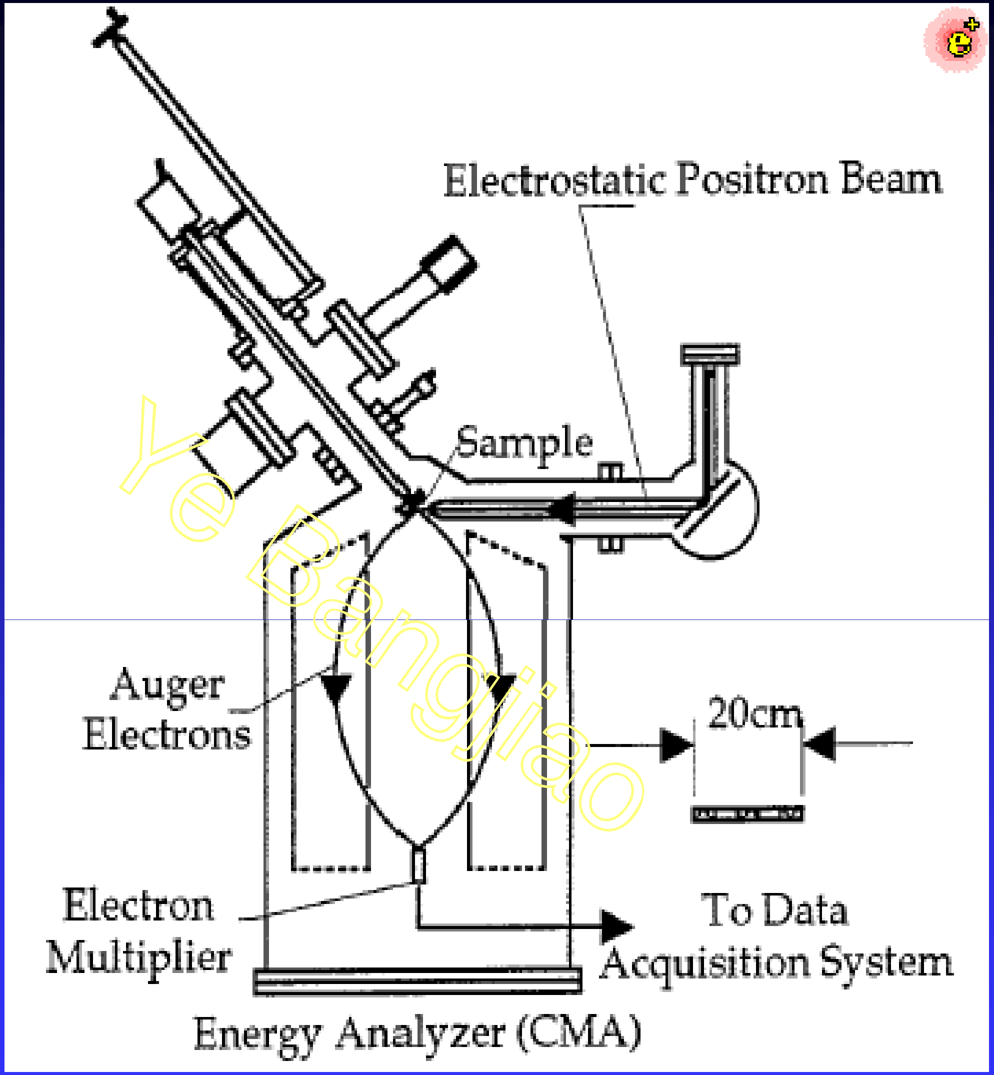

美国德克萨斯大学阿灵顿分校的高分辨**PAES**

Microbeam

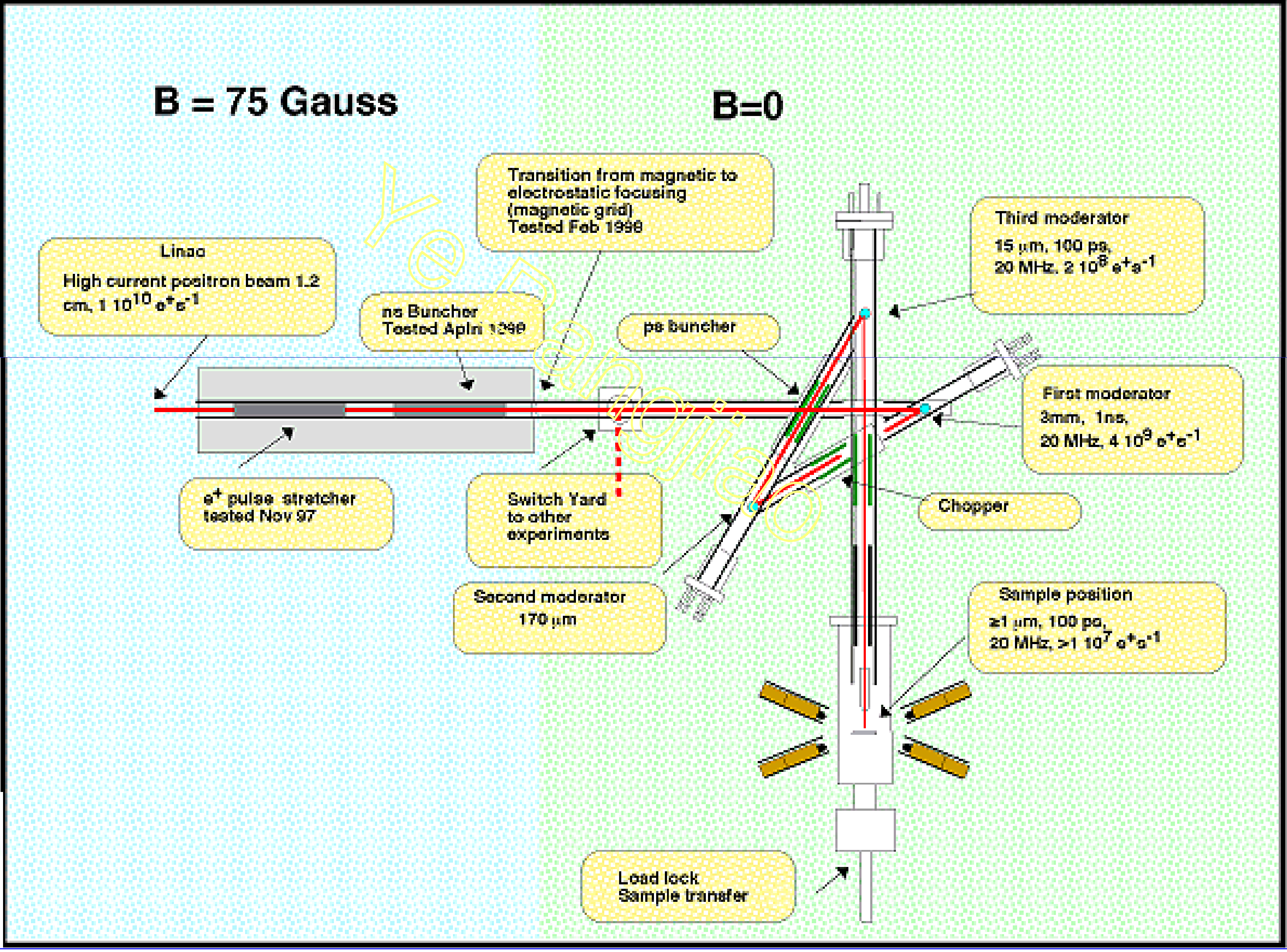

B = 75 Gauss

B=0

Linac
High current positron beam 1.2 cm, 1 10^{10} $e^{+}s^{-1}$

ns Buncher
Tested April 1998

Transition from magnetic to electrostatic focusing (magnetic grid)
Tested Feb 1998

ps buncher

Third moderator
15 μm, 100 ps,
20 MHz, 2 10^{8} $e^{+}s^{-1}$

First moderator
3mm, 1ns,
20 MHz, 4 10^{9} $e^{+}s^{-1}$

e^{+} pulse stretcher
tested Nov 97

Switch Yard
to other
experiments

Chopper

Second moderator
170 μm

Sample position
≥1 μm, 100 ps,
20 MHz, >1 10^{7} $e^{+}s^{-1}$

Load lock
Sample transfer

Scanning positron microscope

- Variable energy micro-beam of monoenergetic positrons
- Lateral resolution of 2 μm is achieved
- Lifetime measurements at different beam energies are possible

↓

- Principle disadvantage: broad positron implantation profile at high energies

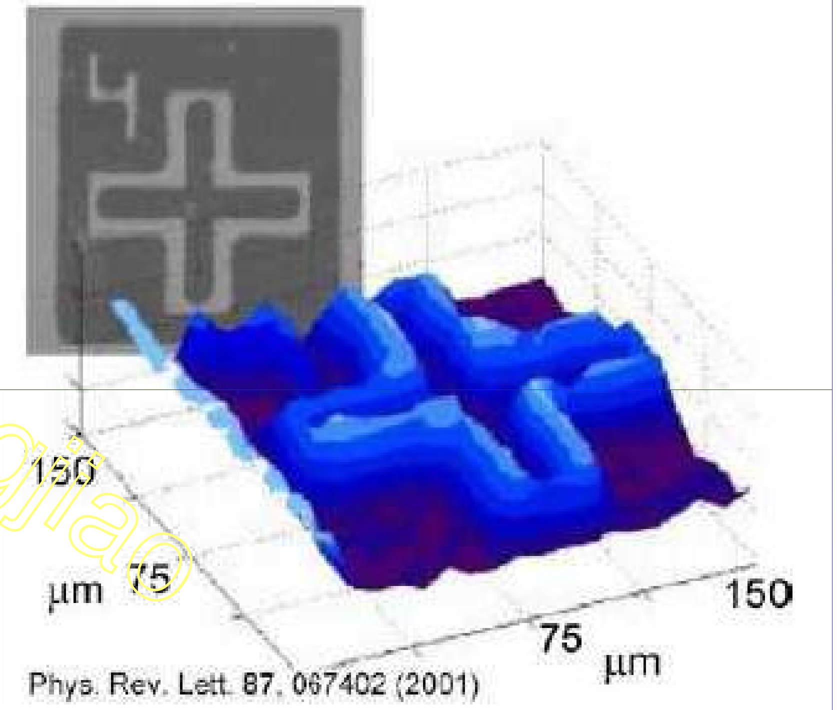

Phys. Rev. Lett. 87, 067402 (2001)

Electron and positron beam image of the surface of a test chip. Light area is SiO_2, dark area is platinum

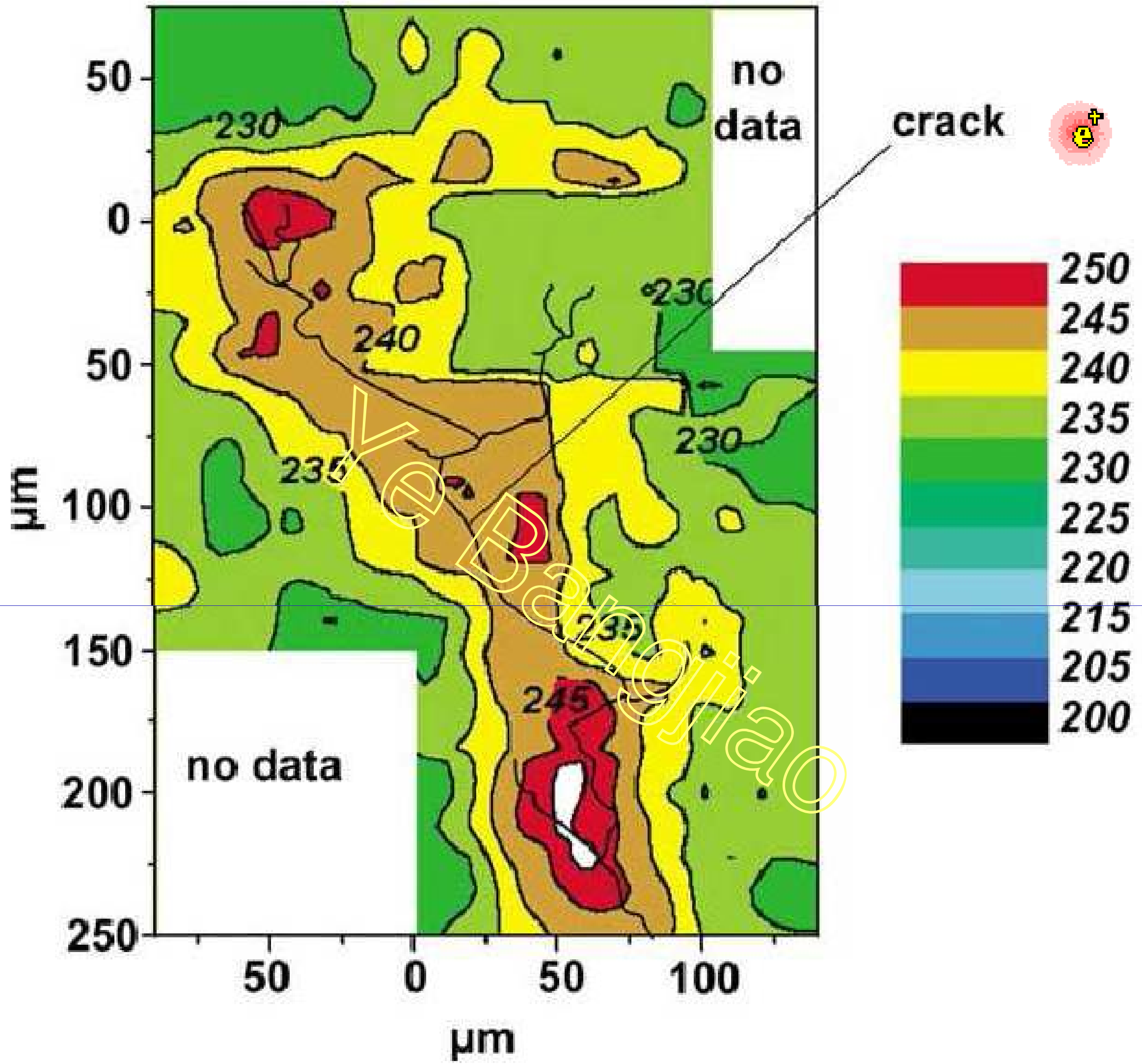

Fatigue crack in copper and map of mean positron fetime [ps] at 5 keV positron implantation energy.

Ye Bangjiao

Thank you!

http://staff.ustc.edu.cn/~bjye/e+/index.htm